Investigating the Importance of the Beta-octyl Glucoside Binding Site for the Toxicity of *C. Perfringens* Epsilon Toxin

Submitted by Leo William Bennett to the University of Exeter as a dissertation for the degree of Masters by Research in Biological Sciences in October 2017.

I certify that all material in this dissertation which is not my own work has been identified and that no material has previously been submitted and approved for the award of a degree by this or any other University.

Leo William Bennett, October 2017

ACKNOWLEDGEMENTS

I would like to thank my supervisors Professor Rick Titball, Dr Monika Bokori-Brown and Dr Sariqa Wagley for their guidance and exceptional support throughout this Masters by Research project. Special thanks also to Gemma Horne for assisting me with software and to those at the University of Exeter Biosciences department whose help was greatly appreciated.

Lastly I would like to thank all those that have helped with proof reading this dissertation and in supporting me along the way.

1 ABSTRACT

C. perfringens epsilon toxin (ε-toxin) is a potent heptameric β-pore forming toxin secreted by *C. perfringens* toxinotypes B and D. ε-toxin causes fatal disease in livestock populations that is characterised by severe neurological disruption. Numerous formaldehyde based veterinary vaccines against ε-toxin are available. However, these suffer from poor immunogenicity and side effects and are unsuitable for human use. Recently, ε-toxin has also been proposed as an aetiological agent for multiple sclerosis following the isolation of *C. perfringens* Type B in a multiple sclerosis (MS) patient. Further research has identified ten times greater ε-toxin immunoreactivity in MS patients compared to healthy controls. The aim of this study is to investigate two areas. Firstly, ε-toxin's beta-octyl glucoside (BOG) binding site was analysed for cytotoxicity against Chinese hamster ovary cells (CHO) expressing the putative myelin and lymphocyte (MAL) receptor using seven site directed mutants (V72A, V72F, F92A, T93A, V166A, V166F, A168F). The V72F, V166F and the A168F mutants demonstrate strongly reduced toxicity in CHO-hMAL cells and show promise as potential recombinant vaccine candidates against ε-toxin. Secondly, sera from control, CIS and MS patients were screened for ε-toxin immunoreactivity by investigating if sera conferred cytotoxic protection to CHO-hMAL cells incubated with ε-toxin. However, high sera lactate dehydrogenase (LDH) enzyme activity distorted experimental results. Consequently, it remains unclear if the sera exhibit immunoreactivity towards WT ε-toxin. The results suggest that fresh standardised sera samples should be used in future to mitigate this issue by ensuring greater experimental control.

2 CONTENTS

APPENDICES

3 LIST OF TABLES

4 LIST OF FIGURES

5 ABBREVIATIONS

ACHN	Human Kidney Adenocarcinoma Cell
Anti-ε PoAb	Anti-ε-toxin Polyclonal Rabbit Antibody
BOG	Beta-octyl Glucoside
CHO	Chinese Hamster Ovary
CIS	Clinically Isolated Syndrome
CNS	Central Nervous System
CPE	*Clostridium perfringens* Enterotoxin
CSF	Cerebrospinal Fluid
DMEM	Dulbecco's Modified Eagle's Medium
DMSO	Dimethyl Sulfoxide
DNA	Deoxyribonucleic Acid
ε-toxin	Epsilon Toxin
EtxYY	Epsilon Toxin Y43A– Y209A
FBS	Fetal Bovine Serum
FSE	Focal Symmetrical Encephalomalacia
GOSH	Great Ormond Street Hospital
HAVCR1	Hepatitis A Virus Receptor 1
LB	Lysogeny Broth
LCMS	Liquid Chromatography-Mass Spectrometry
LDH	Lactate Dehydrogenase
MAL	Myelin and Lymphocyte (protein)
hMAL	Myelin and Lymphocyte (Human Variant)
MDCK	Madin-Darbey Canine Kidney
MS	Multiple Sclerosis
MTT	*3-(4,5-Dimethylthiazol-2-yl)-2,5-diphenyltetrazolium bromidefor*. (Dye compound)
OD	Optical Density
PBS	Phosphate Buffer Saline
PCR	Polymerase Chain Reaction
PLAT	Polycstin-1 Lipoxygenase, Alpha Toxin
PSM	Peptide Spectral Match
RILD	Research Innovation Leaning and Development Centre
SDM	Site Directed Mutagenesis

SDS-PAGE	Sodium Dodecyl Sulphate Polyacrylamide Gel Electrophoresis
SOC	Super Optimal Broth with Catoblite Repression
UK	United Kingdom
US	United States
WT	Wild Type

6 OBJECTIVE

This report is submitted as a dissertation for the degree of Masters by Research in Biosciences. The objective of this report is to present the work and findings from the investigation of two topics, namely:

1) The development of a next generation veterinary vaccine against ε-toxin

2) Investigating the immunoreactivity of multiple sclerosis patients to ε-toxin

The investigation of these topics was undertaken by considering them as two separate projects. These are named Project 1 and Project 2 in this report.

The report is structured as follows:

- Introduction Section 7
- Project 1 – ε-toxin Toxin Mutagenesis Section 8
- Project 2 – Serum Neutralisation of ε-toxin Toxin Section 9

7 INTRODUCTION

This section provides a comprehensive summary of current knowledge regarding the *C. perfringens* bacterium, the different toxins it can produce, and a focussed review of ε-toxin.

7.1 CLOSTRIDIUM PERFRINGENS

C. perfringens, belonging to the *Clostridium* genus, is a non-motile Gram-positive spore-forming bacillus found ubiquitously in the environment. It is closely related to several other pathogenic bacteria including *Clostridium botulinum, Clostridium tetanii* and *Clostridium difficile*. Consistent with other members of the *Clostridium* genus, *C. perfringens* can exist as a vegetative cell or as a dormant spore. The vegetative cells of *C. perfringens* are rod shaped, demonstrate pleomorphism and normally exist in small chains [1]. These cells demonstrate a similar morphology to other Gram-positive bacteria including a thick peptidoglycan cell membrane containing capsular polysaccharides, and an inner cytoplasmic lipid membrane. As a vegetative cell, *C. perfringens* grows as an obligate anaerobic mesophile with optimal propagation achieved at 37°C in environments containing little to no oxygen. *C. perfringens* bacteria have been isolated in a variety of anoxic environments including soil, sewage and marine sediment [2]. However, the bacterium has also been isolated in the intestinal tracts of humans and animals and is known to be present in a variety of food products [1][3]. Under harsh environmental conditions, *C. perfringens* can transition to exist as a highly resistant spore [4]. These spores demonstrate high thermal, ultraviolet and desiccation tolerances enabling the *C. perfringens* bacterium to survive for long periods in hostile environments that are unsuitable for vegetative growth [4]. The prevalence and durability of these spores, particularly in food products, has resulted in the recognition of *C. perfringens* as a serious food safety concern [5]. Furthermore, the ubiquity of *C. perfringens* in these environments has firmly established it as one of the most widely spread pathogens in existence.

The virulence of *C. perfringens* is attributed to its arsenal of seventeen different secretory exotoxins [6]. Four of these toxins are known to exhibit lethal

properties and are considered major toxins. The different strains of *C. perfringens* demonstrate substantial variability in the array of toxins that they can secrete. Consequently, *C. perfringens* classification is divided into five serotypes (A-E) based on the secretion profile of the four major toxins: alpha, beta, epsilon and iota [6]. The five serotypes are listed in Table 7-1.

	TOXIN				
Type	**Alpha**	**Beta**	**Epsilon**	**Iota**	**Enterotoxin**
A	+	-	-	-	±
B	+	+	+	-	±
C	+	+	-	-	±
D	+	-	+	-	±
E	+	-	-	+	±

+ Type produces this toxin

- Type does not produce this toxin

± Some strains of that type produce this toxin

Table 7-1 - Secretion profiles of alpha, beta, epsilon and iota toxin by *C. perfringens* serotypes A, B, C, D and E. [7]

The variety of different toxins secreted by *C. perfringens* is essential in its ability to perform as a pathogenic organism. The toxins all show structural variability and differences in their ability to cause disease. Subsections 7.1.1 to 7.1.5 investigate the main toxins secreted by *C. perfringens* and their roles in human and animal disease.

7.1.1 *C. perfringens* - Enterotoxin

The *Clostridium perfringens* enterotoxin (CPE) is a 35 kDa single polypeptide toxin that currently ranks as the third leading cause of food poisoning in the United Kingdom, United States and Canada. In the United States, the bacterium is responsible for approximately 966,000 gastroenteritis cases each year with

an estimated annual economic loss of $400 million [1][8][9]. CPE is primarily associated with outbreaks at catering institutions where large quantities of food are prepared [10]. The disease is normally initiated through inadequate food preparation and results in isolated outbreaks typically affecting 50-100 people [1]. These gastroenteritis outbreaks are caused by the *C. perfringens* Type A strain, although CPE positive Type C and D strains have also been reported [11]. Despite the prevalence of *C. perfringens*, only an estimated 5% of the global *C. perfringens* population contain the *cpe* gene encoding the enterotoxin [12][13]. The *cpe* gene can be located either chromosomally or on a plasmid. An estimated 70% of *C. perfringens* Type A isolates contain a chromosomal copy of the gene with the remainder carrying the *cpe* gene on a 70-75kB conjugative plasmid [6][8][14]. CPE's protein structure was revealed following analysis from two studies in 2010 (Figure 7-1) [8][15][16]. This identified that CPE contained two domains; a C-terminal receptor binding domain and an N-terminal domain that controls oligomerization and pore formation [8].

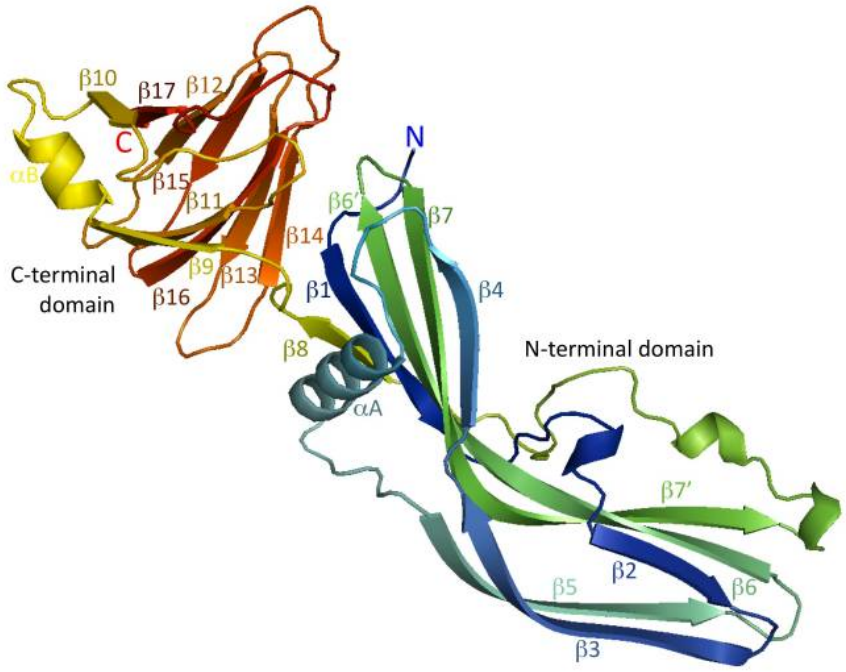

Figure 7-1 - The two-domain protein crystal structure of the CPE toxin [8] [15].

CPE related gastroenteritis is facilitated by the germination of *C. perfringens* Type A spores in food products following completion of the cooking process. *C. perfringens* spores have been isolated in a variety of food products including

spices, condiments, fish, poultry, beef and prepared dishes [1]. The durability of these spores in thermogenic environments enables them to survive most cooking processes. Temperatures ranging between 12°C-60°C promote the germination of *C. perfringens* spores and subsequent vegetative growth. This temperature range is frequently used by the catering industry in warm food holding areas ready for serving [17]. Consequently, cooked foods left in heated holding areas for extended time periods risk initiating a *C. perfringens* gastroenteritis outbreak [5].

If large quantities of contaminated food are ingested, some *C. perfringens* Type A bacteria can survive digestion and translocate to the intestines. These bacteria proliferate within the gut before re-entering sporulation and initiating CPE production. Following sporulation, the *C. perfringens* spores lyse releasing CPE [8]. The CPE is released into the intestinal lumen where it binds to claudin proteins located at epithelial tight junctions in the intestines. The claudin protein structure contains two extracellular loops ECL1 and ECL2 that are critical for CPE binding to the epithelial cell membrane [18][19]. CPE binding to the claudin proteins results in the formation of a non-cytotoxic 90 kDa complex [20]. Several of these complexes oligomerise to form a larger 450 kDa prepore complex named CH-1 [20]. The CH-1 complex contains beta hairpin loops that assemble into a beta barrel that creates a pore within the membrane [21]. Pore formation within the intestinal cell membrane leads to fluid imbalance and the influx of calcium that results in cell death. The disease is characterised by symptoms of diarrhoea and abdominal cramps in the affected patient that typically last 24 hours [22][23]. With extended time the toxin forms an even larger 600 kDa complex named CH-2, however, the role of CH-2 in cytotoxicity is not fully understood [8][24].

CPE is also known to cause acute intestinal damage in other mammalian species including rabbits, cats and dogs. *C. perfringens* is a normal commensal organism in the microflora of these species and has been reported in 80% of dogs [25]. Disease is normally initiated by microfloral disruption that enables *C. perfringens* to become competitively dominant. This can be attributed to changes in diet, antibiotic administration, stress or coinfections in the intestines [26]. CPE related disease is frequently self-limiting in these animals although

some rare cases of suspected fatalities have been reported [27].

7.1.2 *C. perfringens* – Alpha Toxin

Alpha toxin is a 43 kDa sized lethal exotoxin produced by the C*. perfringens* bacterium with a reported lethal dose of 40 ng/ml [28][29][30]. Alpha toxin is encoded by the chromosomally located *cpa* gene that is located in a highly stable area of the bacterial chromosome [31]. Alpha toxin gene expression is regulated by the VirR/VirS two component system; however, the environmental signalling factor stimulating *cpa* expression is currently unknown [32]. Alpha toxin is produced by all five *C. perfringens* toxinotypes with *C. perfringens* Type A producing the largest quantity of alpha toxin (Table 7-1). Enzymatically, alpha toxin demonstrates both phospholipase C and sphingomyelinase activities [33]. This enables alpha toxin to cleave phospholipids and sphingolipids commonly found within eukaryotic cell membranes to initiate cell lysis. Consequently, high concentrations of alpha toxin result in extensive cell lysis from cell membrane damage [17]. The alpha toxin crystal structure was first established in 1998 and revealed that the toxin is structurally divided into two domains [34]. This is presented in Figure 7-2.

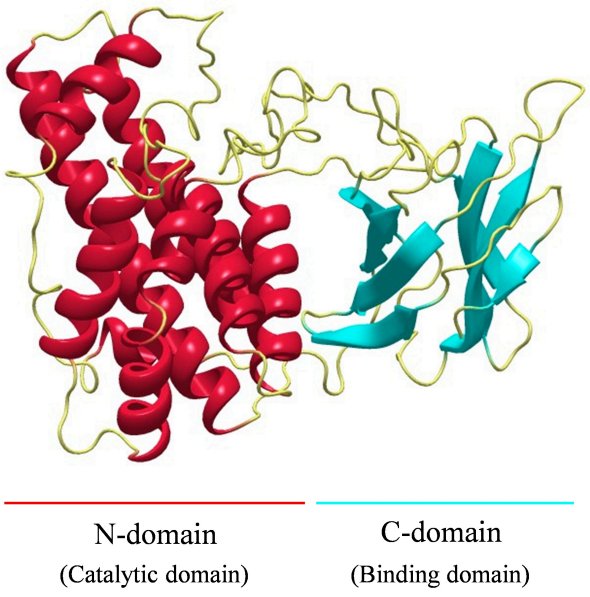

Figure 7-2 - The two domain protein crystal structure of the *Clostridium perfringens* alpha toxin [35]**.**

1) The N-terminal domain contains the residues responsible for alpha

toxin's phospholipase C, sphingomyelinase and cytotoxic activities [36]. The domain consists of nine alpha helices and zinc binding ligands that are essential for alpha toxin's toxicity [33]. The binding of zinc ions to these ligands helps to support the structural integrity of alpha toxin and assists in its phospholipase C activity [17][37]. Treatment of the N-terminal domain with ethylenediaminetetraacetic acid (zinc chelating agent) abolishes alpha toxin's phospholipase C, sphingomyelinase and cytotoxic activities, which strongly suggests that the zinc ions are essential for alpha toxin's functionality. Further studies have indicated that the zinc binding ligands may also serve as part of alpha toxin's catalytic site [33][37][38]. Previous research has identified that the enzymatic activity of the N-terminal domain is clearly required for alpha toxin to elicit toxicity [36]. However, by itself, the N-terminal domain is insufficient to cause disease which suggests that the activity of the C-terminal domain is also required for alpha toxin to initiate toxicity [17].

2) The C-terminal domain also known as PLAT (Ploycystin-1 Lipoxygenase, Alpha-toxin) functions as a membrane binding domain [33]. The PLAT structure is commonly found in membrane associating proteins and consists of an eight stranded antiparallel beta sandwich formed from beta sheets [33]. Current evidence has identified that the C-terminal domain is involved in membrane interactions; however, the C-terminal domain demonstrates no cytotoxic or cytolytic effects. Instead, the C-terminal domain appears to facilitate binding of alpha toxin to host cells that enables the N-terminal domain to elicit toxicity. The molecular action of the C-terminal domain is facilitated by several tyrosine residues and a phenylalanine residue that are critical for membrane binding [39][40]. Furthermore, the C-terminal domain contains calcium-binding ligands that are considered essential for alpha toxin's activity [41]. These calcium ions facilitate structural changes within the C-terminal domain exposing hydrophobic residues which play a key role in phospholipid binding to host cell membranes [17]. Once

associated with the host cell membrane, these calcium ions form bridges which enable hydrophobic residues to insert into the cell membrane in order to initiate cytotoxicity [17].

Alpha toxin is one of the primary etiological agents of gas gangrene also referred to as clostridial myonecrosis in humans. Gas gangrene is an aggressive infection in which healthy tissue is rapidly destroyed resulting in mass necrosis and gas accumulation that can be fatal. Historically the disease was associated with battlefield injuries but has also been connected to natural disasters and, in recent years, intravenous drug use [17]. Gas gangrene is primarily caused by *C. perfringens* that accounts for 80% of cases [42]. The disease is initiated following deep lacerations and crush type injuries that facilitate the introduction of *C. perfringens* into deep tissues [42]. Research into the disease has identified that alpha toxin stimulates platelet, fibrin and neutrophil aggregation by interacting with the platelet fibrinogen receptor glycoprotein IIb/IIIa. [43]. These aggregates occlude blood vessels that obstruct local and regional blood flow in neighbouring tissue [43]. The reduced blood flow promotes an anaerobic environment that is believed to facilitate the spread of *C. perfringens*. Additional studies have identified that polymorphonuclear leukocytes accumulate along the endothelial layer of blood vessels and fail to migrate into the periplasmic space [43]. This appears to be due to the up regulation of intercellular and endothelial adhesion molecules including E-selectin and ICAM-1 [44]. Alpha toxin is cytolytic towards leukocytes that may also contribute to the reduction of inflammatory immune cells to these infected tissues [45]. These data suggest that alpha toxin may also be able to influence the host's immune response to assist the spread of infection [17][46]. The disease is also present in calves, horses and piglets and requires similarly harsh surgical and medical techniques to ensure survival [47][48]. In all these forms of disease, alpha toxin is widely recognised as the primary mode of virulence.

7.1.3 *C. perfringens* – Beta Toxin

Beta toxin is a 34 kDa sized lethal toxin produced by *C. perfringens* [49]. The *cpb* gene located on a *C. perfringens* plasmid encodes the toxin with expression

controlled by the VirR/VirS two-component system [50]. Beta toxin exhibits dermonectrotic effects but demonstrates no haemolytic properties. Unlike other *C. perfringens* toxins, it is highly sensitive to environmental conditions and can be quickly degraded by heat and trypsin digestion [51]. Consequently, beta toxin can only initiate disease under specific environmental conditions. However, individuals subject to a diet rich in trypsin inhibitors are more predisposed to beta toxin disease [51]. Sequence alignments identify that beta toxin shows significant structural similarity with *S. aureus* alpha toxin indicating that beta toxin may belong to the β-pore forming toxin family [52]. The structure of beta toxin can be seen in Figure 7-3:

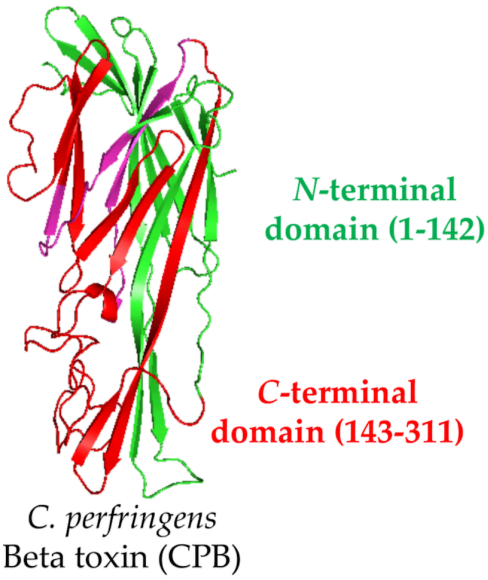

Figure 7-3 - The two domain protein crystal structure of the *C. perfringens* beta toxin [53]**.**

Beta toxin is produced by *C. perfringens* toxinotypes B and C. Both strains can infect animals causing haemorrhagic enteritis and diarrhoea in domesticated livestock species [52][54]. However, Type C infections are recognised as more prolific in neonatal animals [55]. Beta toxin has been identified as the etiological agent of the disease that is characterised by severe mucosal necrosis on the small intestines [50]. In animals, beta toxin infection corresponds to a high mortality rate approaching 100%, resulting in significant economic losses [54].

C. perfringens Type C has also been linked to necrotizing enterocolitis in humans through the action of beta toxin. This disease, also referred to as

pigbel, is not found in western countries. However, the disease was reported in the Highland of Papua New Guinea in 1973, and an outbreak recorded in Germany following the end of World War Two [56][57]. In both cases, the disease was attributed to beta toxin after the sudden consumption of a protein rich diet following a long period of ingesting a low protein diet [52]. Infected individuals possessed lower intestinal trypsin levels indicated they were at higher risk of beta toxin infection. The pigbel disease has a reported mortality rate of 35-40% and results in severe mucosal necrosis, inflammation and haemorrhaging within the small intestine that usually requires surgical treatment [52].

Beta toxin's molecular mechanisms of disease are largely unknown due to a lack of susceptible cell lines for *in vitro* experimentation [52]. However, beta toxin has been shown to bind to vascular endothelial cells at lesion sites and initiates disease through pore formation [58][59]. Pore formation is initiated by beta toxin monomers binding to a currently unknown receptor that is believed to localise on lipid raft microdomains on susceptible cells [60]. Binding is followed by rapid oligomerization into a heptameric pre-pore on the cell surface [51]. Oligomerisation also protects beta toxin from trypsin digestion by burying trypsin targets into the toxin structure [51]. The beta toxin oligomer inserts into the host cell membrane creating a pore that initiates ion uptake into affected cells. This ion disruption results in morphological changes and cell death through programmed necrosis [51][61].

Much remains unknown regarding the pathogenesis of beta toxin. Consequently, more research is required to elucidate the molecular mechanisms of beta toxin mediated disease. Fortunately, beta toxin disease is considered very rare in the world and can be easily avoided by ensuring basic food hygiene, good dietary intake and correct cooking practices.

7.1.4 *C. perfringens* – Iota Toxin

Iota toxin, first described in 1943, is produced solely by *C. perfringens* toxinotype E [62]. It exhibits lethal properties that are associated with enteric disease in animals. Most notably, Iota toxin has been linked to antibiotic

associated enterotoxemia in rabbits and calves, but has rarely been observed in other domesticated livestock [63]. The disease is typically characterised by diarrhoea, haemorrhages and oedema in affected animals and can result in sudden death [63].

Structurally, iota toxin is composed of two unlinked and immunologically distinct proteins Iota-A and Iota-B that are encoded on a plasmid by the *iap* and *iab* genes respectively [64][63]. The 47 kDa Iota-A protein confers the toxin's enzymatic activity while the 81 kDa Iota-B protein facilitates cellular binding and entry of Iota A into host cells [64]. Both Iota toxin proteins are synthesised and secreted during exponential phases of *C. perfringens* growth. However, trypsin proteolytic digestion is required to activate both proteins [65]. Alone, these proteins are non-toxic, but together Iota-A and Iota-B exhibit lethal cytotoxic properties.

Following secretion, the C-terminal domain of the Iota-B binding protein attaches to an unknown receptor found on lipid rafts on the cell surface [62]. Iota-B then oligomerises into a non-toxic heptamer, which facilitates the formation of ion permeable channels in the cell membrane [66]. The Iota-A protein then interacts with Iota-B's exposed N-terminal domain. This interaction facilitates the internalisation of Iota-A into the target cell by receptor-mediated endocytosis. Following this, it is believed that Iota-A is then transported into the cytosol via endosomal trafficking [62]. Once internalised into the cytosol, Iota-A then adenosine diphosphate ribosylates skeletal muscle alpha actin and non-muscle beta/gamma actin at arginine-177 [67][68]. The ribosylation inhibits actin polymerisation preventing the formation and extension of cytoskeletal filaments [69]. This action by Iota-A results in the breakdown of the cell's cytoskeleton causing cell rounding, intoxication and cell death [62].

Iota toxin disease is considered rare and little research has been undertaken to investigate the molecular mechanisms of Iota toxin thoroughly [63]. Consequently, the pathogenesis and molecular interactions of Iota toxin are poorly understood. However, the *C. perfringens* Type E toxinotype that produces Iota toxin is not prevalent in the environment. As a result, Iota toxin is

not recognised as a significant public health or animal health concern.

7.1.5 *C. perfringens* – ε-toxin

ε-toxin is a 32.9 kDa sized heptameric β-pore forming toxin synthesised by *C. perfringens* toxinotypes B and D [70][71]. ε-toxin has a reported intraperitoneal lethal dose of 1.2 ng/kg in mice [72]. This makes ε-toxin the most potent toxin secreted by *C. perfringens* and the third most potent toxin known to man, preceded only by the *C. botulinum* and *C. tetani* neurotoxins [73]. As a result of its marked toxicity, ε-toxin has gained attention from governments around the world who recognise it as a bioterrorism threat. Currently, ε-toxin is registered as a category B biological agent, the second highest bioterrorism security priority recognised by the Centre of Disease Control and Prevention [71]. Pathologically, ε-toxin is a major cause of morbidity and mortality in domestic livestock, most notably in sheep and goat populations around the world [71]. Clinical symptoms of ε-toxin are dose dependent and occur rapidly, normally within minutes to hours after exposure [74]. ε-toxin immunogenicity has recently been described in MS patients suggesting that ε-toxin may be the etiological agent behind the condition [75].

C. perfringens ε-toxin is genetically encoded by the *etx* gene that is located on plasmid vectors. In *C. perfringens* toxinotype D, the *etx* gene can be harboured by at least five different plasmids that vary from 48 to 110 kbp [76][77]. Two of these plasmids can be conjugated between different *C. perfringens* strains [76]. This distribution and acquisition of new plasmids enables *C. perfringens* strains to quickly change toxinotypes, potentially as an adaptive response to changes in their environment. In contrast, Type B harbours the *etx* gene on a single 65 kbp plasmid [78]. The upstream promoter regions between the *etx* gene expressed in Type B and D are dissimilar suggesting that ε-toxin expression is regulated differently between these different toxinotypes [79][80]. *Etx* gene sequencing, cloning and expression were first successfully completed in 1992 and have facilitated the use of recombinant deoxyribonucleic acid (DNA) technologies to further investigate ε-toxin [70]. This has been of particular importance in the context of vaccine development that dominates current

research into ε-toxin. The structure of ε-toxin can be seen in Figure 7-4.

Figure 7-4 - The three domain protein crystal structure of *C. perfringens* ε-toxin [81]**.**

As seen in Figure 7-4, ε-toxin possesses a highly elongated structure that consists of three domains that are critical in mediating ε-toxin's pathological function:

1) Domain I – consists of a large α-helix followed by three shorter helices [71]. Domain I appears to be critical for ε-toxin's initial interaction with host cells and mediating ε-toxin's binding to receptors [81].

2) Domain II – consists of a β-sandwich containing a two-stranded sheet [71]. Domain II has been identified as ε-toxin's pore-forming domain with an amphipathic sequence believed to mediate ε-toxin's membrane insertion and pore forming capabilities [71]. Domain II has also been implicated in ε-toxin's oligomerisation, and stabilisation. The Ser124 and Thr143 residues appear to be important in mediating these characteristics [81].

3) Domain III – consists of a β-sandwich. This domain contains ε-

toxin's cleavage site that is removed during proteolytic activation [71]. Functionally, domain III is believed to control ε-toxin's monomer interactions that enable it to oligomerise into a heptamer [71]. It contains the only parallel strand in the structure.

As seen in Figure 7-5, ε-toxin demonstrates similar characteristics to a range of bacterial pore forming toxins. In particular, it shares strong structural anaology to the *Aeromonas* aerolysin toxin despite only sharing 14% sequence homology [82]. The aerolysin toxin contains an additional domain for interacting with target host cells that is absent in ε-toxin. ε-toxin also demonstrates structural similarity to many other aerolysin-like toxins including the *Laetiporus suphureus* lectin toxin, *Bacillus thurinigiensis* parasporin-2 toxin and *C. septicum's* alpha toxin [79]. However, in all cases, ε-toxin demonstrates far greater potency with lethality at least 100 times greater in mice [71].

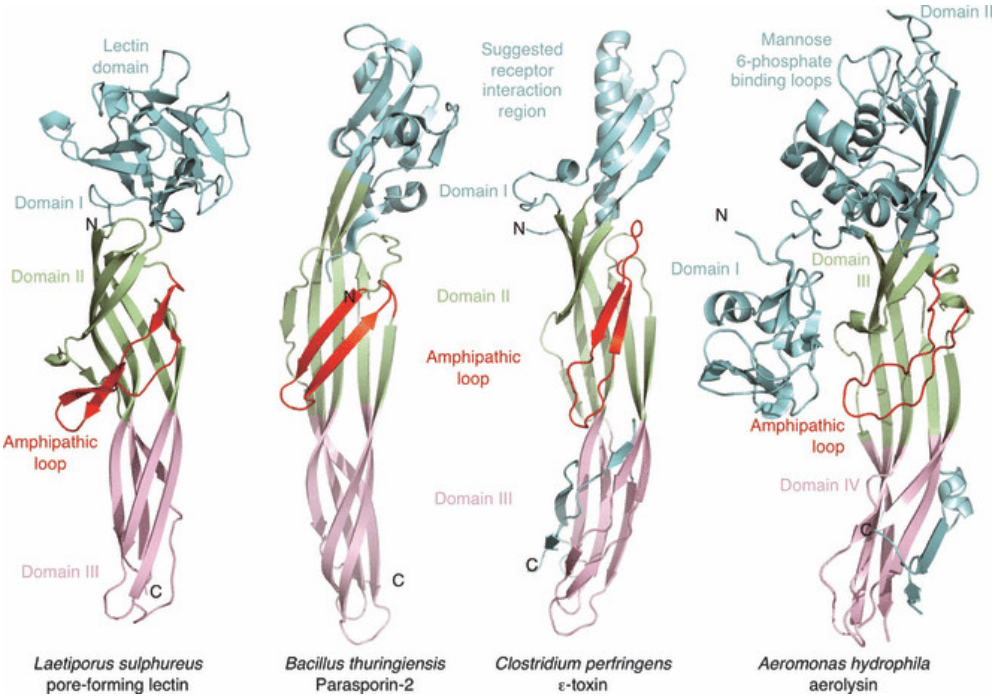

Figure 7-5 - Illustrates the X-ray crystallography three domain protein structures of the *L. sulphureus lectin, B. thurnigiensis Parsporin-2, C. perfringens* ε-toxin and the four domain *A.hydrophila* aerolysin β-pore forming toxins [79]**. The figure shows the putative membrane insertion amphipathic loops in red.**

ε-toxin is secreted by the B and D toxinotypes of *C. perfringens.* Similar to other *C. perfringens* toxinotypes, Types B and D are both found in soil and sediment environments but can also be found in low numbers ($<10^3$ bacteria g^{-1}) in the

digestive tracts of pathologically associated animals [83]. Both toxinotypes represent major causes of disease in domestic livestock; however, the Type D toxinotype causes more ε-toxin induced infections. Type B is the etiological agent of dysentery in new-born lambs and is also responsible for enterotoxemias and enteritis cases in calves, foals and piglets [71]. The Type D toxinotype is found globally and is responsible for the fatal enterotoxemias of goats, sheep and new-born lambs [71]. Type D disease is most common in rapidly growing lambs, less frequent in sheep and goats and occasionally in other species [71]. In both Type B and D infections, ε-toxin is considered to be the main mode of virulence and lethality in affected animals. Consequently, these sometimes rapidly fatal diseases in domestic livestock populations can lead to significant economic and agricultural losses.

Both *C. perfringens* Type B and D can reside naturally in low number in the microfloral environment of ruminant animals without damaging the host. Disease is initiated when *C. perfringens* Types B and D are stimulated to produce ε-toxin in the intestines of the host animal. This is normally associated with the overgrowth of these bacteria above a threshold of $>10^6$ bacteria g^{-1} [71]. A variety of factors can stimulate the *C. perfringens* bacteria to transition to a pathogenic organism. ε-toxin producing *C. perfringens* can rapidly proliferate in the digestive tracts of new-born animals, whereby the microflora that supresses *C. perfringens* colonization is undeveloped and non-functional. This is particularly common in the case of *C. perfringens* Type B lamb dysentery that can occur within the first few days of life [71]. The overconsumption or sudden transition to a carbohydrate rich diet is associated with the proliferation of *C. perfringens* that causes enterotoxemia in older animals [71][79]. The sudden influx of undigested carbohydrates such as starch distresses the local microflora and serves as excellent growth substrate for *C. perfringens* [71]. A variety of other factors have been linked to the development of ε-toxin disease in animals including; parasitic infections, pregnancy, tranquiliser use and antibiotic consumption [73][84].

Acute forms of ε-toxin disease in animals commonly involve neurological symptoms including violent convulsions, ataxia, lateral recumbency, cerebral swelling and coma [71]. Non-neurological symptoms include laboured

breathing, high blood pressure and oedema of various organs. Histological patterns between animal species can vary considerably. For example, sheep are known to suffer relatively greater brain damage compared to goats, which suffer greater intestinal and colonic damage through lesion formation [73]. The contrasting pathologies of ε-toxin in different animal species may be explained by differences in bacterial growth kinetics between different animal species [85]. For example, micro-environmental differences between animals possessing four chambered stomachs and linear digestive systems will invariably impact the growth of *C. perfringens* and the subsequent production of ε-toxin [85]. However, although ε-toxin's pathology varies between animal species, some symptoms including central nervous system (CNS) damage are observed consistently between all infected animals species [73].

The symptoms of ε-toxin disease develop quickly, usually within minutes to a few hours following exposure, and are rapidly fatal. Older animals typically develop a more chronic form of the disease referred to as Focal Symmetrical Encephalomalacia (FSE) that is commonly observed in sheep [71]. A recent FSE case was reported in a Brazilian goat population that demonstrated neurological symptoms, blindness and recumbency up to fourteen days [86]. Post-mortem examinations reveal extensive systematic damage in infected animals with ε-toxin disease present in multiple organs including the heart, lungs, liver, stomach and brain [73]. ε-toxin most notably accumulates throughout the kidneys, except in the medulla and proximal tubes [81]. ε-toxin has also been reported in bladder epithelial cells. The effects of ε-toxin accumulation in animal kidneys are also clearly evident in post-mortem examinations. Pulpy kidney disease is typically observed shortly after the animal has died from Type D enterotoxemia, and is characterised by the post-mortem swelling and autolysis of the kidneys [73][87]. The high ε-toxin activity in the kidneys during *C. perfringens* infections may explain why the few discovered cell lines susceptible to ε-toxin are from canine, mouse and human kidneys. However, it has also been suggested that ε-toxin's apparent affinity to the kidneys may be related to renal function. It has been proposed that the kidneys deliberately absorb ε-toxin in an attempt to filter out and reduce toxin levels in the bloodstream, and to mitigate harmful effects in other organs

[81][87]. However, this theory has not been proven.

Terminal phases of ε-toxin disease are characterised by severe neurological disorders in infected animals. This is induced by ε-toxin's ability to rapidly disrupt the blood brain barrier increasing vascular permeability in order to initiate neurological disease. The effects of ε-toxin on the blood brain barrier are well described, however, the mechanism by which ε-toxin induces permeability changes to the blood brain barrier is not fully understood [88]. After bypassing the blood brain barrier, ε-toxin binds to multiple brain structures including the hippocampus, thalamus, striatum, olfactory bulb, colliculi and cerebral white matter [81]. In mice, the toxin most notably associates with the cerebellum, however, immunofluorescence of murine brain slices identified that ε-toxin also binds to defined regions of the mouse cerebellar cortex [79][89].

ε-toxin's cytotoxic activity within the brain has been well characterised through a variety of different research studies. This has found that ε-toxin specifically targets and kills myelin forming cells within the CNS and demonstrates particular affinity for oligodendrocytes [88][90]. However, other cell lines including astrocytes, microglia and neurons appear to be insensitive to ε-toxin exposure [88]. Further research identified that ε-toxin is unable to bind to immature oligodendrocytes indicating that changes in gene expression during maturation are required to initiate ε-toxin's binding [88]. Furthermore, the cytotoxic activity of ε-toxin on oligodendrocytes appears to be independent of ε-toxin's pore forming capabilities. Experiments using fluorescently labelled BAPTA1 probes demonstrated that the probes were retained by oligodendrocytes exposed to ε-toxin [91]. This strongly suggests that ε-toxin does not form pores within oligodendrocytes. However, studies have identified that ε-toxin exposure triggers demyelination in oligodendrocytes that occurs in a time and dose dependent manner [88]. This degradation of the myelin sheath that protects axons likely explains many of the neurological symptoms experienced by animals during ε-toxin infections.

However, a number of studies indicate that ε-toxin induces neurological damage by stimulating neurotransmitter release. For example, ε-toxin stimulates dopamine secretion in hippocampal cells, and increases intracellular Ca^{2+} levels

that promote excessive neuronal transmitter firing [81]. *In vitro* examinations also reveal that ε-toxin stimulates glutamate release during oligodendrocyte and granule cell binding [81]. Oligodendrocytes and granule cells are known to regulate glutamate expression. Therefore ε-toxin damage to these cells may correspond to increased glutamate levels by inhibiting regulatory systems [91]. Stimulated glutamate release following ε-toxin exposure leads to seizures and neuronal damage within the hippocampus [79][92]. These data indicate that glutamate is released during direct toxin interactions with granule cells and may contribute to the observed neurological symptoms observed in infected animals [92]. Post-mortem examinations of affected animal brain tissue, note the formation of microscopic and occasionally macroscopic lesions. These brain lesions are associated with the localised killing and demyelination activity of ε-toxin that typically result in the liquefaction of local white matter areas [81][93]. The widespread neurological damage inflicted by ε-toxin results in cerebral swelling and necrosis within infected animals and is believed to be due to multiple factors [73].

Before the use of commercial vaccines against *C. perfringens* Type D, more lambs died from enterotoxemia than all other diseases combined [73][94]. Consequently, significant efforts have been made over the years by the veterinary industry to combat ε-toxin related infections in livestock populations. A number of commercially available vaccines have been developed to protect livestock and are used extensively in veterinary medicine industries around the world [71,95]. These vaccines are produced from formaldehyde-inactivated ε-toxin or *C. perfringens* culture filtrates. The formaldehyde introduces conformational changes within ε-toxin's structure that detoxify the protein. These toxoid vaccines are then filtered to remove the toxic formaldehyde to minute levels that are several hundred times lower than the dose required to cause harm [96]. These formaldehyde vaccines are inexpensive to produce and are used globally in sheep and goat populations. However, the crude design and production of formaldehyde vaccines mean that they are too dangerous for use in humans [95]. Consequently, no ε-toxin vaccines are commercially available for use in humans. Animal vaccination involves two vaccine doses 2-6 weeks apart followed by either an annual or quarterly boosters in sheep and

goats respectively [79][73]. This accounts for the reduced immunoreactivity in goats compared to sheep. The vaccine is injected along with an aluminium hydroxide adjuvant that helps to promote a stronger immune response [79].

While cheap to make and use, formaldehyde vaccines have several reported setbacks. Firstly, the vaccine formulation is rarely pure. Depending on how the vaccine is prepared, it will contain a variety of other bacterial proteins and in the case of culture filtrates it can contain whole bacterial cells [79][97]. The lack of purification means that there is significant batch variability and immunogenic variability between different ε-toxin formaldehyde vaccines. Inflammatory responses have been reported in animals following vaccination that have led to reduced food consumption [79][98]. Conversely, a study of seven ε-toxin formaldehyde vaccines in Brazil identified that only two were sufficiently potent [99]. These data indicate that the formaldehyde method of vaccine production results in considerable immunogenic variability that is unacceptable for reliable immunization. Finally, the formaldehyde used to detoxify proteins is toxic to living organisms and therefore has to be removed by filtration. This introduces potentially unnecessary risks to producing vaccines with this method that could be avoided using other techniques. As a result of these issues, efforts have been concentrated on investigating other alternative techniques of vaccination. One approach is to use site directed mutagenesis (SDM) to produce genetic toxoids of ε-toxin. This produces an attenuated form of the toxin by introducing amino acid substitutions. Two genetic toxoids for ε-toxin have been generated using isoleucine to cysteine mutations [100]. These mutants significantly reduce toxicity in Madin-Darbey Canine Kidney (MDCK) cells by restricting toxin insertion and disrupting toxin oligomersation [73]. However, despite these advancements the development of a reliable vaccine technology for ε-toxin immunization remains one of the biggest challenges facing the veterinary industry.

7.1.5.1 ε-toxin's toxin Production

ε-toxin is synthesised as a 32.9 kDa sized protein during exponential *C. perfringens* growth within the host environment [71]. The toxin contains a leader sequence that facilitates its transport out of the bacterial cytosol into the

extracellular environment [73]. This protein can bind to sensitive cell lines but is unable to oligomerise and therefore fails to elicit cytotoxicity. This first inactive form of ε-toxin requires proteolytic digestion in order to activate its cytotoxic activities [71]. It is therefore referred to as the epsilon prototoxin. Subsequent proteolytic digestion can either be completed by trypsin and chymotrypsin host enzymes or via *C. perfringens* secreted λ protease [71]. Proteolytic activation of ε-toxin requires the removal of both amino and carboxyl terminal residues from the prototoxin. Proteolytic activation removes between 10-13 N-terminal and 22-29 C-terminal residues depending on the protease catalysing the digestion [81] [101]. ε-toxin potency varies depending on which proteases complete the digestion. Maximum ε-toxin potency is achieved through the combined activation of trypsin and chymotrypsin resulting in the loss of 13 N-terminal and 29 C-terminal residues [81][102]. ε-toxin digestion results in the formation of a 28.6 kDa activated mature toxin that is >1000 fold more potent compared to the original prototoxin [101]. Removing the C-terminal residues from the prototoxin facilitates conformational changes that enable ε-toxin to heptamerise on targeted cells and subsequently elicit disease [71]. Recent research has identified a *C. perfringens* Type D strain that uses an intracellular protease to activate ε-toxin, which is subsequently released following autolysis of the bacterial cell [103]. However, the protease responsible for this activity is currently unknown.

After proteolytic activation, ε-toxin acts locally on intestinal epithelial cells. The mechanism of how ε-toxin bypasses the intestinal epithelial layer into the blood stream is not currently understood. Transmission electron microscopy studies of infected mice and rat intestinal epithelial cells revealed that ε-toxin likely increases the permeability of the small intestines by opening mucosal tight junctions [79][104]. The opening of these junctions can induce the accumulation of fluids and macromolecules into the intestinal lumen leading to diarrhoea [81]. This suggests that ε-toxin modulates intestinal permeability to assist its absorption into the bloodstream. Research has also suggested that sialidases produced by *C. perfringens* play a crucial role in initiating ε-toxin disease [81]. Sialidases are known to assist ε-toxin's oligomerisation within the intestinal environment and may help to expose receptors for ε-toxin on the intestinal

epithelial layer [81]. Sialidase activity, which increases when in contact with the trypsin enzyme, also plays an important role in facilitating the initial colonisation of *C. perfringens* in the intestines, by promoting adhesion to host cells [105]. The absorption of ε-toxin in the intestines is not associated with histological or ultrastructural changes to the intestinal epithelium [71]. Furthermore, intestinal lesions are not frequently observed in *C. perfringens* type D enterotoxemia cases [71][104]. This suggests that ε-toxin absorption may exploit the paracellular pathway by passing through intercellular spaces between intestinal epithelial cells to enter the host blood stream [71]. After gaining access to the bloodstream the toxin can then be disseminated across the host where it can elicit disease in a variety of different organs.

Research using a rat model identified that ε-toxin targets endothelial cells and increases vascular permeability following intradermal injection [106]. This appears to be due to direct interactions between ε-toxin and vascular endothelial cells [106]. Further experiments using intravenously injected fluorescently tagged ε-toxin identified that ε-toxin bound to the luminal surface of endothelial cells of most blood vessels [107][108]. Observed necrotic cells within the endothelium following ε-toxin exposure suggests that ε-toxin decreases the integrity of the endothelial cell layer by killing cells rather than exploiting intercellular junctions [106]. The importance of these mechanisms is not understood partly because many-cultured endothelial cell lines are insensitive to ε-toxin exposure. In fact, ε-toxin demonstrates cytotoxicity in a very limited range of cell lines with most research being conducted in MDCK, mpkCCD$_{cl4}$ and human G-402 cell lines [109]. This lack of susceptible cell lines may be because cultured cells do not express the appropriate ε-toxin receptor when grown *in vitro* [71][110].

In recent years, research has focussed on investigating ε-toxin's molecular and cellular mechanisms of action. Research using MDCK cells has identified that ε-toxin monomers bind to host cells using a specific receptor that is currently unknown [71]. The restricted nature of this receptor results in highly localised and concentrated levels of ε-toxin monomers that facilitate this oligomersation process [111]. ε-toxin monomers bind to the outside of the host cell and are not internalised during the intoxication process [112]. The binding of toxin

monomers is accompanied by the formation of a large 155 kDa or 220 kDa complex, whereby the toxin monomers oligomerise into a heptamer on the cell surface [81][112]. This complex inserts into the host cell membrane forming a transmembrane pore that facilitates the passage of molecules up to 1 kDa in size [112]. The formation and activity of the pore are understood to be temperature dependent [73]. Pore formation induces an increase in the host cell's membrane permeability resulting in a rapid decrease in intracellular potassium and an influx in sodium, chloride and calcium ions [71]. Secondary effects of ε-toxin intoxication include cytoskeletal dysfunction followed by mitochondrial breakdown and disruption to cell monolayers [73]. This is characterised by changes in cell morphology including cell swelling and membrane blebbing [71]. Ultimately, the cell undergoes rapid cell death through necrosis. The signalling cascade initiating this response is not understood but may be triggered through adenosine triphosphate depletion or the sudden loss of potassium ions [113]. This intoxication process results in lesion formation that can be observed in the different organs including the kidneys, lungs and brain during ε-toxin disease [81].

The lipid environment of targeted cell membranes appears to play a crucial role in mediating ε-toxin's initial binding to host cells. Research has identified that ε-toxin specifically localises to cholesterol and sphingolipid rich lipid raft microdomains on the cell surface [114][115][116]. This strongly suggests that the currently unknown ε-toxin binding receptor is located on these lipid raft micro domains. Research has shown that both activated and inactivated forms of ε-toxin can bind to these lipid rafts, however, inactivated epsilon prototoxin is unable to form heptamers to initiate pore formation [73]. Cholesterol levels in the lipid rafts are functionally critical in mediating ε-toxin‘s activity, with cholesterol depleted lipid rafts demonstrating an inhibitory effect on ε-toxin's oligomerisation [114]. Research using human kidney adenocarcinoma (ACHN) cells has identified that the Caveolin 1 and 2 proteins appear to promote cytotoxicity by stimulating ε-toxin oligomerisation [117]. ACHN cells devoid of the Caveolin proteins result in significantly reduced ε-toxin oligomerisation [73]. Consequently, this research provides strong evidence to suggest that the lipid composition of host cells appears to play a crucial role in mediating ε-toxin's

receptor access, oligomerisation and pore formation.

ε-toxin's binding specificity for specific cell types suggests that it binds to a particular receptor. *In vivo* ε-toxin preferentially binds to brain and kidney cells, however, cytotoxicity assays on seventeen different human cell lines identified only the G-402 cell lines to be highly susceptible to the toxin [109]. It has been documented that some cell lines sensitive to ε-toxin *in vivo* become insensitive when cultured *in vitro* [82][118]. This is likely due to the changes in receptor expression during *in vitro* cell culturing. This has impeded research aimed at investigating ε-toxin's binding receptor.

Previous research has shown that ε-toxin can oligomerise on membrane vesicles. However, little activity was observed on protein free vesicles suggesting that ε-toxin binds to a protein or glycoprotein based receptor [82]. Recently, research indicated that the hepatitis A virus receptor one (HAVCR1) facilitated ε-toxin binding and cytotoxicity in MDCK cells [119]. HAVCR1 is a class one O-linked membrane glycoprotein that can exist in several isoforms. The 100 kDa variant of HAVCR1 appears to bind to several tyrosine residues (Y29, Y30, Y36 AD Y196) accessible within domain one of ε-toxin to initiate binding [119]. Mutating these tyrosine residues prevented ε-toxin binding and cytotoxicity in MDCK cells [82]. In particular, replacement of Y30 and Y196 residues with alanine generated mutants with significantly reduced cytotoxicity in MDCK cells. A Y30A-Y196A combined mutant demonstrated a 430-fold reduction in cytotoxicity compared to wild type (WT) ε-toxin in MDCK cells [120] The mutant was non-toxic in mice and demonstrated potential for forming the basis of a recombinant vaccine against enterotoxemia in ruminant animals [120]. However, a contrasting study identified that the Y30A-Y196A mutant did not affect ε-toxin binding or toxicity in ACHN cells or CHO cells expressing the MAL protein [73][121]. These data indicate that ε-toxin binds to a secondary receptor, which has been suggested to be the MAL protein. Recently a Beta-octyl glucoside (BOG) molecule was found to bind within domain three of ε-toxin's crystal structure [73]. The BOG molecule bound to a different location to the HAVCR1 binding site and may be a possible binding site for MAL. Other research indicates that several other cell surface proteins are involved in ε-toxin intoxication. However, HAVCR1 is the only protein consistently linked to

increased expression and ε-toxin susceptibility in other cell lines [73]. This therefore suggests that the HAVCR1 protein acts as a receptor or co-receptor for ε-toxin but that ε-toxin possesses other binding receptors to establish cytotoxicity.

In 2013, theoretical modelling, using the National Library of medicine databases, was employed to investigate other potential ε-toxin binding receptors that localise to lipid raft microdomains of endothelial cells and myelin [85]. This revealed the MAL protein that fitted these specific criteria and ε-toxin's activity profile. MAL is a highly hydrophobic tetraspan membrane proteolipid that resides in epithelial cells, oligodendrocytes, Schwann cells and T lymphocytes. In oligodendrocytes and Schwann cells, MAL localises to myelin membranes [122]. Functionally, MAL has been implicated in the formation and stabilisation of lipid rafts and in the formation of immunological synapses [123][124]. The introduction of the *mal* gene has been reported to transform previously insensitive cell lines to cells that demonstrate high sensitivity to ε-toxin exposure. For example, oligodendrocytes expressing the MAL protein are sensitive to ε-toxin while MAL deficient oligodendrocytes are insensitive to ε-toxin exposure [88]. Similarly, Chinese hamster ovary (CHO) cells are naturally resistant to ε-toxin. However, when expressing the MAL protein, these cells become immediately sensitive to ε-toxin [85]. Subsequent research also noted that CHO cells expressing the rat variant of the MAL protein demonstrated 100x greater sensitivity to ε-toxin compared to cells expressing human MAL [85]. These data strongly suggest that the MAL protein is necessary and potentially involved in ε-toxin's cell surface binding, oligomerization and pore forming capabilities.

MAL's structural integrity appears to be critical in establishing protein interactions with ε-toxin. In particular, MAL contains two extracellular loops, ECL1 and ECL2 that appear to be highly important in facilitating MAL's binding activity with ε-toxin [85][125]. Analysis of the primary structure of ECL2 revealed a subtle residue difference between rat and human MAL variants. Human MAL contains a glutamate residue at position 114 whereas rat MAL contained a phenylalanine residue [85]. Glutamate is a highly polar side chain whereas phenylalanine is not. The contrast between these residues may explain the

disparity between ε-toxin's lethality between human and rat species. If MAL is the binding receptor for ε-toxin, then ECL2 is likely to play an essential role in ε-toxin's pathology and cell surface binding capabilities [85].

It is possible that the MAL protein is not a direct binding receptor for ε-toxin but instead forms part of a co-receptor, receptor complex, or acts as a chaperone facilitating the building of a receptor complex without interacting with ε-toxin. Studies have noted that the MAL microenvironment is well suited for ε-toxin's activity [85][126][124]. The MAL protein localises in close proximity and high concentrations within lipid raft microdomains [85]. This could facilitate ε-toxin monomers localising within binding range of each other, thereby favouring direct monomer interactions and oligomerisation. Consequently, the current evidence strongly suggests that MAL is required for ε-toxin's binding activity through direct or possibly indirect protein interactions.

ε-toxin's ability to elicit cytotoxicity in humans is controversial. To date, only two cases of ε-toxin producing *C. perfringens* Type D infections have been medically reported in humans [81][127][128]. Both infections were isolated in agricultural workers in 1955. However, ε-toxin's ability to infect some human cell lines, including the G-402 human kidney cell line, suggests that ε-toxin exposure does pose a genuine risk to human health. In particular, inhalation of ε-toxin may result in pulmonary tissue damage and could facilitate ε-toxin's absorption and subsequent dissemination in the bloodstream [81]. Using data extrapolation, ε-toxin's LD_{50} dose in humans has been estimated at 1 mg/kg via the respiratory route [129]. This has been recognised by multiple government biodefense agencies that consider ε-toxin to pose a realistic biosecurity threat against civilian and livestock populations. Biodefence research has identified that aerosolisation would be required to weaponize purified ε-toxin and disperse it effectively over large areas [130]. This poses a significant barrier to exploiting ε-toxin as a bioterrorism agent, since aerosolisation would require a particle size between 1-3 μM in order to sufficiently establish pathogenicity [130]. However, despite ε-toxin being recognised to pose a security threat, there are still currently no available vaccines that are suitable for use in humans.

ε-toxin brain exposure in animals causes severe white matter damage in

ruminant animals by specifically targeting myelin-forming cells within the CNS to initiate cell death [88]. ε-toxin's demyelination activities in ruminant animals have gained attention from researchers who note similar observations in brain lesions formed in MS [85]. MS is a degenerative neurological disorder that is characterised by the demyelination of nerve cells within the brain and spinal cord of humans. The disease is incurable and is one of the most common CNS disorders in the world affecting an estimated 2.3 million people globally, with varying rates in different countries and populations [131]. The link between MS and ε-toxin is not new, with previous researchers recognizing the localisation of MS cases in areas of highly concentrated sheep populations [132]. This suggested a possible link with a veterinary pathogen. However, the link gained renewed attention in 2012, following the isolation of an ε-toxin producing *C. perfringens* Type B strain in a young woman with enhanced brain lesions clinical manifestations of MS [75]. This marked the first time in medical history that *C. perfringens* Type B had been isolated in humans. The detection of *C. perfringens* in humans is challenging since the bacterium can exist as an endospore that is highly resistant to DNA extraction techniques [75]. However, the authors of the study identified that the woman remained positive for *C. perfringens* Type B eight months later [75].

Mechanistically, ε-toxin's pathology and demyelination activity in animals fits the profile of MS in humans. ε-toxin exposure in animals also results in other MS like symptoms including visual impairment, muscular discoordination and spastic paralysis [71][116]. Subsequent studies have investigated sera from MS patients for immunoreactivity towards ε-toxin. MS sera and cerebrospinal fluid (CSF) obtained from sera banks identified that MS patients demonstrated ten times greater immunoreactivity to ε-toxin compared to healthy controls [75]. ε-toxin immunoreactivity was observed in 10% of MS and 1% of healthy controls [75]. These low percentages may be explained by the difficulty for humans to generate substantial humeral immunity [75]. These results may therefore underestimate the true number of MS patients who have been previously exposed to ε-toxin. Despite this, collectively the data provides a compelling link between ε-toxin exposure and the development of MS. However, further research is required to fully confirm whether ε-toxin is responsible for the

development of MS in humans.

Currently there are two challenges facing researchers who are investigating ε-toxin. The first is lack of a modern toxoid vaccine that can be used to reliably prevent ε-toxin disease in domestic livestock populations. As previously discussed, current formaldehyde based vaccines are crude and suffer several disadvantages that make them unreliable vaccination strategies. There is now an emphasis on producing a genetic toxoid vaccine that would provide a more reliable method of livestock vaccinations against ε-toxin. The second challenge is to elucidate the risk that ε-toxin poses to human health. The recent isolation of an ε-toxin producing *C. perfringens* Type B strain suggests a possible link between ε-toxin and the development of MS in humans. This link needs to be further investigated to confirm the role of ε-toxin in human health. The research conducted in Projects 1 and 2 aim to address both of these challenges by:

1) Investigating the suitability of new mutagenesis targets for the development of a next generation veterinary vaccine against ε-toxin.

2) Investigating MS sera samples for immunoreactivity towards ε-toxin. This data will identify the percentage of MS patients who have been previously exposed to the ε-toxin.

8 PROJECT 1 –E-TOXIN'S TOXIN MUTAGENESIS

8.1 PROJECT OBJECTIVES

C. perfringens ε-toxin vaccines are available for veterinary use. However, current vaccines are based on formaldehyde treated *C. perfringens* cultures or formaldehyde inactivated toxin [133][99]. These imprecise methods suffer from batch variability and immunogenicity issues that make these vaccines unreliable [141][120]. Consequently, efforts are now being directed towards developing a recombinant ε-toxin vaccine based on SDM. Currently, two possible ε-toxin binding receptors have been proposed, HAVCR1 and MAL. Research suggests that residues present on ε-toxin are important for binding to MDCK cells possibly by interacting with a HAVCR1 protein receptor. Mutagenesis of these residues abolishes ε-toxin's toxicity in MDCK cells but does not affect toxicity in CHO-hMAL cells. This indicates that there is a secondary receptor for ε-toxin, which has been suggested to be MAL. Recently, research identified a BOG molecule bound to ε-toxin's crystal structure [121]. It is possible that this BOG binding site is also involved as a binding site for MAL [121].

In order to construct a safe recombinant vaccine for ε-toxin, toxicity has to be abolished in both the MDCK and CHO-hMAL cell lines. Consequently, Project 1 aims to investigate the importance of ε-toxin's BOG binding site for cytotoxicity against CHO-hMAL cells. To achieve this, the role of seven amino acids within the BOG binding site were analysed for their toxicity towards CHO-hMAL cells.

The methods to achieve the objectives of Project 1 are as follows:

1) SDM will be employed to mutate residues within the BOG binding domain of ε-toxin. The proposed mutations are: V72F, V72A, F92A, T93A, V166A, V166F and A168F.

2) Plasmid DNA, encoding individual ε-toxin mutants, will be transformed and overexpressed into the Rosetta DE3 protein expression strain and grown in ZYM-5052 media.

3) Completed protein expression mutants will be purified and extracted

using His and PD10 protein purification columns.

4) ε-toxin mutant protein concentrations, purity and folding patterns will be analysed for each individual mutant.

5) ε-toxin mutants will be tested for cytotoxicity in the CHO-hMAL cell line using the LDH cytotoxicity assay.

8.1.1 Project Hypothesis

Site directed mutagenesis of amino acids within the BOG binding domain will reduce epsilon toxin cytotoxicity to CHO-hMAL cells by reducing epsilon toxin binding.

8.2 MATERIALS AND METHODS

This section contains a detailed account of the different materials and methods used to complete all individual experiments undertaken in Project 1.

8.2.1 Plasmid

The pET-26b(+) vector containing the WT ε-toxin gene was generated in Professor R. Titball's laboratory by M. Bokori-Brown (unpublished). The pET26b(+) plasmid was the only vector used for the ε-toxin mutagenesis study (Addgene plasmid # 69862-3).

8.2.2 Oligonucleotide Primer Design

Mutagenic primers for ε-toxin were designed using the QuikChange Primer Design Program. The pET26b-etxD plasmid FASTA sequence was obtained and nucleotide base changes encoding the required amino acid substitution were selected to produce reverse primers. Reverse primers were reverse complemented to produce the forward primers. Oligonucleotide primers used in Project 1 can be seen in Appendix B.

8.2.3 Site Directed Mutagenesis – Mutant Strand Synthesis Reaction

The primers encoding the ε-toxin mutations were incorporated into the pET26b-etxD plasmid by SDM. The mutagenesis reaction was prepared by mixing the reagents presented in Table 8-1.

Reagent	Volume (µl)
10X Buffer	5
Plasmid (5 ng/µl)	5
Primer One (100 ng/µl)	1.25
Primer Two (100 ng/µl)	1.25
dNTPs	1
QuikSolution Change	1.5
H_2O	34
QuikChange Enzyme	1

Table 8-1 - SDM Reaction Constituents

SDM was completed using the QuikChange Lightning Mutagenesis Kit (Promega) following the corresponding protocol [134]. Briefly, SDM constituents were cooled on ice and mixed together. In all cases the QuikChange enzyme was the last addition to the reaction mixture.

8.2.4 Site Directed Mutagenesis – Mutant Strand DNA Amplification

Polymerase chain reaction (PCR) was used to amplify the mutant plasmid DNA. PCR thermal cycling was completed using the cycles listed in Table 8-2.

Reaction Step	Temperature (°c)	Time (sec)	Cycles
Initial Denaturation	95	120	
Denaturation	95	20	
Primer Annealing	60	10	17
Primer Extension	68	210	
Final Extension	68	300	
Final Hold	10	∞	

Table 8-2 - PCR Conditions.

Mutant plasmid DNA samples were amplified by PCR using a C1000™ Thermo Cycler (BioRad) following the QuikChange Lightning Mutagenesis Kit Protocol [134]. Briefly, DNA samples were denatured at 95°C, primers were annealed to the plasmid template at 60°C and primer extension was completed at 68°C. Completed PCR samples were held at 10°C.

8.2.5 Heat Shock Bacterial Transformation – XL10-Gold Ultra-competent *E.coli*

Mutant plasmid DNA was transformed into XL10-Gold Ultra-competent *E.coli* by heat shock following the QuikChange Lightning Mutagenesis Kit Protocol [134]. Briefly, mutant plasmid DNA was mixed with 2 µl of the *Dpn*I enzyme and incubated at 37°C for five minutes. 45 µl aliquots of XL10-Gold *E.coli* cells were gently thawed on ice, mixed with 2 µl of β-mercaptoethanol and incubated on ice for two minutes. 2 µl of each mutant plasmid DNA sample was added to a separate XL10-Gold *E.coli* aliquot. The DNA samples were incubated on ice for 30 minutes. Samples were heat shocked for 30 seconds at 42°C and immediately returned to ice for two minutes.

Each sample was inoculated with 100 µl of super optimal broth with catabolite repression (SOC) medium and incubated for one hour in an orbital shaking incubator at 37°C, 250 rpm. 100% of each sample was plated on lysogeny broth (LB) agar containing kanamycin (50 µg/ml). Plated samples were incubated

overnight at 37°C and 5% CO_2.

8.2.6 MINI Prep (DNA Purification)

For each mutant sample, three transformed XL10-Gold *E.coli* colonies were inoculated into 5 ml of LB broth containing Kanamycin (50 mg/ml). Bacterial samples were grown overnight in a shaking incubator set at 37°C, 250 rpm before centrifugation at 10,000g for 20 minutes. The Thermo scientific MINI-prep Protocol A was then followed [135]. Briefly, bacterial cells were re-suspended, lysed, neutralised and centrifuged. The supernatant was extracted and the samples washed to purify DNA. DNA was eluted in 30 µl of sterile water. DNA concentrations were quantified using a Thermo Scientific NanoDrop ND-2000C machine. DNA samples were stored at -20°C.

8.2.7 DNA Sequencing and Analysis

Successful mutagenesis was confirmed by DNA sequencing following the Eurofins DNA submission guide. Briefly, plasmid DNA samples were diluted with deionised water to a concentration between 50-100 ng/µL [136]. 15 µL of each mutant DNA sample was pipetted aseptically to separate 1.5 mL micro-centrifuge tubes fitted with safe-lock screw cap seals to prevent evaporation. DNA samples were analysed using Value Read (Eurofins Genomics). Two DNA aliquots were submitted for each mutagenesis sample. One aliquot was analysed using the T7 forward primer, the other was analysed using the T7 Terminal backwards primer.

Sequencing data was analysed using the BioEdit program and compared to a reference plasmid containing the WT ε-toxin gene [137]. T7 Terminal genetic sequences were reverse complemented before sequences were compared using the ClustalW multiple alignment tool. Non-conserved sequences were deleted and sequences checked for successful SDM within the target site.

8.2.8 Bacterial Amplification – *E.coli* Rosetta DE3

Confirmed SDM mutants were transformed into the Rosetta DE3 *E.coli* expression strain by heat shock [138]. Briefly, 10 µl aliquots of Rosetta DE3 were prepared in pre-chilled 1.5 ml Eppendorf tubes for each sample. For each

mutant DNA sample, 10 ng/µl stocks were produced through dilution in deionised water. 1 µL of diluted plasmid DNA was added to a Rosetta DE3 *E.coli* aliquot and incubated on ice for five minutes. Transformation samples were heat shocked at 42°C for 30 seconds before being immediately returned to ice for two minutes.

Transformation samples were inoculated with 90 µl of SOC medium and incubated for one hour in an orbital shaking incubator set at 37°C, 200 rpm. 100% of the transformation sample was plated on LB agar containing kanamycin (50 µg/ml) and chloramphenicol (34 µg/ml). Plated samples were incubated overnight at 37°C, 5% CO_2.

8.2.9 ZYM-5052 Media Preparation

ε-toxin mutant protein expression was maximised using ZYM-5052 autoinducer media. ZYM-5052 media was prepared based on an adaptation of the protocol by Studier et al. [139]. Briefly, 10g of tryptone and 5g of yeast extract were added to 960 ml of deionised water. Following sterilisation by autoclaving, 20 ml of 50x M-solution, 20 ml of 50x "5052" solution, 1 ml of 2 M $MgSO_4$, 200 µl of 1000X trace metals were added to the solution. ZYM-5052 media was stored in a ventilated cold room at 5°C.

8.2.10 Protein Expression in ZYM-5052 Media

ZYM-5052 aliquots were prepared according to the number of transformation samples. Kanamycin (50 µg/ml) and Chloramphenicol (34 µg/ml) were added to the ZYM-5052 aliquot in a $^1/_{1000}$ dilution. 100 ml of ZYM-5052 solution was used for each protein expression sample. $^1/_{10}$ of the total flask volume was filled with ZYM-5052 media to ensure oxygenic conditions. 100 µl of each transformation sample was pipetted aseptically into the ZYM-5052 media. Cells were grown for three hours at 37°C at 300 rpm before further incubation for 24 hours at 20°C at 300 rpm.

Following incubation, cell density was measured using an Ultrospec-10 spectrophotometer (GE Healthcare). Briefly, 100 µl of each sample was mixed with 900 µl of ZYM-5052 media. Experimental optical density (OD) readings

were compared to a blank that contained 1000 µl of ZYM-5052.

Nalgene® 500 ml centrifuge bottles were used for centrifuging each sample. The weight of each bottle was measured and, using a class two safety cabinet, the bacterial solution poured into individual Nalgene® bottles before establishing the solution weight. ZYM-5052 media was added to samples to balance the weight (±1g) for centrifugation completed for ten minutes at 10,000g, 4°C. Using a class two safety cabinet, the supernatants were removed and the pellets allowed to dry. Pellet weights were calculated by subtracting the known weight of the bottle. Bacterial pellets were stored in the Nalgene® bottles at -80°C.

8.2.11 Protein Purification Preparation

Bacterial pellets were mixed with lysis agents to prepare them for protein purification (Table 8-3). The solution was carefully pipetted up and down to detach and suspend bacterial cells into the solution. The solution was incubated on a rocker for twenty minutes at room temperature and centrifuged at 16,000g for twenty minutes at 4°C.

Reagent	Volume (µl)
Bugbuster	5
R-Lysozyme	5
Benzonase Nuclease	1.25

Table 8-3 - Protein Purification Bacterial Lysis Reagents

8.2.12 Protein Purification – HisTrap HP Buffers

A HisTrap HP Column was used to purify the mutant ε-toxin protein. The HisTrap HP column buffers for protein purification were produced in the proportions shown in Table 8-4.

Buffer Type	Imidazole (µl)	Phosphate Buffer (µl)	H_2O (ml)
Binding Buffer	100	1250	8.65
Wash Buffer	300	1250	8.45
Elution Buffer	750	375	1.875

Table 8-4 - Protein Purification HisTrap HP Column Buffers

8.2.13 Protein Purification – HisTrap HP Column

HisTrap HP protein purification was completed following the GE Healthcare protocol [140]. Briefly, the HisTrap HP column tip was removed and excess liquid drained. The column was loaded onto a stand and equilibrated with 10 ml of binding buffer. The prepared sample was added and allowed to pass through the column. The column was washed using 10 ml of prepared wash buffer. Finally, the protein was eluted in 3 ml of elution buffer.

8.2.14 Protein Purification – PD-10 Desalting Column

PD-10 Desalting protein purification was completed following the GE Healthcare gravity protocol [141]. Briefly, the PD-10 column tip was removed, and excess liquid drained. The column was equilibrated with 25 ml of phosphate buffer saline (PBS). Following equilibration, 2.5 ml of the protein sample was added. Finally, the protein was eluted in 3.5 ml of PBS buffer, transferred into 500 µl aliquots and stored at -20°C.

8.2.15 Protein Analysis

8.2.15.1 NanoDrop

ε-toxin mutant concentrations were quantified using a Thermo Scientific NanoDrop ND-2000C machine. Briefly, the NanoDrop machine was calibrated using 2 µl of deionised H_2O. Using the A280 program, the NanoDrop machine was blanked with PBS before 2 µl of experimental sample was analysed for

protein concentration.

8.2.15.2 SDS-PAGE Analysis

The molecular weight and purity of ε-toxin mutants were analysed by Sodium Dodecyl Sulphate Polyacrylamide Gel Electrophoresis (SDS–PAGE). ε-toxin mutants were boiled for ten minutes on a heat block, pulsed for two minutes in a micro-centrifuge at full speed and mixed with 10 µL of 4x LDS loading buffer solution. A precast twelve well NU-PAGE 4-12% Bis-Tris gel (ThermoFisher Scientific) was washed with deionised water before loading into the SDS-PAGE chamber. Using 1x MES solution, the central chamber was fully filled with outer chambers being half filled.

5 µl of Perfect Protein Marker 10-225kD ladder (Merck) was loaded onto the NU-PAGE gel alongside 10 µl of each protein sample. The gel electrophoresis was run for 45 minutes at 180V, 400mA. Following electrophoresis, the gel was removed and washed with deionised water. Gel staining was completed by submerging the gel in SimplyBlue SafeStain (ThermoFisher Scientific) and microwaving for 30 seconds. The gel was incubated on a rocker at room temperature for one hour. The SimplyBlue SafeStain was removed and the gel submerged in deionised water. The gel was incubated overnight at room temperature on a rocker. Imaging was completed using the ChemiDoc™ XRS system Epiwhite mode and ImageLab™ software (BioRad).

8.2.15.3 Mass Spectrometry

ε-toxin mutagenesis and sample purity was analysed using Liquid Chromatography Mass Spectrometry (LCMS). One aliquot for each ε-toxin mutant was standardised to a concentration of 1 mg/ml. From this 50 µl (50 µg) samples were pipetted aseptically into 2 ml screw cap tubes with an O-ring to prevent sample loss by evaporation. Samples were sent on dry ice to the University of Bristol Proteomics Facility for LCMS analysis. Each sample was trypsin digested before separation by high performance liquid chromatography and spectroscopy analysis. Protein samples were ionised and the protein mass identified through mass spectrometry. Digested peptides for each mutagenesis sample were compared and scored according to their spectral match with

digested Etx-YY peptides. Peptide spectra match (PSM) scores were analysed between cut-off percentage confidence limits (identified at >1% False Discovery Rate, <5% False Discovery rate). This ensured a 95% confidence level in the mass spectrometry peptide analysis. For non-contaminated samples, the total PSM score for every peptide was calculated. In contaminated samples, the peptides were screened for the presence of the expected mutation and screened again for the contaminant. The PSMs for each peptide matching with the expected mutant and contaminant were calculated.

8.2.16 CHO-hMAL Resuscitation

Frozen 1 ml CHO-hMAL cell samples, stored in cryovials at -80˚C, were resuscitated in a water bath at 37˚C. Cryovials were thawed by gentle agitation at 37˚C until no ice crystals were present in the sample. The O-ring and cryovial cap were kept out of the water to reduce the risk of contamination. Cell thawing was completed quickly to reduce dimethyl sulfoxide (DMSO) toxicity to CHO-hMAL cells.

Once fully thawed, the cryovials were decontaminated using 70% ethanol. Working in a class two biological safety cabinet, the 1 ml CHO-hMAL sample was transferred into a 15 ml Falcon tube. 10 ml of pre-warmed Dulbecco's Modified Eagle Medium (DMEM) containing 10% Fetal Bovine Serum (FBS) was added to the CHO-hMAL cell suspension in the 15 ml Falcon tube. The CHO-hMAL cell solution was transferred to a T25 flask and incubated overnight at 37˚C, 5% CO_2. The cell medium was replaced with fresh DMEM 10% FBS the following day to remove all DMSO. CHO-hMAL cells were grown to 90% confluency in the T25 before transferral to a T75 flask.

8.2.17 CHO-hMAL Cell Culturing (T25 Flask)

CHO-hMAL cells were viewed for confluency using an inverted light microscope. T25 flasks <90% confluent were returned for incubation at 37˚C, 5% CO_2.

T25 flasks that demonstrated ~90% confluency were prepared for cell splitting. Working in a class two biological safety cabinet, cell media was removed and

the flask was washed twice with 5 ml of PBS. To detach the CHO-hMAL cells, 1 ml of heat inactivated trypsin was added and the flask incubated at 37˚C, 5% CO_2 for two minutes. After detachment, cells were diluted in 4 ml of DMEM and mixed thoroughly to separate CHO-hMAL aggregates. The full contents were transferred to a T75 flask along with 10 ml of DMEM. T75 flasks were incubated at 37˚C, 5% CO_2 until 90% confluent.

8.2.18 CHO-hMAL Cell Culturing (T75 Flask)

CHO-hMAL cells were viewed for confluency under an inverted light microscope. T75 flasks <90% confluent were returned for incubation at 37˚C, 5% CO_2.

T75 flasks that demonstrated ~90% confluency were prepared for culturing. Working in a class two biological safety cabinet cell media was removed and the flask was washed twice with 10 ml of PBS. To detach the CHO-hMAL cells from the flask, 3 ml of heat inactivated trypsin was added and the flask incubated at 37˚C, 5% CO_2 for ten minutes. After detachment, the cells were diluted in 7 ml of DMEM and mixed thoroughly to separate CHO-hMAL aggregates. The full contents were transferred to a 15 ml Falcon tube. Using this cell solution, T75 flasks were set up for future experiments. 3 ml of cell solution was added to T75 flasks for next day experiments, 1.5 ml used for mid-week experiments and 0.5 ml for end of week experiments. These cell solutions were filled to 15 ml with DMEM 10% FBS. Completed flasks were incubated at 37˚C, 5% CO_2 until confluency reached 90%.

8.2.19 CHO-hMAL Cell Culturing - Assay Preparation

CHO-hMAL cells were viewed for confluency using an inverted light microscope. T75 flasks <90% confluent were returned for incubation at 37˚C, 5% CO_2 and checked.

T75 flasks that demonstrated ~90% confluency were prepared for culturing. Working in a class two biological safety cabinet, cell media was removed and the T75 flask was washed twice with 10 ml of PBS. To detach the CHO-hMAL cells, 3 ml of heat inactivated trypsin was added and the flask incubated at

37˚C, 5% CO_2 for ten minutes. Detached cells were diluted in 7 ml of DMEM and mixed thoroughly to separate CHO-hMAL aggregates. The full contents were transferred to a 15 ml Falcon tube. In a 1.5 ml Eppendorf, a $^1/_{10}$ cell dilution was produced by mixing 800 µl of DMEM, 100 µl of CHO-hMAL cell suspension and 100 µl of 0.4% Tryphan Blue (Sigma-Aldrich). 20 µl of the $^1/_{10}$ cell dilution was pipetted onto a haemocytometer for cell counting and viewed using an inverted light microscope. Cells stained by the Tryphan Blue were excluded from the cell count.

Cell suspension and DMEM volumes required to produce the CHO-hMAL seeding density of $3x10^6$ cells/ml was identified using the haemocytometer cell count. A 10 ml aliquot of CHO-hMAL cell solution at the seeding density of $0.3x10^6$ cells/ml was produced in a 15 ml Falcon tube. Using a pipette, 100 µL of CHO-hMAL cells at seeding density were pipetted into wells on a 96 well plate. Completed 96-well plates were incubated overnight at 37°C, 5% CO_2. 96-well plates were inspected before beginning experimentation.

8.2.20 Cytotoxicity Assay - ε-toxin Mutants

Following the manufacturer's instructions, a CytoTox96® Non-Radioactive LDH Cytotoxicity Assay (Promega) was used, to analyse ε-toxin mutant cytotoxicity against CHO-hMAL cells. Briefly, WT ε-toxin concentration (mg/ml) was identified using a NanoDrop 1000 (BioRad) and converted to molar concentration using the equation in Equation 1.

$$Convert \frac{mg}{mL} to\ uM = \frac{Concentration}{Molecular\ Weight}\ x10^6$$

Equation 1 - Concentration conversion (mg/ml to molar concentration).

ε-toxin mutants were diluted to a starting concentration of 0.2 mg/ml using PBS. 10 µl of the inactivated ε-toxin was pipetted into a 1.5 ml Eppendorf and mixed with 10 µl of 4xLDS buffer for SDS PAGE analysis (Section 8.2.15.2). A $^1/_{100}$ volume of 0.2 mg/ml trypsin solution was used to activate ε-toxin. This solution was incubated at room temperature for 30 minutes to ensure complete toxin activation. 10 µl of trypsin-activated ε-toxin was pipetted into a 1.5 ml Eppendorf and mixed with 10 µl of 4xLDS Buffer for SDS PAGE analysis (Section

8.2.15.2). Using a 96-well V-bottomed plate, activated ε-toxin mutants were diluted in PBS through a two-fold dilution.

Using a previously seeded 96 well plate, old cell media was replaced with 80 µl of pre-warmed DMEM. 20 µl of each two-fold dilution containing activated ε-toxin was transferred to respective wells on the seeded plate. 20 µl of the control samples were each added to three seeded control wells (Table 8-5). The 96-well plate was incubated at 37°C, 5% CO_2 for three hours. Following incubation, 50 µl of cell culture medium was transferred from each well to a fresh 96-well plate and mixed with 50 µL of reconstitution substrate mix. Following a 30 minute incubation in the dark at room temperature, the wells were mixed with 50 µl of stop solution and cytotoxicity measured at 490 nm using a microplate reader (BioRad). The mean PBS negative control was subtracted from all experimental values and data analysed for neutralisation activity and the cytotoxic 50% dose calculated using non-linear regression analysis. The cytotoxic 50% dose was calculated using non-linear regression analysis.

WT ε-toxin Cytotoxicity LDH Assay Controls	Control Type
PBS	Negative
0.1X Triton X	Positive

Table 8-5 - Experimental controls employed for the LDH Assay investigating Wild Type ε-toxin Cytotoxicity to CHO-hMAL cells.

8.2.21 Cytotoxicity Assay - ε-toxin Mutant CT_{50} Calculation

Following the LDH Cytotoxicity Assay (described in 8.2.20), the CT_{50} dose of the ε-toxin site directed mutants was compared to the Etx-YY background CT_{50}. Using Graphpad Prism 7, the CT_{50} values of each of the SDM samples was divided by the CT_{50} of the Etx-YY background to illustrate the fold difference in CT_{50}.

8.3 RESULTS

This section describes the results obtained from all experiments completed in Project 1.

8.3.1 Amino Acid Mutagenesis Selection

The work in Project 1 aims to investigate the mutagenesis of seven critical residues within the BOG binding domain and their effects towards ε-toxin's toxicity against CHO-hMAL cells. The introduced mutations were V72A, V72F, F92A, T93A, V166A, V166F and A168F. These residues were chosen since they were previously shown to bind to the BOG ligand (Figure 8-1) [121]. Mutagenesis was completed using a variant form of ε-toxin containing the Y43A-Y209A mutations within the HAVCR1 binding domain (Figure 8-1). This form of ε-toxin, referred to as Etx-YY, was used as the DNA template for mutagenesis and retained full cytotoxic activity against CHO cells expressing human MAL.

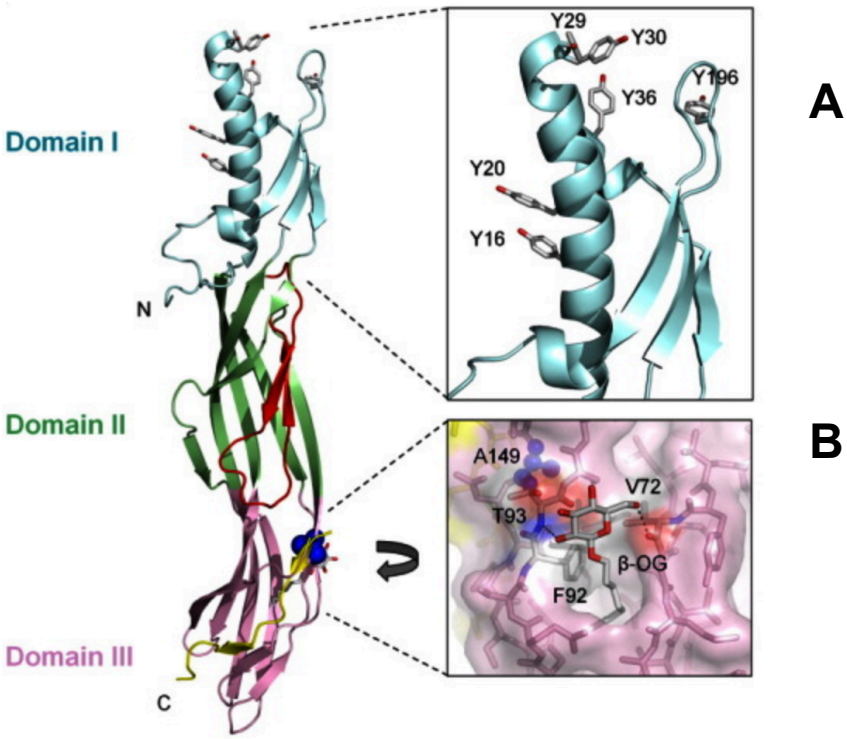

Figure 8-1 - The three domain protein crystal structure of the *Clostridium perfringens* epsilon prototoxin [121]**. The figure illustrates the putative membrane insertion loop of domain II in red. (A) Illustrates previously mutated residues in domain I. Of these the Y43A and Y209A were shown to markedly reduce binding to MDCK cells. (B) Illustrates residues within domain III involved in the co-ordination of a single BOG molecule. Amino acid numbering excludes the 13 N-terminal peptide sequence.**

8.3.2 Bacterial Transformation – DNA Sequencing

Following bacterial transformation, successful mutagenesis was confirmed by nucleotide sequencing. The ε-toxin mutant plasmids were subsequently referred to by their respective mutations (V72A, V72F, F92A, T93A, V166A, V166F and A168F). ε-toxin SDM targets can be seen in Figure 8-2.

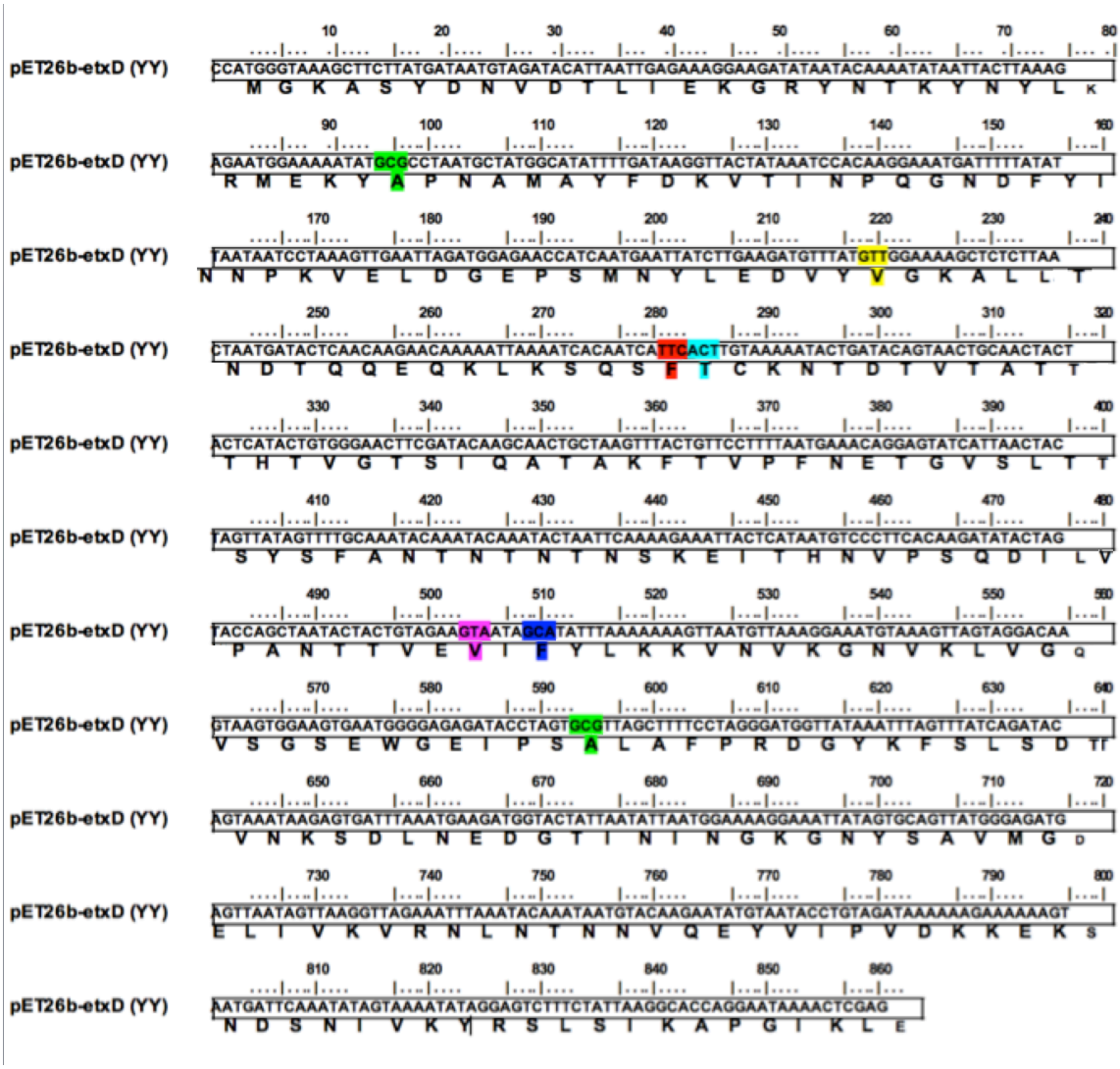

Mutation Positions:

Green	=	Etx-YY mutations
Yellow	=	V72A and V72F mutations
Red	=	F92A mutation
Turquoise	=	T93A mutation
Lilac	=	V166A and V166F mutations
Blue	=	A168F mutation

Figure 8-2 - DNA and amino acid sequences of V72A, V72F, F92A, T93A, V166A, V166F and A168F ε-toxin mutants introduced into the Etx-YY background. Individual V72A, V72F, F92A, T93A, V166A, V166F and A168F amino acid substitutions introduced into the Etx-YY background by SDM

were confirmed by nucleotide sequencing the mutated etx gene. Completed nucleotide sequences for all seven mutagenesis samples as presented in Appendix A.

8.3.3 Protein Purification – Protein Concentrations

ε-toxin mutant concentrations ranged from 1.29 mg/ml to 2.61 mg/ml with a mean concentration of 1.86 mg/ml (Figure 8-3). All seven mutants demonstrated lower protein concentrations compared to the Etx-YY concentration of 2.82 mg/ml.

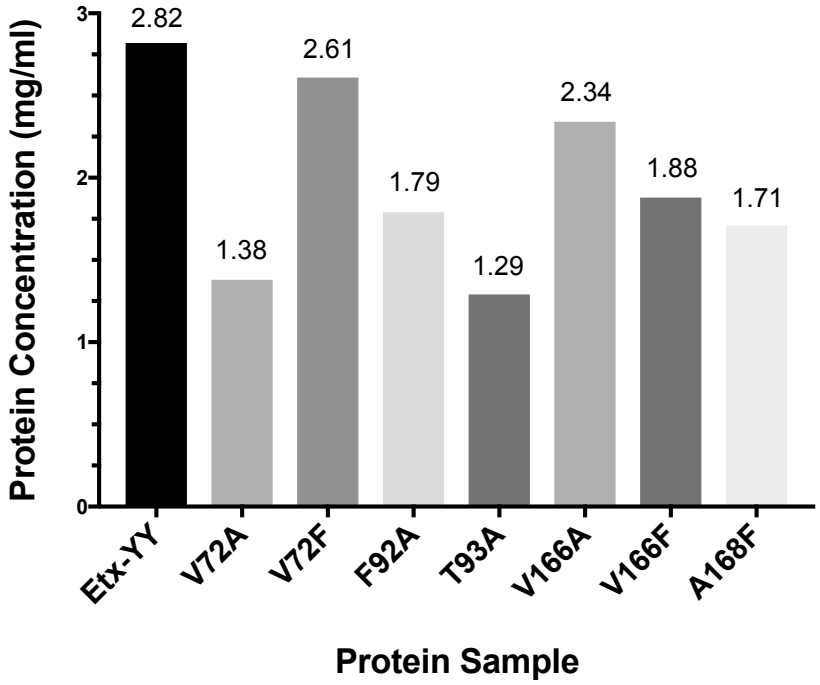

Figure 8-3 - Concentrations of ε-toxin mutants. Mutant proteins were expressed in *E.coli*, purified using nickel affinity and PD10 column chromatography and concentrations measured using a NanoDrop spectrophotometer at 280nm. Results shown were taken from a single measurement expressed as mg/ml.

8.3.4 Protein Purification – SDS PAGE protein purity analysis

ε-toxin mutant purity was analysed by SDS-PAGE, which revealed that a single protein band was present for each of the ε-toxin mutant samples (Figure 8-4). The protein bands of all seven mutants correspond to the 35 kDa marker on the protein ladder (10-225 kDa).

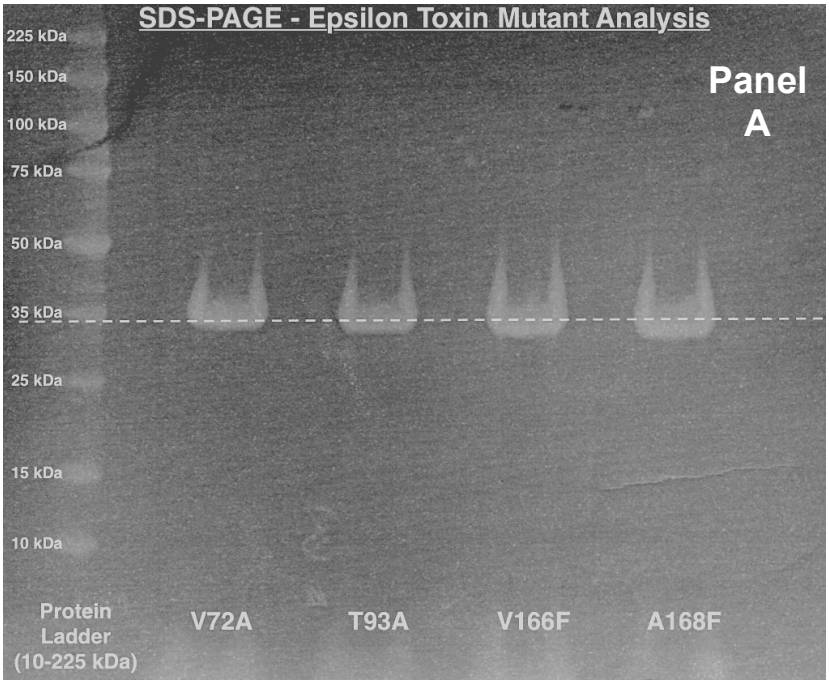

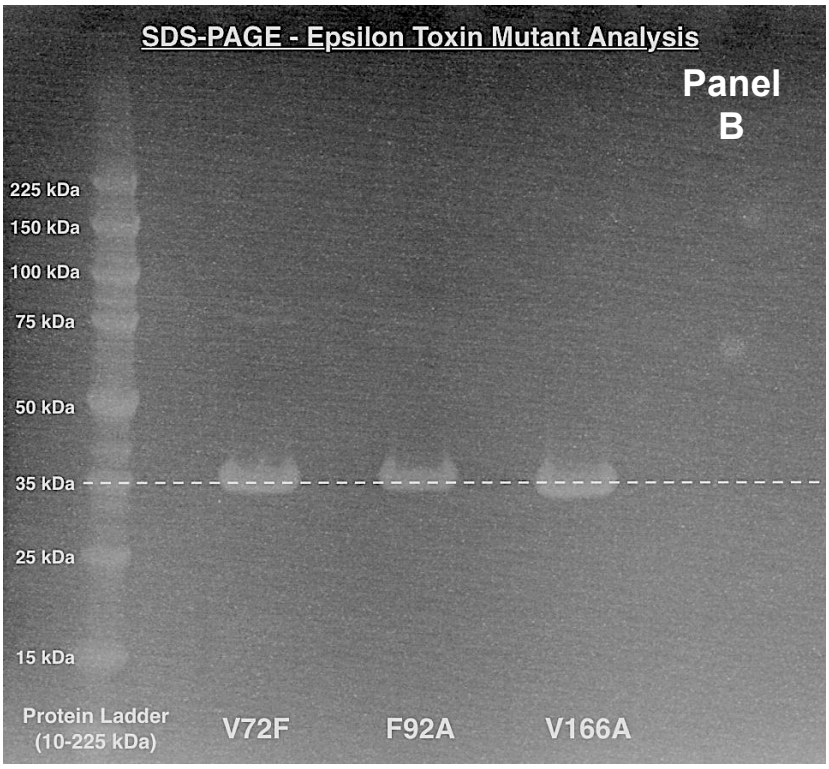

Figure 8-4 - SDS-PAGE analysis of ε-toxin mutants with SimplyBlue gel staining. Mutant proteins were subject to electrophoresis on a 4-12%SDS-PAGE following boiling and centrifugation treatment. Imaging was completed using Chemidoc™ Epiwhite mode. (A) shows V72A, T93A, V166F and A168F mutant samples compared to a 10-225 kDa protein ladder. (B) shows V72F, F92A and V166A mutant samples compared to a 10-225 kDa protein ladder.

8.3.5 LDH Assay – ε-toxin Mutant CHO-hMAL Cytotoxicity

ε-toxin mutant cytotoxicity against CHO-hMAL cells was investigated using an LDH assay through a two-fold dilution. OD readings of LDH release correlate to the cytotoxicity profile for each ε-toxin mutant and were compared to the Etx-YY background (Figure 8-5). V72A and T93A mutants retained full CHO-hMAL cytotoxicity for five dilutions and exhibited similar cytotoxicity profiles to the Etx-YY background. The F92A and V166A mutants demonstrated reduced CHO-hMAL cytotoxicity compared to the Etx-YY background but retained cytotoxicity at higher concentrations between 0.5 and 1 mg/ml. The V72F, V166F and A168F mutants abolished CHO-hMAL cytotoxicity at all concentration ranges compared to the Etx-YY background.

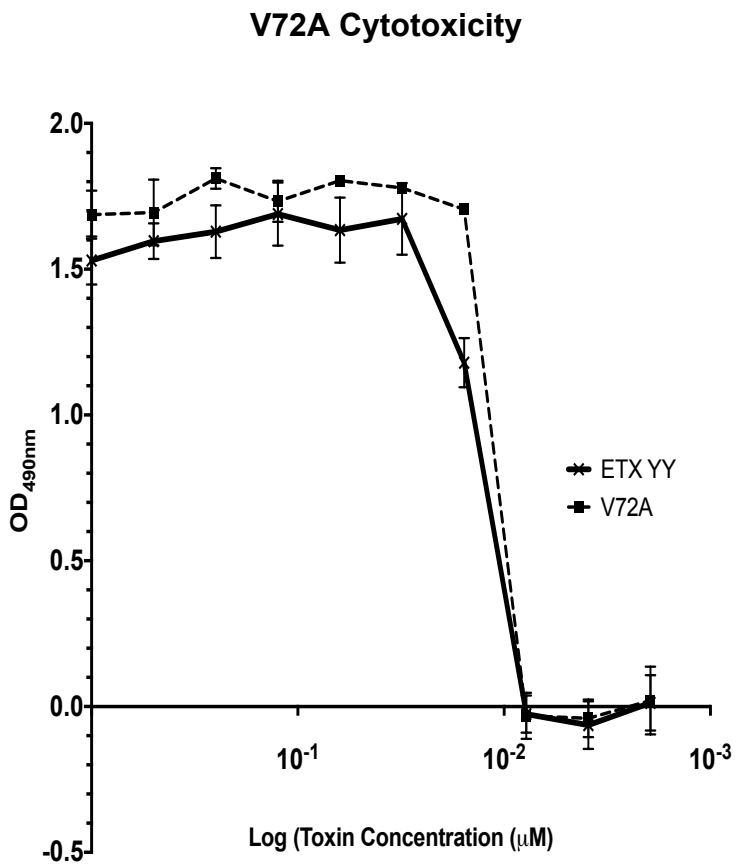

V72F Cytotoxicity

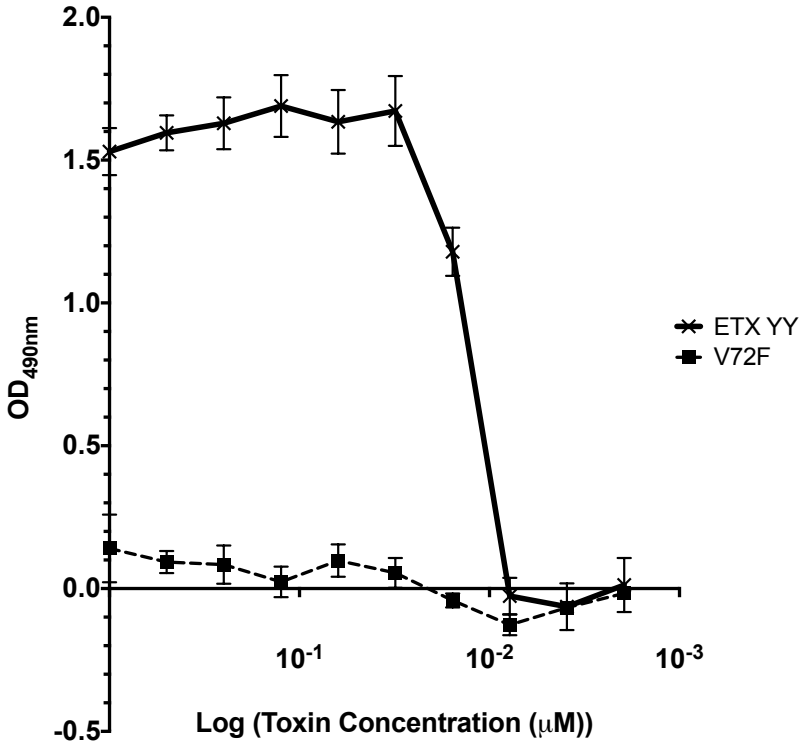

F92A Cytotoxicity

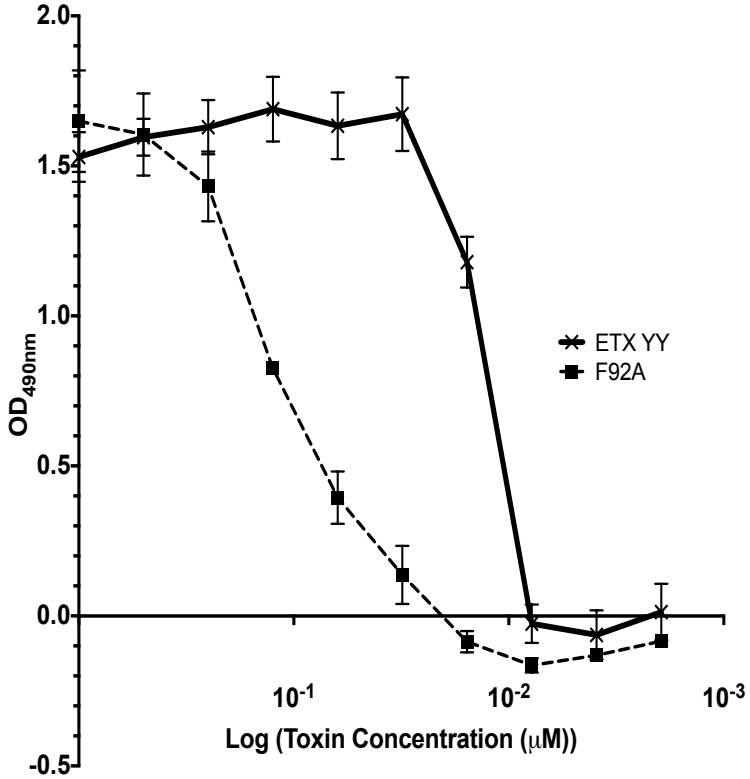

T93A Cytotoxicity

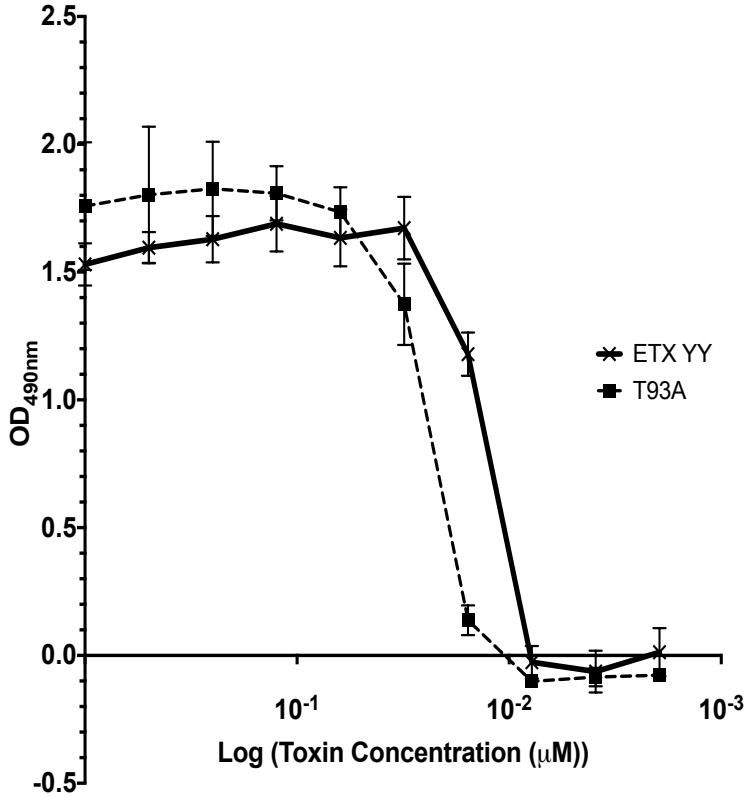

V166A Cytotoxicity

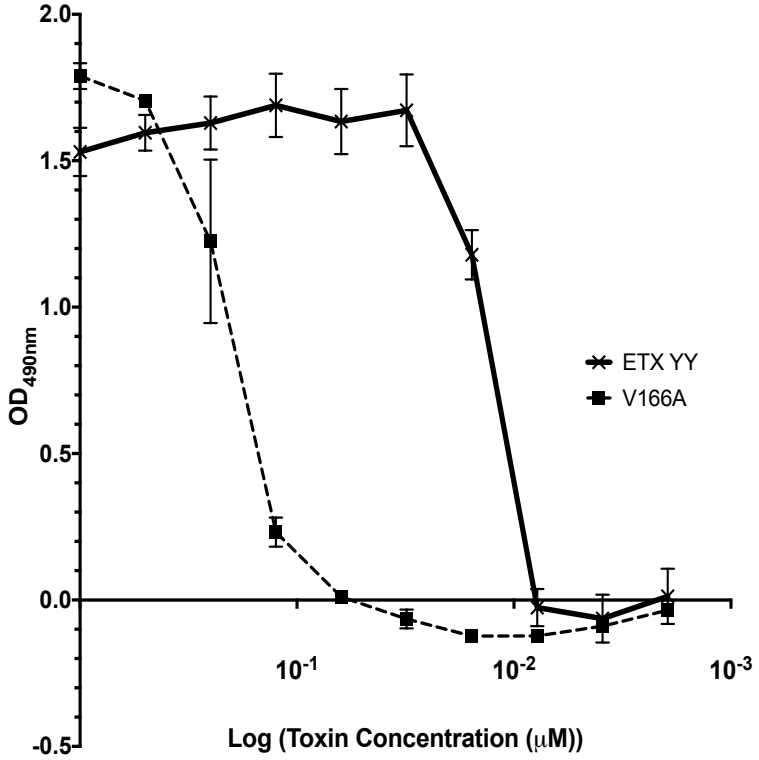

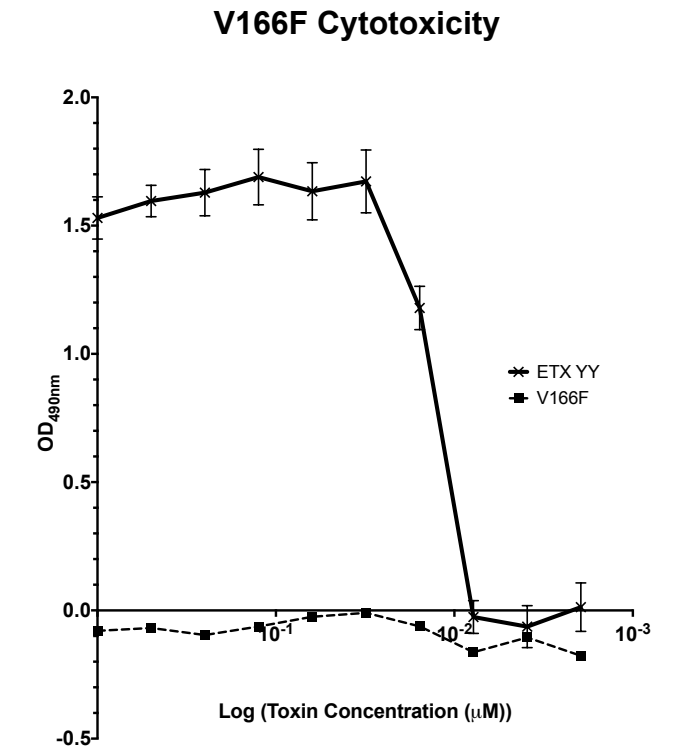

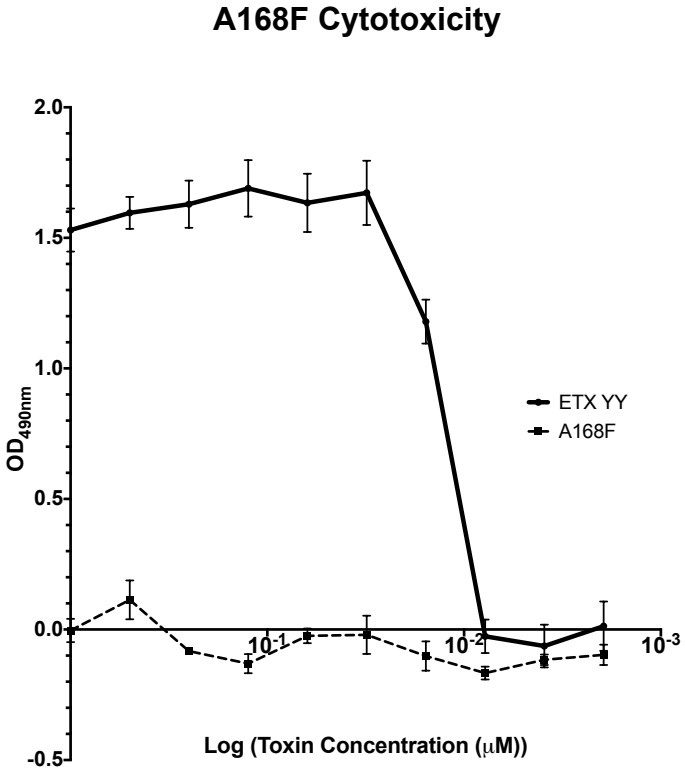

Figure 8-5 - Cytotoxicity analysis of ε-toxin mutants compared to Etx-YY. Mutant proteins and Etx-YY were diluted through a two-fold dilution starting at a concentration of 0.2 mg/ml. The figure illustrates the optical density measuring mean LDH release from CHO-hMAL cells incubated with Etx-YY or ε-toxin mutant. Results shown are from two replicates

measured at OD_{490nm}. The error bars represent the standard error of the mean.

8.3.6 LDH Assay - ε-toxin Mutant CHO-hMAL CT_{50}

The ε-toxin mutant CT_{50} concentrations against CHO-hMAL cells were determined using the LDH assay data in Figure 8-5 and are listed in Table 8-6 along with their respective 95% confidence intervals.

ε-toxin mutant	CT_{50} concentration (mg/ml)	95% Confidence Intervals
V72A	$5.9x10^{-3}$	$\pm 2.1x10^{-3}$
V72F	>0.2	N/A
F92A	$18.6\ x10^{-3}$	$\pm 6.7x10^{-3}$
T93A	$6.3\ x10^{-3}$	$\pm 2.3x10^{-3}$
V166A	$44.5\ x10^{-3}$	$\pm 15.9x10^{-3}$
V166F	>0.2	N/A
A168F	>0.2	N/A
Etx-YY	$2.9x10^{-3}$	$\pm 1.0\ x10^{-3}$

Table 8-6 - ε-toxin mutant CT_{50} concentration against CHO-hMAL cells

Figure 8-6 illustrates the fold difference of the ε-toxin mutant CT_{50} concentrations compared to the Etx-YY CT_{50}. The V72A and T93A mutants exhibited a two-fold CT_{50} reduction in CHO-hMAL cytotoxicity. The F92A and V166A mutants showed a 6.4 and 15.3 fold CT_{50} reduction against CHO-hMAL cells respectively. The V72F, V166F and A168F mutants abolished cytotoxicity at all assay concentrations up to 0.2 mg/ml (Figure 8-5). Consequently, the CT_{50} concentrations for these samples exceed a 68.8 fold attenuation compared to the Etx-YY background.

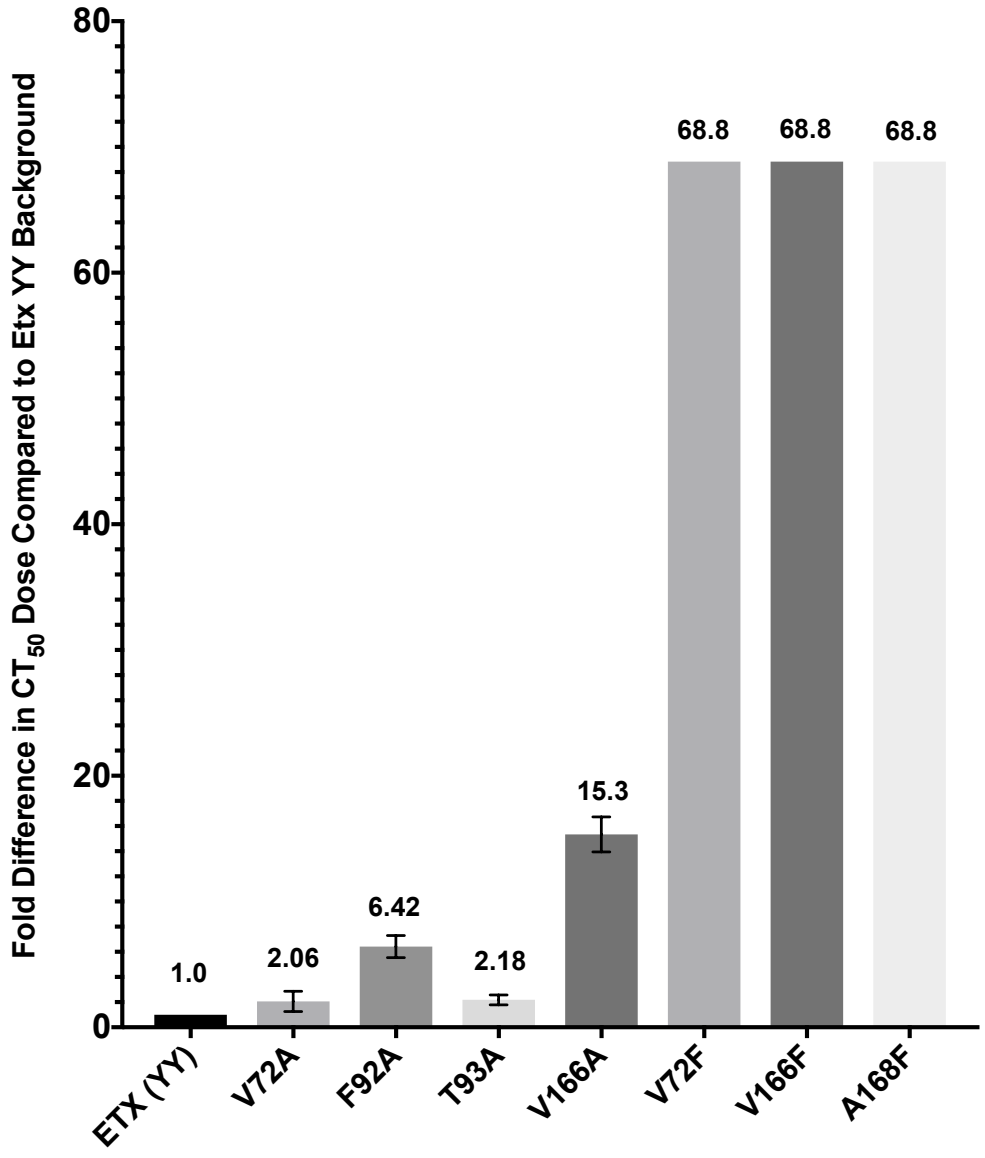

Figure 8-6 - Comparing the CT_{50} concentration differences between Etx-YY and the individual ε-toxin mutants. The fold difference was calculated by divided individual mutant CT_{50} concentrations by the Etx-YY CT_{50} concentration. Results shown were taken from two replicates. The error bars represent the standard error of the mean.

8.3.7 Protein Purification – Mass Spectrometry analysis

LCMS was employed to confirm successful ε-toxin mutagenesis and sample purity (Figure 8-7**)**. The V72F, F92A, T93A and A168F samples demonstrated zero PSMs for the Etx-YY background and PSM scores of 61, 836, 655 and 871 for their respective mutations. These data confirmed the successful mutagenesis and purity of these samples.

The V72A and V166A samples demonstrated respective PSM scores of ten and three for the Etx-YY background and scores of 112 and 36 for their respective mutations. These data confirmed the successful mutagenesis of these samples but revealed that they were contaminated with the Etx-YY background.

The V166F sample demonstrated zero PSMs for the Etx-YY background and PSM scores of 29 for the V166F mutation and two for the A168F mutation. These data confirmed successful V166F mutagenesis but revealed that the sample was contaminated with the A168F sample.

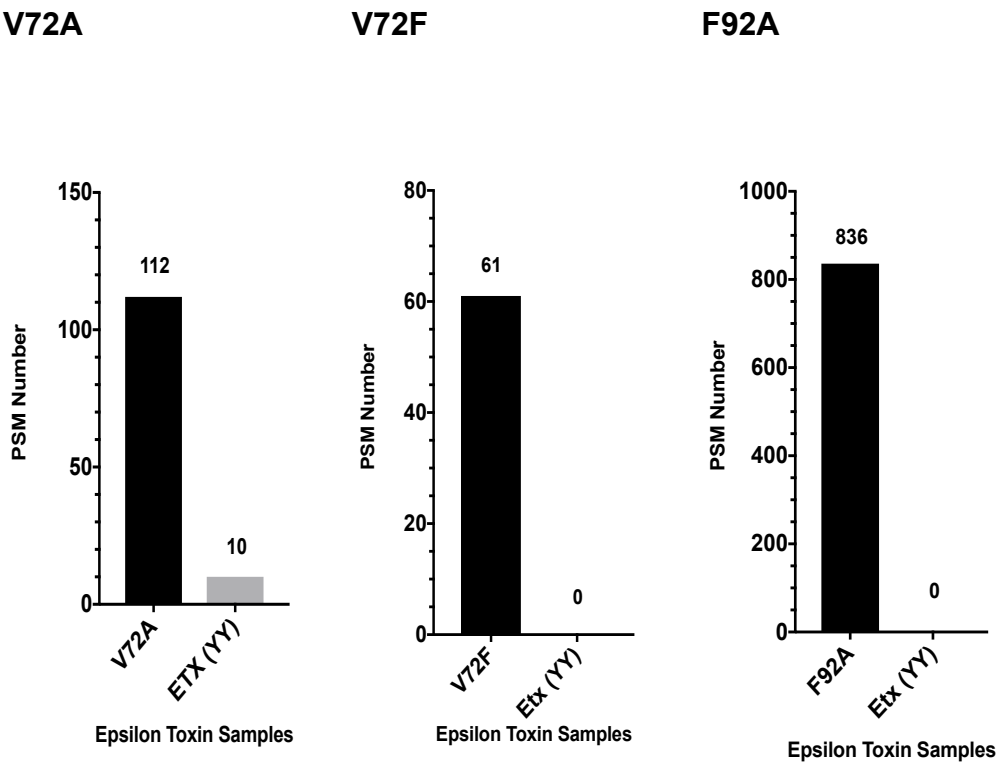

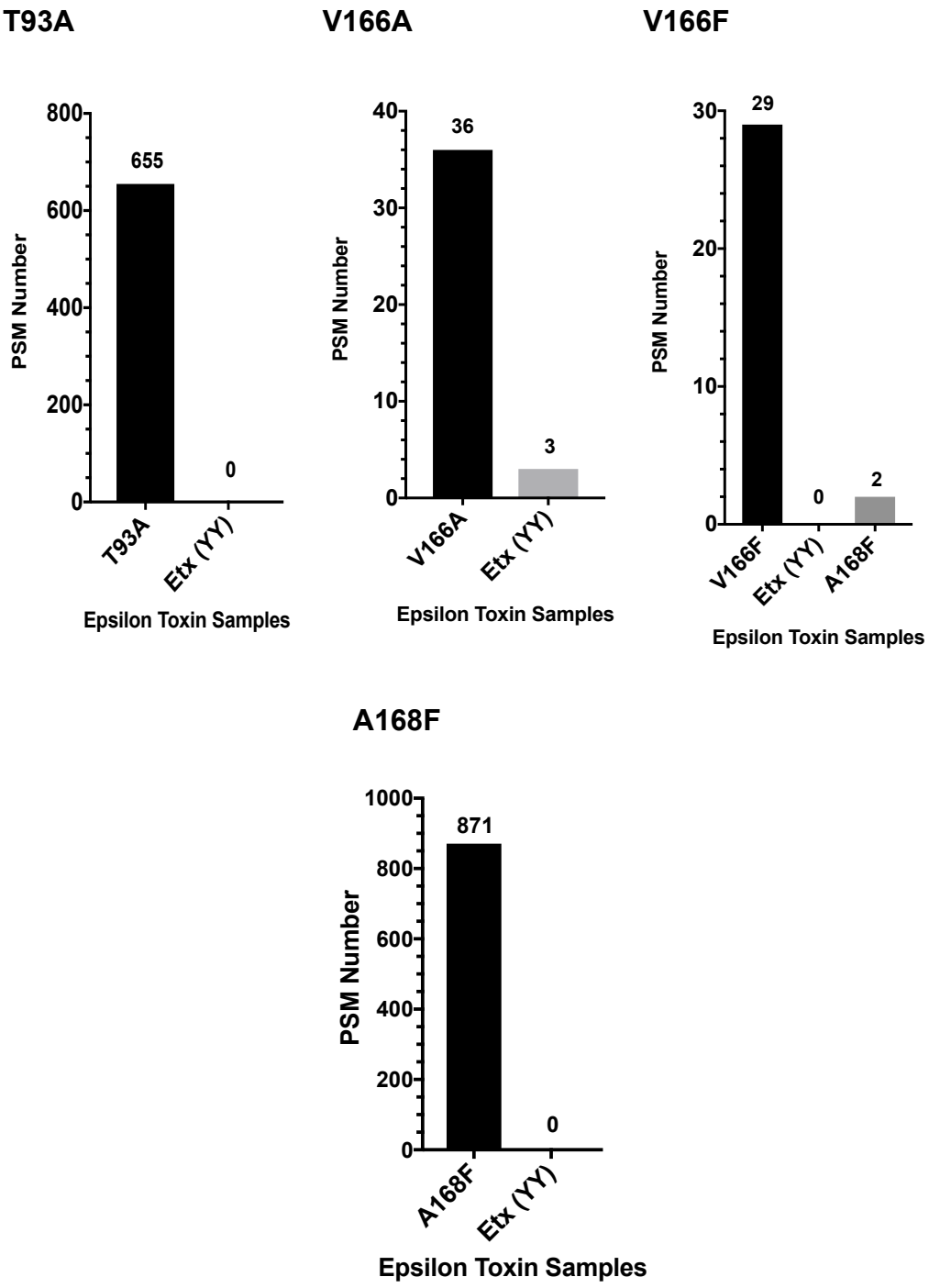

Figure 8-7 - Mass spectrometry analysis of ε-toxin mutants. Results show the total PSM number for proteins present in each ε-toxin mutant sample. The PSM number equates to the total number of peptides matched to each protein. The mass spectrometry analysis was completed by the University of Bristol Proteomics Group. Results shown were taken from a single measurement.

8.3.8 Mass Spectrometry – V72A and V166A Contamination Analysis

Etx-YY contamination was analysed by investigating if the Etx-YY contaminant present in the V72A and V166A samples was sufficiently concentrated to interfere with cytotoxicity data (Section-8.3.5). To do this, the Etx-YY concentration present in the 0.2 mg/ml V72A and V166A cytotoxicity assay samples was estimated using the percentage Etx-YY PSM scores in Table 8-7. The number of two fold dilutions required to dilute the Etx-YY contaminant concentration to its CT_{50} concentration was then compared to the number of two fold dilutions required to obtain the CT_{50} of the contaminated samples (Equation 2) and (Table 8-8).

Epsilon Toxin Mutant	Etx-YY PSM Percentage	Etx-YY Concentration in 0.2 mg/ml Cytotoxicity Assay
V72A	8.9%	$17.8x10^{-3}$ mg/ml
V166A	7.6%	$15.2x10^{-3}$ mg/ml.

Table 8-7 - Illustrates the relative percentage Etx-YY PSM scores and concentrations present in the 0.2 mg/ml cytotoxicity assay starting concentrations for the contaminated V72A and V166A samples

Initial equation…

$$\frac{EtxYY\ Contaminant\ Concentration}{2^x} = EtxYY\ CT50$$

Where x = Number of two fold dilutions

Therefore for V72A…

$$\frac{0.0178}{2^x} = 0.0029$$

Thus…

$$x = \frac{Log(6.14)}{Log(2)} = 2.62$$

Therefore for V166A…

$$\frac{0.0152}{2^x} = 0.0029$$

Thus…

$$x = \frac{Log(5.24)}{Log(2)} = 2.29$$

Equation 2 - Number of two fold dilutions required to dilute Etx-YY contaminant concentration to the V72A and V166A CT_{50} concentrations.

Epsilon Toxin Mutant	CT_{50} – Two Fold Dilutions	Etx-YY Contaminant CT_{50} Two Fold Dilutions in 0.2 mg/ml Cytotoxicity Assay
V72A	6.11	2.62
V166A	2.17	2.29

Table 8-8 - Illustrates the number of two fold dilutions required to obtain the CT_{50} concentration of the V72A and V166A samples and the Etx-YY contamination present in the 0.2 mg/ml starting concentration of the V72A and V166A samples.

V72A and V166A PSM analysis revealed that 8.9% and 7.6% of the sample composed of the Etx-YY contaminant respectively. This equates to a respective $17.8x10^{-3}$ mg/ml and $15.2x10^{-3}$ mg/ml Etx-YY concentration present in the 0.2 mg/ml starting concentration of the V72A and V166A cytotoxicity assay samples (Table 8-7). Dilution analysis using Equation 2 revealed that 2.62 and 2.29 two-fold dilutions were required to dilute the V72A and V166A Etx-YY contamination to the Etx-YY CT_{50} concentration respectively. Table 8-8 shows that the number of two-fold dilations required to obtain the V166A CT_{50} compares closely to the number of dilutions required to obtain the Etx-YY contaminant CT_{50} concentration. However, the number of two-fold dilations required to obtain the V72A CT_{50} does not compare closely to the number of dilutions required to obtain the Etx-YY contaminant CT_{50} concentration (Table 8-8).

8.4 DISCUSSION

NanoDrop protein analysis revealed that the purified ε-toxin mutant concentrations were greater than the WT ε-toxin CT_{50} (Section 9.3.1). ε-toxin mutant concentrations were generally consistent suggesting that the HisTrap HP and PD-10 were reliable protein purification methods (Figure 8-3). However, protein concentrations were obtained from single NanoDrop measurements only. Consequently, there is a risk that small molecular sample contaminants, including nucleic acids and lipoproteins, could have influenced the A280 absorption readings [142]. This would culminate in inaccurate protein concentration results. ε-toxin mutant concentrations shown in Figure 8-3 could be validated using a secondary protein quantification technique, such as the Bradford, Lowry, or BCA assays. With these methods, ε-toxin mutant concentrations would be analysed spectrophotometrically by a colour change. Absorption readings could then be compared to a known protein standard such as the Etx-YY protein background or bovine serum albumin [143]. These methods are unaffected by small sample contaminants and could therefore quantify ε-toxin mutant concentrations more accurately compared to a NanoDrop spectrophotometer. However, all seven ε-toxin mutants contain a high cysteine content that may produce artificially high results using the BCA assay [142]. Consequently, more accurate protein concentration results may be obtained using the Lowry or Bradford assays instead.

SDS-PAGE analysis revealed that the protein bands of all seven ε-toxin mutants correlated closely to the 33 kDa size of WT ε-toxin. This suggested that these samples contained the desired ε-toxin mutants [73] (Figure 8-4). Contaminant bands were not visible, therefore if any sample contamination existed it would be at very low concentrations. However, the SDS-PAGE method cannot distinguish molecular differences between these proteins and therefore could not confirm the purity or successful mutagenesis of these samples. To further investigate this, samples were analysed by mass spectrometry. Mass spectrometry analysis confirmed the purity and successful mutagenesis of the V72F, F92A, T93A, and A168F samples (Figure 8-7). However, the V72A and V166A mass spectrometry analysis revealed that these samples were contaminated with Etx-YY protein. The Etx-YY contaminant

accounted respectively for 8.9% and 7.6% of the total V72A and V166A PSM scores suggesting that the contamination in both samples was considerable. The Etx-YY contamination could have been introduced through two possible means, described in 1) and 2) below. In both possibilities, bacteria encoding the Etx-YY contaminant would have grown during protein expression and would not be separated from the desired V72A and V166A mutants during protein purification. This would result in a contaminated final elution that could have affected the cytotoxicity profiles of the V72A and V166A samples.

1) The Etx-YY contamination could have been introduced into the V72A and V166A samples through human error. This would have most likely occurred during the bacterial transformation or protein purification of these samples.

2) The V72A and V166A mutants may have reverted back to the Etx-YY background as a result of back mutations. Theoretically this could have occurred at any point following bacterial transformation. Reversion mutations are unlikely to occur unless there is an evolutionary driver favouring the reverted protein. The V72A and V166A mutations are not known to be evolutionarily detrimental to transformed bacteria. Consequently, it is considered unlikely that the Etx-YY contamination was introduced through a reversion mutation event.

Mass spectrometry also confirmed that the V166F mutant was contaminated with A168F (Figure 8-7). The A168F contaminant accounted for 6.7% of the total V166F PSM score suggesting that the contamination was substantial. The contamination was most likely introduced as a result of human error since protein expression and purification experiments were completed separately under aseptic conditions.

The cytotoxicity analysis performed in Figure 8-5 and Figure 8-6 was completed using only two replicates for each mutagenesis sample. Consequently, the data can only provide the spread of the results without a reliable indication of a statistical mean value. Despite the small spread of the results, the reliability of

the cytotoxicity analysis in Figure 8-5 and Figure 8-6 would be improved with more replicates.

The purity of the V72F, A168F, F92A and T93A samples confirmed that their cytotoxicity profiles were representative of their mutations. The cytotoxicity data revealed that the V72F and A168F samples were non-toxic to CHO-hMAL cells at all concentrations used in the cytotoxicity assay (Figure 8-5). The abolished cytotoxicity of the V72F and A168F mutants suggests that these residues are critical for ε-toxin cytotoxicity by potentially altering the structural integrity of the BOG binding site. The F92A and T93A mutants also demonstrated reduced CHO-hMAL cytotoxicity compared to the Etx-YY protein but retained cytotoxicity at higher concentrations (Figure 8-5). This suggests that the F92 and T93 residues are involved but inessential for ε-toxin cytotoxicity. One possible explanation is that the F92A and T93A mutations fail to introduce a significant structural change to abolish ε-toxin's cytotoxicity, therefore enabling ε-toxin to retain its cytotoxic properties. This could be because the BOG binding site remains functional but with reduced binding efficiency, which could explain why both mutants retain some cytotoxicity. Consequently, the cytotoxicity data from the V72F, A158F, F92A and T93A samples suggest that the BOG binding site is potentially responsible for ε-toxin's cytotoxicity towards CHO-hMAL cells, possibly mediated by binding to the MAL protein as a receptor.

The V166F sample also demonstrated abolished CHO-hMAL cytotoxicity, but was contaminated with the non-cytotoxic A168F mutant (Figure 8-7). A168F's non-cytotoxic properties suggest that it was unlikely to have affected the V166F cytotoxicity results. Consequently, the V166F cytotoxicity data is likely to be representative of a pure V166F sample, however, this may not be true for concentrations beyond the range used in the assay. The cytotoxicity results therefore suggest that the V166F mutation inhibits ε-toxin cytotoxicity, potentially by altering the structural integrity of the BOG binding site (Figure 8-5). However, future experiments are required to re-purify and test the V166F sample to confirm its effect on ε-toxin cytotoxicity.

The V166A sample also demonstrated reduced CHO-hMAL cytotoxicity but retained cytotoxicity at higher concentrations (Figure 8-5). This may be because

the alanine substitution fails to introduce a significant structural change to abolish ε-toxin's cytotoxicity. However, mass spectrometry results in Section 8.3.8 confirmed that the V166A sample was contaminated with Etx-YY protein. Contamination analysis suggests that the Etx-YY contaminant was sufficiently concentrated to influence V166A's cytotoxicity profile (Figure 8-7). Consequently, it is possible that the Etx-YY contamination was responsible for V166A's cytotoxicity against CHO-hMAL cells at high concentrations. Cytotoxicity results from the V166F mutant indicate that the V166 residue is critical for ε-toxin's cytotoxic properties. This suggests that a purified V166A sample may demonstrate significantly reduced CHO-hMAL cytotoxicity levels, potentially comparable to the V166F sample. These results further suggest that the BOG binding site is important for ε-toxin's cytotoxicity.

The V72A mutant failed to reduce CHO-hMAL cytotoxicity at all concentrations used in the assay (Figure 8-5). This may be because the alanine substitution fails to introduce a significant structural change to influence ε-toxin's cytotoxicity potentially because the BOG binding site remains fully functional. This is supported by the V72F mutant that targeted the same residue but demonstrated significantly reduced CHO-hMAL cytotoxicity compared to the V72A sample. This suggests that the V72 residue is critical for ε-toxin's cytotoxic properties but that the type of amino acid substitution is critical in influencing the cytotoxicity of ε-toxin. Mass spectrometry results in Section 8.3.8 revealed that the V72A sample was contaminated with the Etx-YY protein. However, the contamination was not sufficiently concentrated to explain V72A's cytotoxicity profile (Figure 8-7)(Equation 2). Although the Etx-YY contaminant could have impacted the results, the data suggests that the V72A mutation fails to introduce a significant structural change to influence ε-toxin's cytotoxicity. However, due to the Etx-YY contaminant, future experiments are required to re-purify and test the V72A sample in order to confirm its effect on ε-toxin cytotoxicity.

The cytotoxicity data demonstrated a clear disparity in the effectiveness of different amino acid substitutions. Alanine substitutions for the V72 and V166 residues demonstrated poor levels of cytotoxicity reduction; however, phenylalanine substitutions demonstrated strong levels of cytotoxicity reduction. These data suggest that the type of amino acid substitution is critical in

influencing ε-toxin's cytotoxicity. This is potentially related to the physiochemical properties of these different amino acids.

Alanine and valine share structural similarities resulting in both amino acids possessing similar molecular weights and hydrophobicity characteristics. This may result in an alanine substitution being inconsequential (Table 8-9). Furthermore, alanine rarely exhibits steric effects meaning that it is unlikely to change a protein's conformation or reactivity [144]. This suggests that the V72A and V166A substitutions may be unable to change the BOG binding site structure, and may explain why they were unsuccessful. Phenylalanine also shares similar hydrophobicity and structural characteristics but possesses a larger molecular weight due to the presence of an aromatic ring (Table 8-9). This bulkier aromatic side chain will result in a greater steric effect within the BOG binding site structure. This steric effect could have prevented BOG binding in the V72F and V166F samples, and therefore explain why phenylalanine was more effective in reducing ε-toxin's cytotoxicity compared to alanine.

Amino Acid Name	Structure	Side Chain Polarity	Hydropathy index*	Molecular Weight (Da)
Alanine	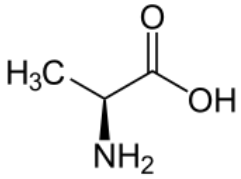	Nonpolar	1.8	89.09
Phenylalanine	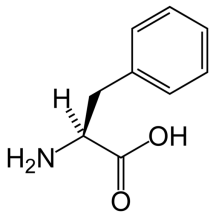	Nonpolar/ aromatic	2.8	165.9
Valine	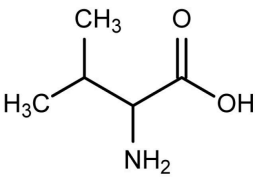	Nonpolar	4.2	117.15

*Hydropathy Index: a number representing the hydrophobic or hydrophilic properties of the side-chain of an amino acid [145]

Table 8-9 - Physiochemical properties of alanine, phenylalanine and valine

[146].

The results presented within Project 1 largely support the hypothesis. Despite contamination of the V72A, V166A and V166F samples, the cytotoxicity data of all seven ε-toxin mutants demonstrated reduced CHO-hMAL cytotoxicity compared to the Etx-YY background (Figure 8-6). This decreased cytotoxicity suggests that there could be reduced binding between the ε-toxin mutants and the CHO-hMAL cells. One possible explanation for this is that the mutations prevent direct or indirect interactions between the BOG binding domain and the putative MAL receptor. However, there is a risk that the folding of the ε-toxin mutants is incorrect. In this case, the cytotoxicity data obtained in Figure 8-6 would not be representative of the ε-toxin mutations. Protein folding analysis of the ε-toxin mutants is therefore required to investigate if the decreased cytotoxicity is due to reduced ε-toxin binding or incorrect protein folding. The results also reveal a clear disparity between the effectiveness of different amino acid substitutions. Consequently, this suggests that the type of amino acid substitution is also critical in affecting the BOG binding domain and ε-toxin's cytotoxicity towards CHO-hMAL cells. Notwithstanding these issues, the results obtained in this project support the hypothesis statement that: 'Site directed mutagenesis of amino acids within the BOG binding domain will reduce epsilon toxin cytotoxicity to CHO-hMAL cells by reducing epsilon toxin binding'.

8.5 FUTURE WORK

8.5.1 Samples V72A, V166A and V166F

Mass spectrometry data revealed that the V72A, V166A and V166F samples were contaminated (Figure 8-7). V72A and V166A were contaminated with Etx-YY protein and V166F was cross-contaminated with A168F. The contamination in these samples could have affected the cytotoxicity data obtained for these samples. Consequently, it is unclear how these mutations affect the cytotoxicity of ε-toxin. To resolve this, it is recommended that these samples be repeated, checked for contamination and tested for cytotoxicity. The testing of pure V72A, V166A and V166F samples will confirm if they can be considered as possible vaccine candidates against ε-toxin.

8.5.2 Samples F92A and T93A

Data from mutants targeting the V72 and V166 residues suggest that the alanine substitutions are ineffective at reducing ε-toxin's cytotoxicity. Both the F92A and T93A samples involved alanine substitutions and demonstrated poor levels of cytotoxic protection to CHO-hMAL cells. Consequently, it may be of interest to investigate alternative amino acid substitutions for these residues to fully confirm their involvement in ε-toxin's cytotoxicity.

8.5.3 Samples V72F and A168F

The A168F and V72F samples both demonstrated strong levels of cytotoxicity reduction and were identified as pure samples by the mass spectrometry analysis. Several further experiments are required before these mutants can be pursued as vaccine candidates against ε-toxin:

1) The V72F and A168F CT_{50} concentrations for CHO-hMAL cells remain unknown, as they lie beyond the 0.2 mg/ml starting concentration used in the cytotoxicity assays (8.2.20). Future experiments could investigate the V72F and A168F mutants at concentration ranges above 0.2 mg/ml. These experiments would identify the CT_{50} concentrations for these mutants against CHO-

hMAL cells.

2) Future cytotoxicity assays could investigate the V72F and A168F cytotoxicity profiles in different cell lines. Previous work identified that the background Etx-YY protein was non-toxic to MDCK cells. However, experimentation is required to confirm that the V72F and A168F mutants remain non-toxic to MDCK cells. Previous work also identified that the Etx-YY background retained cytotoxicity to ACHN cells. It has since been hypothesised that the ε-toxin BOG binding site attaches to the NK receptor of ACHN cells to establish cytotoxicity [121]. Future work could therefore elucidate whether the V72F and A168F mutations targeting the BOG binding site also influences ε-toxin's cytotoxicity against ACHN cells.

3) The protein folding of the V72F and A168F mutants remain unconfirmed. Incorrect folding could affect the protein conformation of these mutants that might compromise their cytotoxicity profiles. Protein folding analysis can be investigated using circular dichrorism, X-ray Crystallography or nuclear magnetic resonance to analyse protein folding between the ε-toxin mutant and WT ε-toxin [147][148][149]. These methods would confirm if the V72F and A168F mutants are correctly folded, and therefore, if the cytotoxicity profiles are representative of the introduced mutations.

8.6 CONCLUSIONS

Using the method described in this project, several ε-toxin mutagenesis samples were successfully expressed purified and analysed for cytotoxicity against CHO-hMAL cells. In particular, the V72F, V166F and the A168F samples showed at least a 68.8 fold cytotoxicity reduction to CHO-hMAL cells and demonstrate significant promise as ε-toxin vaccine candidates. Phenylalanine mutants resulted in greater cytotoxicity reductions compared to alanine substitutions that may be related to physiochemical differences between these amino acids. Mass spectrometry data revealed that the V72A, V166A and V166F samples were contaminated. Consequently, future work is required to re-

purify the contaminated samples and investigate the V72F and A168F mutants for protein folding and further analysis in other cell lines.

9 PROJECT 2 – SERUM NEUTRALISATION OF E-TOXIN

9.1 PROJECT OBJECTIVES

In 2012, *C. perfringens* Type B was isolated in a patient with clinical presentations of MS [75]. *C. perfringens* Type B secretes ε-toxin that bypasses the blood brain barrier and demyelinates axons in ruminant animals. These demyelination activities show striking similarities to the pathology of MS. Recent research identified greater ε-toxin immunoreactivity in MS patients compared to controls [75]. This suggested that MS patients have previous exposure to ε-toxin that may have contributed to their disease. Consequently, the aim of this study was to investigate whether the anti-ε-toxin antibodies present in MS sera could bind and neutralise ε-toxin. To achieve this, ε-toxin was mixed with sera and incubated with CHO cells expressing the putative MAL binding receptor for ε-toxin [85]. Neutralisation of ε-toxin by serum antibodies would confer cytotoxic protection to the CHO-hMAL cells that can be quantified using a cytotoxicity assay.

The methods to achieve the objectives of Project 2 are as follows:

1) Identify ε-toxin's cytotoxic 50% dose against CHO-hMAL cells using a cytotoxicity assay.

2) Demonstrate neutralisation of ε-toxin using previously obtained anti-ε-toxin antibodies. Antibody/ε-toxin solutions are incubated with CHO-hMAL cells and checked for cytotoxicity.

3) Investigate neutralisation of ε-toxin using sera obtained from MS, CIS and control patients. Sera/ ε-toxin solutions are incubated with CHO-hMAL cells and checked for cytotoxicity.

4) Sera neutralisation capabilities against ε-toxin can be compared. These data will be used in conjugation with research from another project to further corroborate or dismiss the link between ε-toxin and MS.

9.1.1 Project Hypothesis

Compared to control sera, MS and CIS patient sera will confer greater cytotoxic protection to CHO-hMAL cells against ε-toxin due to the presence of anti ε-toxin antibodies.

9.2 Materials and Methods

This section contains a detailed account of the different materials and methods used to complete all individual experiments undertaken in Project 2.

9.2.1 CHO-hMAL Culturing

CHO-hMAL cells were resuscitated and grown in T25 and T75 tissue culture flasks, or for assays as described previously (Sections 8.2.17, 8.2.18, 8.2.19).

9.2.2 SDS-PAGE – Wild Type ε-toxin Trypsin Activation

SDS-PAGE analysis was used to check WT ε-toxin trypsin activation and was completed as previously described (Section 8.2.20).

9.2.3 Wild Type ε-toxin Cytotoxicity Assay

A CytoTox96® Non-Radioactive LDH Cytotoxicity Assay (Promega) was used to calculate the cytotoxic 50% dose of WT ε-toxin against CHO-hMAL cells as previously described (Section 8.2.20).

9.2.4 Wild Type ε-toxin Neutralisation Using an Anti-ε PoAb

WT ε-toxin neutralisation using an anti-ε-toxin was analysed with a CytoTox96® Non-Radioactive LDH Cytotoxicity Assay following the manufacturer's instructions (Promega). WT ε-toxin neutralisation was completed using an anti-ε-toxin polyclonal rabbit antibody (anti-ε PoAb). Briefly, WT ε-toxin concentration (mg/ml) was identified using a NanoDrop 1000 (BioRad) and converted to molar concentration (Equation 1). WT ε-toxin was diluted to a starting concentration of 50xCT_{50} with PBS. 10 µL of inactivated 50 µM ε-toxin was mixed with 10 µl of 4xLDS Buffer for SDS PAGE analysis (Section 9.2.2). Following WT ε-toxin trypsin activation, 10 µL of activated ε-toxin was mixed with 10 µl of 4xLDS

Buffer for SDS PAGE analysis (Section 9.2.2).

Using a 96-well V-bottomed plate, an anti-ε PoAb was diluted in PBS through a two-fold dilution. Wells were mixed with equal volumes of activated ε-toxin ($50xCT_{50}$) and incubated at room temperature for one hour. Using a previously seeded 96 well plate (Section 8.2.19), 100 µl of old cell media was replaced with 80 µl of pre-warmed DMEM. 20 µl of each ε-toxin and anti-ε PoAb solution was transferred to respective wells on the seeded plate. 20 µl of the positive and negative controls were each added to three control wells (Table 9-1). The seeded 96-well plate was incubated at 37°C, 5% CO_2 for three hours. Following incubation, 50 µl of cell culture medium from all control and experimental wells was transferred to a fresh 96-well plate and mixed with 50 µl of reconstitution substrate mix. Following a 30 minute incubation in the dark at room temperature, the wells were mixed with 50 µl of stop solution and cytotoxicity measured at 490 nm using a microplate reader (BioRad). The mean PBS OD score was subtracted from all experimental values and data analysed for neutralisation activity.

ε-toxin Neutralisation LDH Assay Controls	Control Type
PBS	Negative
0.1X Triton X	Positive
$1xCT_{50}$ WT- ε-toxin	Positive

Table 9-1 - Experimental controls employed for the LDH assay investigating WT ε-toxin neutralisation using an anti-ε PoAb

9.2.5 Serum Neutralisation of Wild Type ε-toxin

WT ε-toxin neutralisation using human sera was analysed with a CytoTox96® Non-Radioactive LDH Cytotoxicity Assay following the manufacturer's instructions (Promega). Briefly, WT ε-toxin concentration (mg/ml) was identified using a NanoDrop 1000 (BioRad) and converted to molar concentration (Equation 1). WT ε-toxin was diluted to a starting concentration of $10xCT_{50}$ with

PBS. 10 µL of the inactivated 50 µM ε-toxin was mixed with 10 µl of 4xLDS Buffer for SDS PAGE analysis (Section 9.2.2). Following WT ε-toxin trypsin activation, 10 µL of activated ε-toxin was mixed with 10 µL of 4xLDS Buffer for SDS PAGE analysis (Section 9.2.2).

Using a 96-well V-bottomed plate, equal volumes of human sera and activated ε-toxin (10xCT_{50}) were mixed and incubated at room temperature for one hour. Using a previously seeded 96 well plate (Section 8.2.19), 100 µl of old cell media was replaced with 80 µl of pre-warmed DMEM. 20 µl of the serum/ WT ε-toxin solution was transferred to respective wells on the seeded plate. 20 µl of the positive and negative controls were each added to three control wells (Table 9-2). The 96-well plate was incubated at 37°C, 5% CO_2 for three hours. Following incubation, 50 µl of cell culture medium from all control and experimental wells was transferred to a fresh 96-well plate and mixed with 50 µl of reconstitution substrate mix. Following a 30 minute incubation in the dark at room temperature, the wells were mixed with 50 µl of stop solution and cytotoxicity measured at 490 nm using a microplate reader (BioRad). The mean PBS negative control was subtracted from all experimental values and data analysed for neutralisation activity.

ε-toxin Neutralisation LDH Assay Controls	**Control Type**
PBS	Negative
1xCT_{50} WT- ε-toxin + anti.-ε PoAb	Negative
0.1X Triton X	Positive
1xCT_{50} WT ε-toxin	Positive

Table 9-2 - Experimental controls employed for the LDH assay investigating WT ε-toxin neutralisation using human sera.

9.2.6 Serum Cytotoxicity to CHO-hMAL Cells

A CytoTox96® Non-Radioactive LDH Cytotoxicity Assay (Promega) was used to analyse serum cytotoxicity to CHO-hMAL cells following the manufacturer's instructions.

Using a 96-well V-bottomed plate, equal volumes of human sera (20 samples) and PBS were mixed together. Using a previously seeded 96 well plate (Section 8.2.19), 100 µl of old cell media was replaced with 80 µl of pre-warmed DMEM without FBS. 20 µl of the serum-PBS mix was added to seeded wells and 20 µl was added to non-seeded wells. 20 µl of the positive and negative controls were each added to three seeded control wells (Table 9-3). The 96-well plate was incubated at 37°C, 5% CO_2 for three hours. Following incubation, 50 µl of culture medium from all control and experimental wells was transferred to a fresh 96-well plate and mixed with 50 µl of reconstitution substrate mix. Following a 30 minute incubation in the dark at room temperature, the wells were mixed with 50 µL of stop solution and cytotoxicity measured at 490 nm using a microplate reader. (BioRad). OD scores for sera in seeded and non-seeded wells were compared to identify serum cytotoxicity to CHO-hMAL cells.

Serum Cytotoxicity LDH Assay Controls	Control Type
PBS	Negative
0.1X Triton X	Positive

Table 9-3 - Experimental controls employed for the LDH Assay investigating serum cytotoxicity to CHO-hMAL cells.

9.2.7 Sera LDH Activity

Sera LDH levels were analysed using a CytoTox96® Non-Radioactive LDH Cytotoxicity Assay following the manufacturer's instructions (Promega). Briefly, 15 µl of each human serum sample was transferred aseptically to wells on a non-seeded 96-well plate and mixed with 15 µl of PBS. 20 µl of the serum-PSB solution was added to 80 µl of DMEM without FBS and serum colour measured at 490 nm using a micro-plate reader (BioRad). 20 µl of the positive and negative control samples were each added to three wells containing 80 µl of DMEM without FBS (Table 9-4).

50 µl of experimental and control samples were transferred to a new 96-well plate and mixed with 50 µl of reconstitution substrate mix. Following a 30 minute incubation in the dark at room temperature and sera LDH activity measured at 490 nm using a microplate reader (BioRad). Serum colour levels were subtracted from experimental values and data compared with the controls.

Serum LDH Activity Experimental Controls	Control Type
PBS	Negative
LDH Positive Control (Promega)	Positive

Table 9-4 - Experimental controls employed for the LDH assay investigating serum LDH activity.

9.2.8 LDH Isoenzyme Testing (Great Ormond Street Hospital)

Selected CIS and control serum samples were sent to Great Ormond Street Hospital (GOSH) for LDH isoenzyme analysis by electrophoresis. Briefly, 5 µl samples were loaded onto a rinsed pre-cast 6.5% polyacrylamide gel in a tank-containing buffer (2.4 g Tris base, 11.6 g glycine/litre). Electrophoresis was completed at 12 mA for 90 minutes. The gel was removed and washed in developer solution (H_2O-18.4 ml, 1M-Tris 4 ml, tetrazolium-blue 12 ml, phenzinemethosulphate 4 ml, Na-lactate 4 ml and NAD 1.3 mL at 40°C for 20 minutes. The gel was washed with water and visualised. Isoenzyme quantification was completed by measuring the pixel density for each

isoenzyme band. The density of each isoenzyme band was calculated and expressed as a percentage for the whole sample [150].

9.2.9 MTT Assay – Wild Type ε-toxin Cytotoxicity Assay

The cytotoxic 50% dose of WT ε-toxin against CHO-hMAL cells was calculated using a CytoTox96® Non-Radioactive MTT Assay following the "Same Day Method" as per the manufacturer's instructions (Promega). Briefly, WT ε-toxin concentration (mg/ml) was identified using a NanoDrop 1000 (BioRad) and converted to molar concentration (Equation 1). ε-toxin mutants were diluted to a starting concentration of 50 µM using PBS. 10 µl of the inactivated 50 µM ε-toxin was mixed with 10 µl of 4xLDS Buffer for SDS PAGE analysis (Section 9.2.2). Following WT ε-toxin trypsin activation, 10 µl of activated ε-toxin was mixed with 10 µl of 4xLDS Buffer for SDS PAGE analysis (Section 9.2.2). Using a 96-well V-bottomed plate, activated ε-toxin mutants were diluted in PBS through a two-fold dilution.

Using a previously seeded 96 well plate, old cell media was replaced with 80 µl of pre-warmed DMEM. 20 µl of each dilution was transferred to their respective wells on the seeded plate. 20 µl of the control samples were each added to three seeded control wells (Table 9-5). The 96-well plate was incubated at 37°C, 5% CO_2 for three hours. Cell media was replaced with 85 µl of DMEM and 15 µl of MTT dye solution. Following a further four hour incubation at 37°C, 5% CO_2, 100 µl of stop/solubilisation solution was added to all wells and incubated at room temperature for one hour. Cytotoxicity was measured at 490 nm using a microplate reader (BioRad). The mean PBS value was subtracted from all experimental values and data analysed for neutralisation activity. The cytotoxic 50% dose calculated using non-linear regression analysis.

Wild Type ε-toxin Cytotoxicity MTT Assay Controls	Control Type
PBS	Negative
0.1X Triton X	Positive

Table 9-5 - Experimental controls employed for the MTT Assay investigating Wild Type ε-toxin cytotoxicity to CHO-hMAL cells.

9.2.10 MTT Assay – Wild Type ε-toxin Neutralisation using Anti-ε PoAb

The cytotoxic 50% dose of ε-toxin against CHO-hMAL cells using a CytoTox96® Non-Radioactive MTT Assay following the "Same Day Method" as per the manufacturer's instructions (Promega). Briefly, WT ε-toxin concentration (mg/ml) was identified using a NanoDrop 1000 (BioRad) and converted to molar concentration (Equation 1). WT ε-toxin was diluted to a starting concentration of $10xCT_{50}$ with PBS. 10 µl of the inactivated 50 µM ε-toxin was mixed with 10 µl of 4xLDS Buffer for SDS PAGE analysis (Section 9.2.2). Following WT ε-toxin trypsin activation, 10 µl of activated ε-toxin was mixed with 10 µl of 4xLDS Buffer for SDS PAGE analysis (Section 9.2.2).

Using a 96-well V-bottomed plate, an anti-ε PoAb was diluted in PBS through a two-fold dilution. Each well was mixed with equal volumes of activated ε-toxin ($10xCT_{50}$) and incubated at room temperature for one hour. Using a previously seeded 96 well plate (Section 8.2.19), 100 µl of old cell media was replaced with 80 µl of pre-warmed DMEM. 20 µl of each two-fold dilution was transferred to respective wells on the seeded plate diluting the activated ε-toxin to $1xCT_{50}$. 20 µl of the control samples were each added to three seeded control wells (Table 9-6). The 96-well plate was incubated at 37°C, 5% CO_2 for three hours. Cell media was replaced with 85 µl of DMEM and 15 µl of MTT dye solution. Following a four hour incubation at 37°C, 5% CO_2, 100 µl of stop/solubilisation solution was added to all wells and incubated at room temperature for one hour. Cytotoxicity was measured at 490 nm using a microplate reader (BioRad). The mean PBS value was subtracted from all experimental values and data analysed for neutralisation activity.

ε-toxin Neutralisation MTT Assay Controls	Control Type
PBS	Negative
0.1X Triton X	Positive
1xCT_{50} WT- ε-toxin	Positive

Table 9-6 - Experimental controls employed for the MTT Assay investigating WT ε-toxin neutralisation using an anti-ε PoAb

9.3 RESULTS

This section describes the individual results obtained from all experiments completed in Project 2.

9.3.1 Wild Type ε-toxin CT_{50} Calculation

Using the LDH cytotoxicity assay, WT ε-toxin's cytotoxic 50% (CT_{50}) dose against CHO-hMAL cells was determined through a two-fold dilution (Figure 9-1). Non-linear regression analysis identified the WT ε-toxin CT_{50} as 0.32 μM against CHO-hMAL cells.

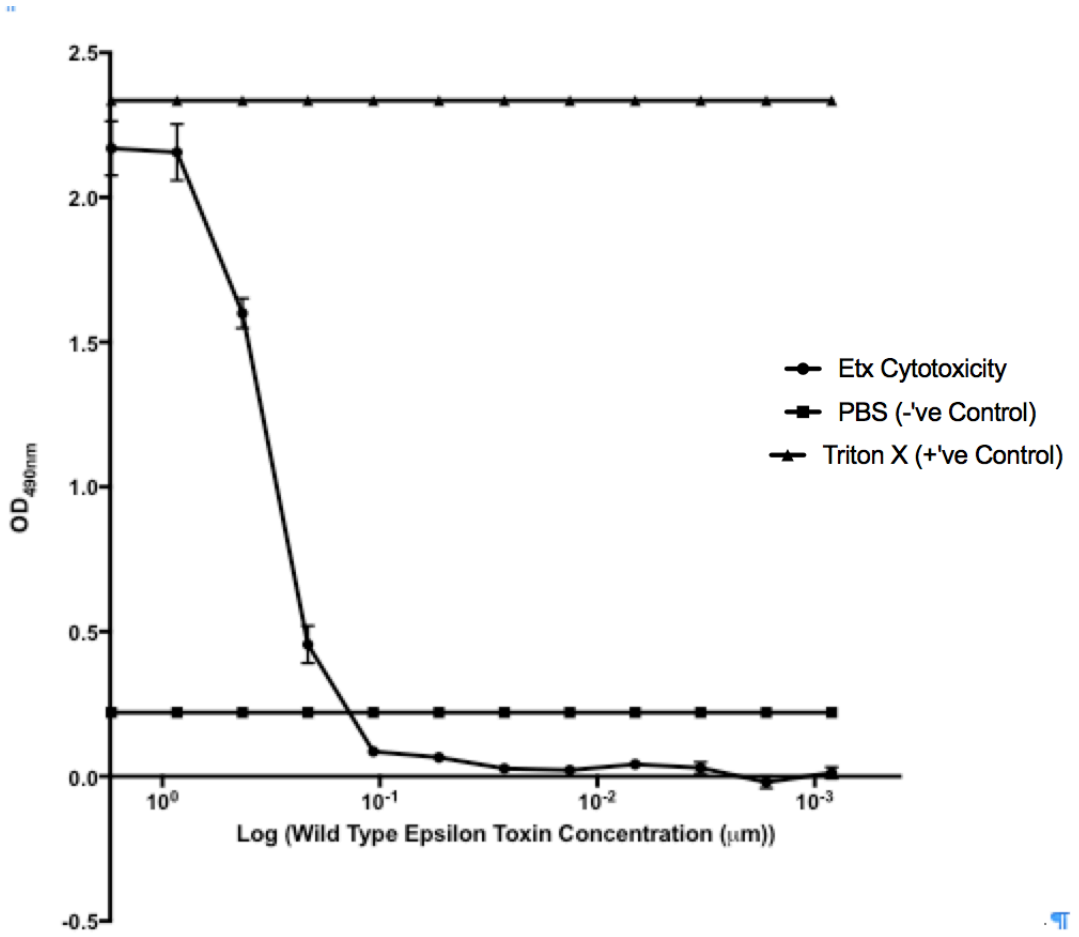

Figure 9-1 - Illustrates optical density measuring mean LDH release from CHO-hMAL cells. Cells were incubated with WT ε-toxin, a PBS negative control or TritonX positive control. WT ε-toxin was diluted through a two-fold dilution starting at a concentration of 1.7 μM. Results are from two replicates measured at OD_{490nm}. The error bars represent the standard error of the mean.

9.3.2 Wild Type ε-toxin Neutralisation Using an Anti-ε PoAb

WT ε-toxin neutralisation was demonstrated with an anti-ε PoAb using an LDH cytotoxicity assay. Figure 9-2 illustrates that WT ε-toxin ($1xCT_{50}$) cytotoxicity increases to $1xCT_{50}$ positive control levels as the anti-ε PoAb concentration decreases. Complete WT ε-toxin neutralisation was observed between anti-ε PoAb concentrations of 0.9 and 0.225 mg/ml.

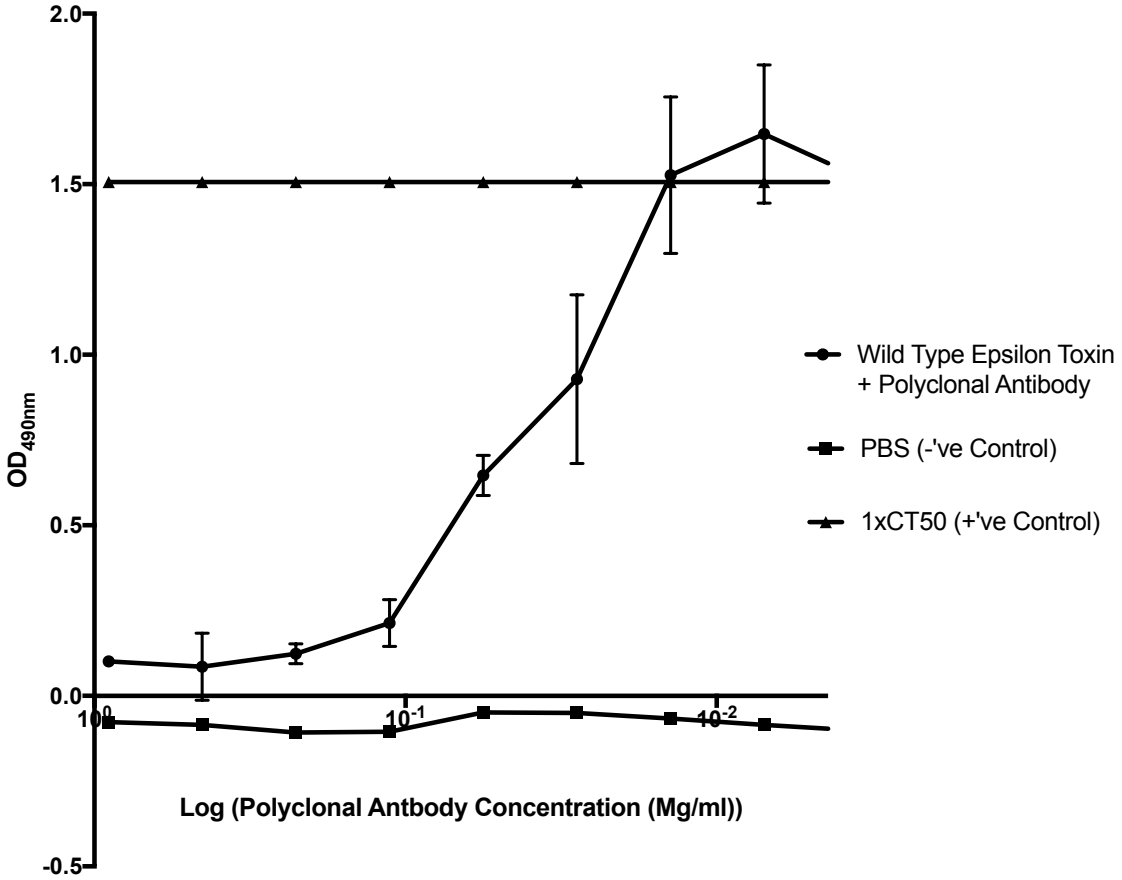

Figure 9-2 - Illustrates optical density measuring mean LDH release from CHO-hMAL cells. Cells were incubated with WT ε-toxin ($1xCT_{50}$) mixed with anti-ε-PoAb, a PBS negative control or TritonX positive control. The anti-ε-PoAb was diluted through a two-fold dilution starting at a concentration of 0.9 mg/ml. Results shown are from two replicates measured at OD_{490nm}. The error bars represent the standard error of the mean.

9.3.3 Wild Type ε-toxin Serum Neutralisation Assay (Sample Group 1)

WT ε-toxin neutralisation by control, CIS and MS sera was completed using an LDH cytotoxicity assay. Sera were mixed with a $1xCT_{50}$ dose of WT epsilon toxin and cytotoxicity results were normalised against the $1xCT_{50}$ positive control. Figure 9-3 shows that control, CIS and MS sera demonstrated greater

LDH activity compared to the 1xCT_{50} positive control. Evidence of ε-toxin neutralisation by control, CIS and MS sera was not observed.

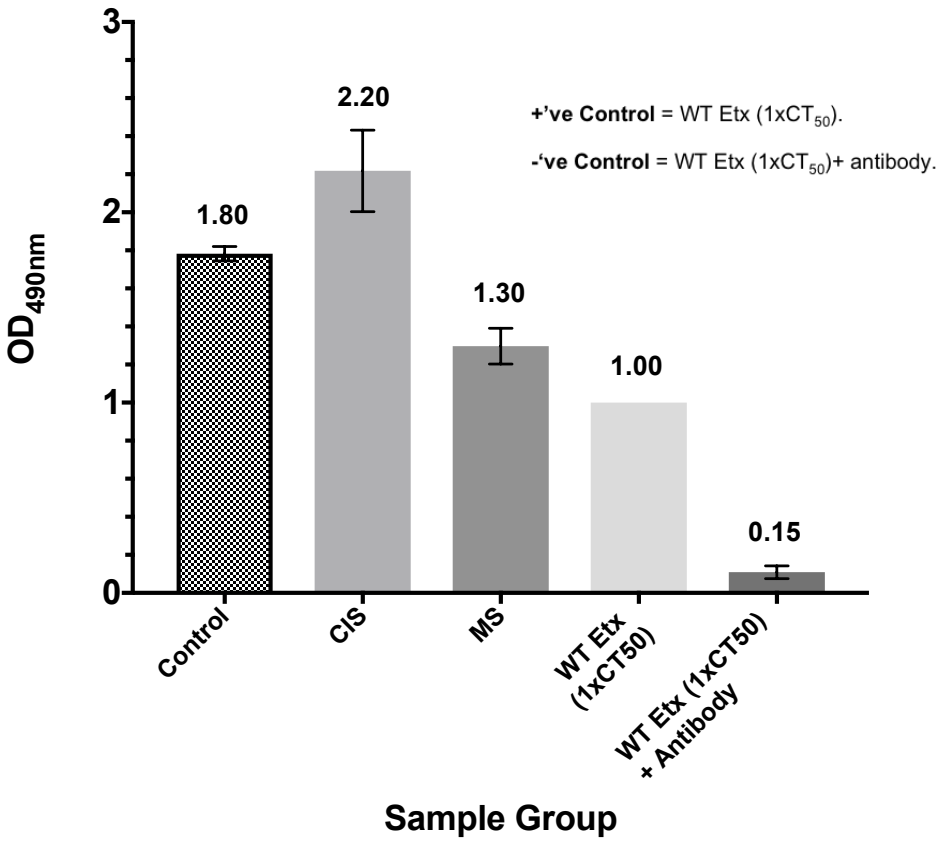

Figure 9-3 - Illustrates optical density measuring mean LDH release from CHO-hMAL cells. Cells were incubated with WT ε-toxin (1x CT_{50}), mixed with control, CIS or MS patient sera, WT ε-toxin (1x CT_{50}) positive control and WT ε-toxin (1x CT_{50}) mixed with a neutralising concentration of anti-ε-PoAb as the negative control. Data shown was normalised against the 1xCT_{50} positive control and adjusted for serum colour variation. Results are from two replicates of sera samples in Appendix C.1 measured at OD_{490nm}. The error bars represent the standard error of the mean.

9.3.4 Serum Cytotoxicity to CHO-hMAL cells (Sample Group 1)

Serum mediated cytotoxicity to CHO-hMAL cells was investigated using an LDH cytotoxicity assay. Figure 9-4 illustrates consistent LDH levels between the control, CIS and MS sera groups and the PBS negative control. These data show that the sera are not cytotoxic to the CHO-hMAL cells.

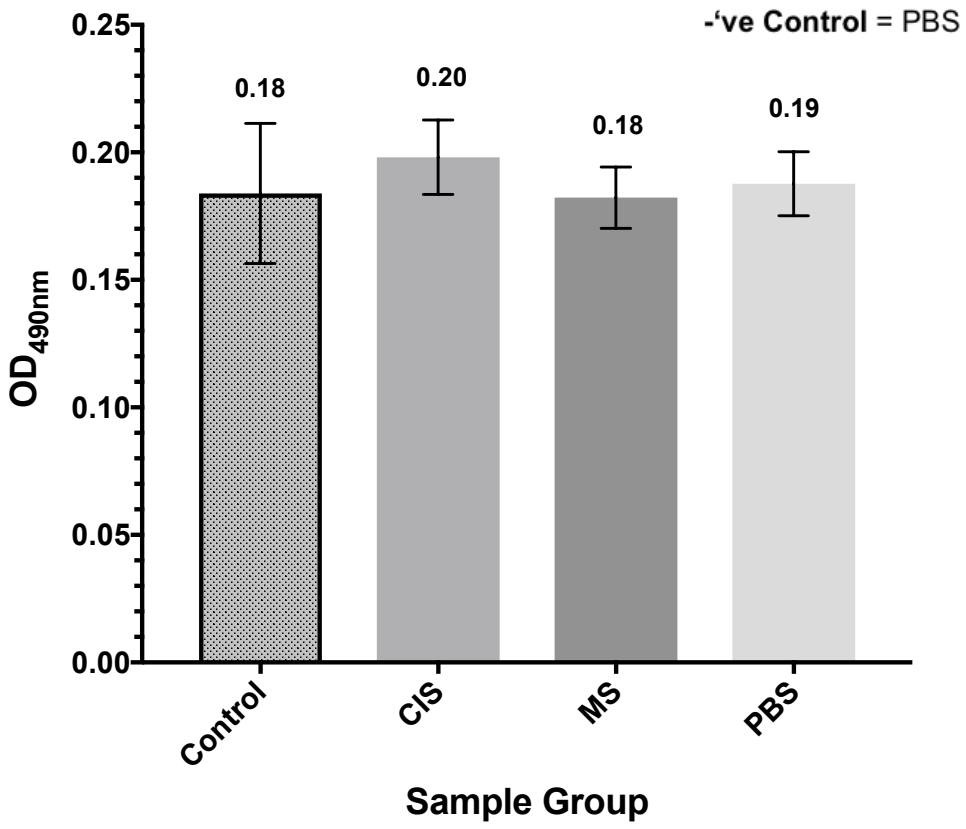

Figure 9-4 - Illustrates optical density measuring mean LDH release from CHO-hMAL cells incubated with control, CIS or MS sera compared to a PBS negative control. Results shown are from two measurements recorded at OD_{490nm} of sera samples listed in Appendix C.1. The error bars represent the standard error of the mean.

9.3.5 Serum LDH Levels (Sample Group 2)

Sera LDH activity was investigated using an LDH assay. Data in Figure 9-5 shows that all three sera groups demonstrated increased LDH activity compared to the PBS negative control. The CIS sera group demonstrated the most LDH activity followed by the control group and lastly the MS group. The difference in LDH activity between the CIS and Control sera groups and the CIS and MS sera groups were statistically significant at ($P \leq 0.01$) and ($P \leq 0.05$) respectively.

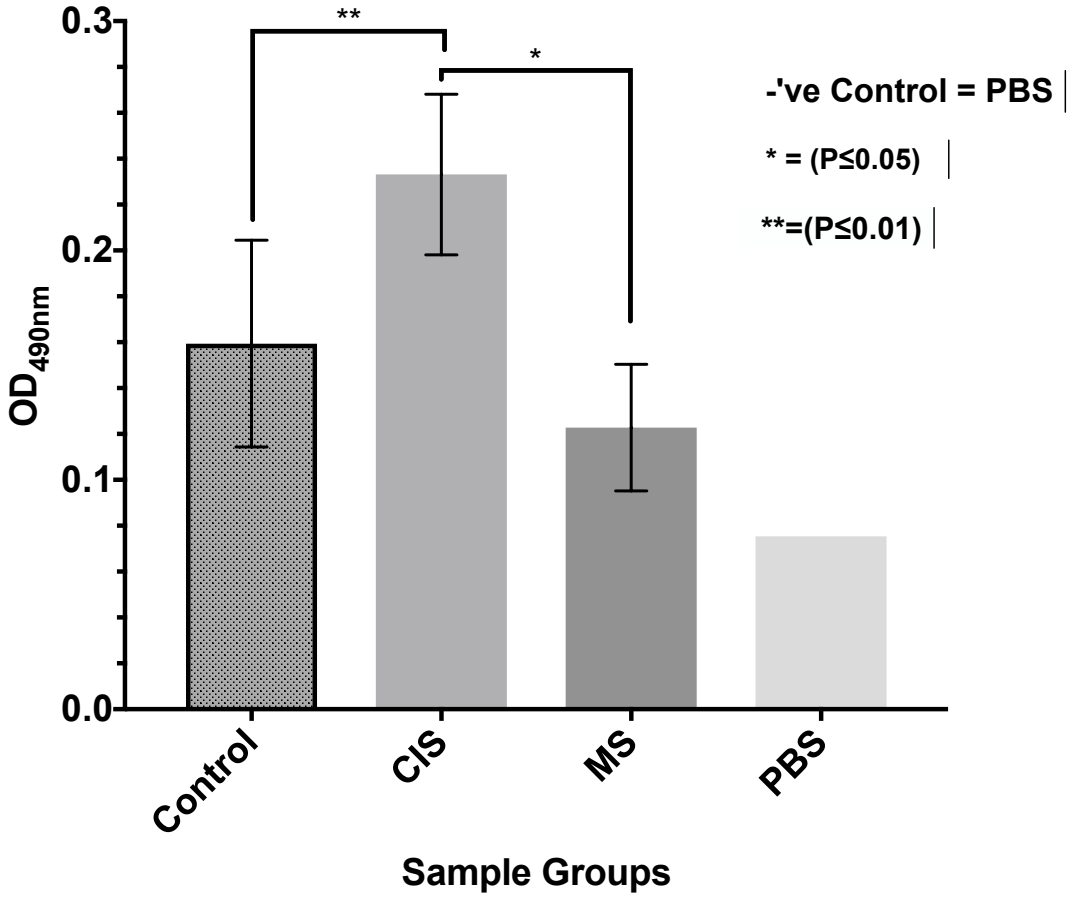

Figure 9-5 - Illustrates optical density measuring mean LDH activity in control, CIS and MS sera compared to a PBS negative control. Statistically significant differences were identified between control and CIS sera at P≤0.01 and between CIS and MS sera at P≤0.05. Results shown are from two measurements recorded at OD_{490nm} of sera samples listed in Appendix C.2. Data analysed using the Kolmogorov-Smirnov unpaired statistical test. The error bars represent the standard error of the mean.

9.3.6 GOSH - LDH Isoenzymes

Differences in sera LDH activity between control and CIS sera (Section 9.3.5) were investigated by GOSH using an LDH isoenzyme electrophoresis assay. Figure 9-6 illustrates the mean percentage LDH isoenzyme level present in control and CIS sera. Elevated LDH isoenzyme 1 and 4 levels were observed in CIS patients compared to control patients. However, LDH isoenzymes 2, 3 and 5 showed deceased activity in CIS patients compared to control patients.

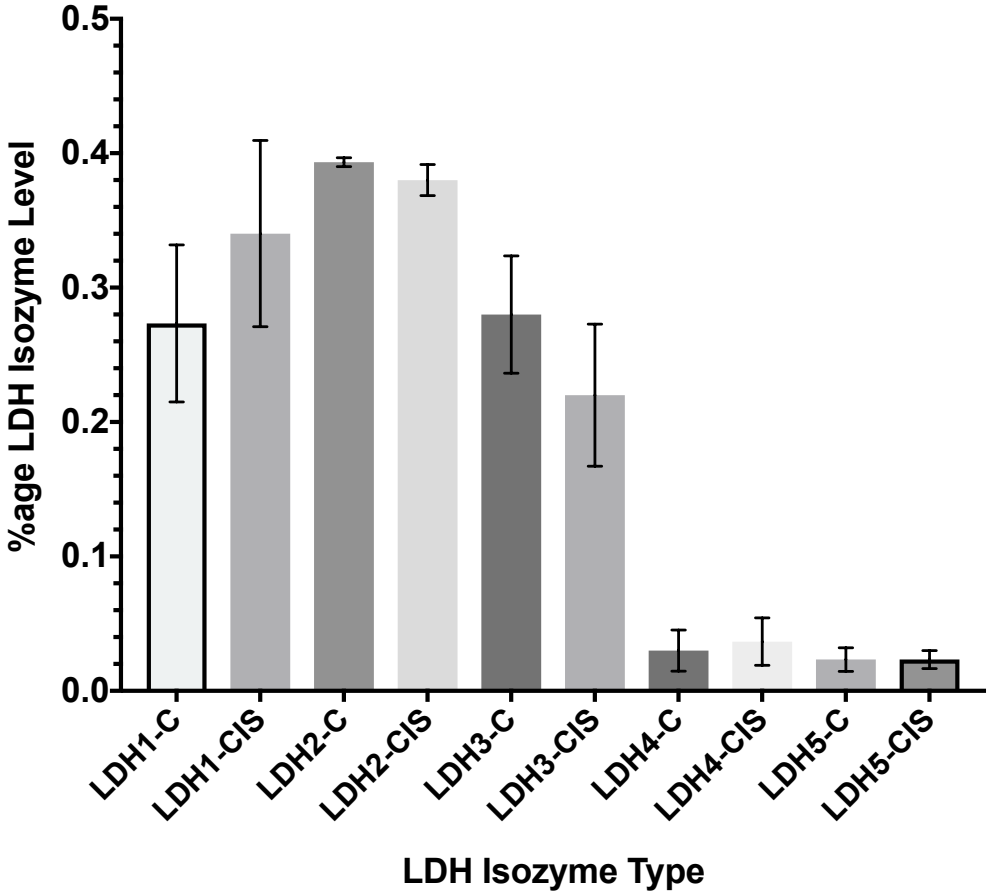

Figure 9-6 - Illustrates mean percentage LDH Isoenzyme levels in CIS and control sera groups. The experiment was performed using an LDH isoenzyme electrophoresis assay completed by GOSH. Three sera samples were tested for both the CIS (CIS300, CIS302, CIS314) and control group (BUH228, BUH236, BUH239). Results shown are the mean LDH isoenzyme level of each sera group obtained from one measurement at OD_{490nm}. The error bars represent the standard error of the mean of the three samples analysed for the control or CIS sera group.

9.3.7 Great Ormond Street Hospital LDH Isoenzyme Data vs. LDH Assay Data

Sera LDH levels were compared between the LDH cytotoxicity assay results (X-axis) and GOSH LDH Isoenzyme results (Y-axis) to check for reproducibility (Figure 9-7). The plotted data from both assays followed a line of best fit showing that the LDH assay yielded similar sera LDH results compared to the LDH isoenzyme electrophoresis method.

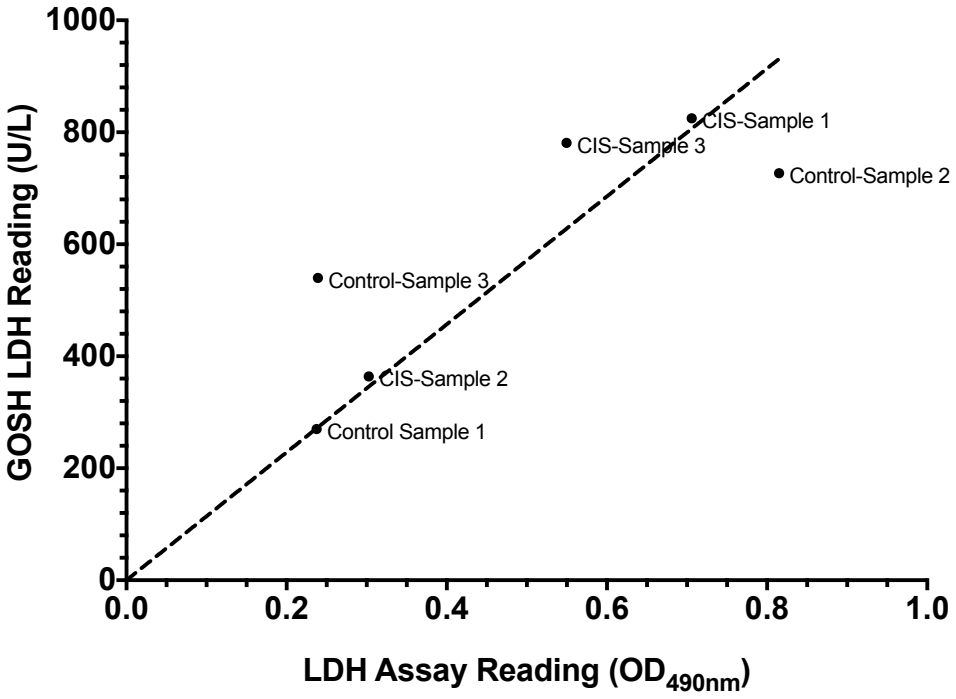

Figure 9-7 - Comparing LDH measurements of sera samples analysed using the LDH cytotoxicity assay (X-axis) and the GOSH LDH Isoenzyme Assay (Y-axis). Results shown are the mean LDH levels of the three CIS and control sera samples from both assays. A line of best fit has been plotted.

9.3.8 Serum LDH Levels Grouped According to Sample Origin

Serum LDH results (Section 9.3.5) were categorised according to their patient group and hospital of origin to investigate if differences in serum handling conditions at different hospitals were affecting sera LDH results. Figure 9-8 shows that serum LDH results varied considerably between corresponding sera groups obtained from different hospitals. Statistically significant sera LDH results were observed between the Exeter Research Innovation Learning and Development Centre (RILD) and Exeter Medical School control sera ($P \leq 0.001$), the Exeter RILD and Barts NHS Trust control sera ($P < 0.05$), the Exeter Medical School and Barts NHS Trust control sera ($P \leq 0.0001$) and the Exeter Medical School and Barts NHS Trust MS sera ($P \leq 0.01$) (Figure 9-8).

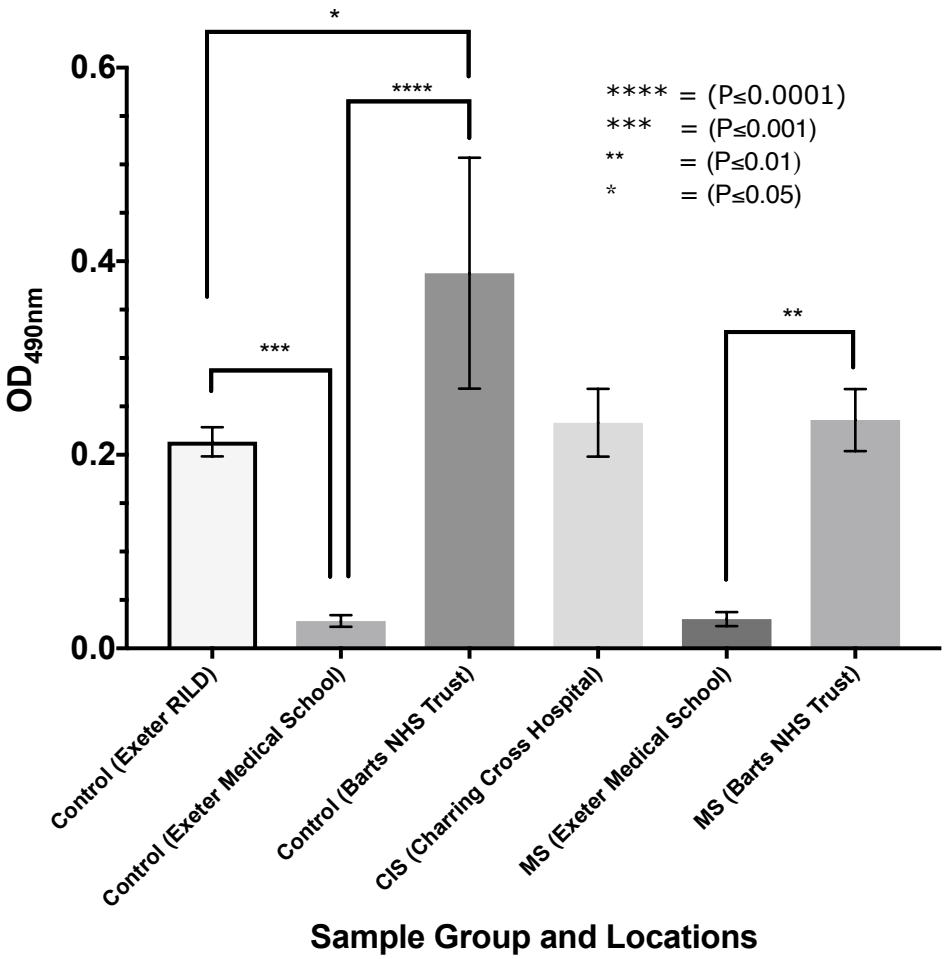

Figure 9-8 - Illustrates optical density measuring mean sera LDH activity categorised by sera group and hospital origin. Statistically significant differences were identified between Exeter RILD and Exeter Medical School at P≤0.0001, Exeter Medical School and Barts NHS Trust at P≤0.001 and Exeter Medical School and Barts NHS Trust at P≤0.001. Results shown are from the mean of sera samples for each patient group listed in Appendix C.2 from one measurement at OD_{490nm}. Data analysed using the one-way ANOVA statistical test. The error bars represent the standard error of the mean.

9.3.9 Serum LDH Levels (Old Controls vs. New Controls)

In response to the variable sera LDH results (Section 9.3.8), the sera LDH activity of fresh control sera samples obtained from the Exeter serum bank were analysed using an LDH cytotoxicity assay. This sera group consisted of 20 identically treated serum samples that had completed two freeze thaw cycles. The fresh control sera demonstrated greater LDH activity compared to previously tested samples with reduced LDH variability between individual samples (Figure 9-9). Differences in sera LDH activity between the control

groups were significant at (P ≤ 0.01).

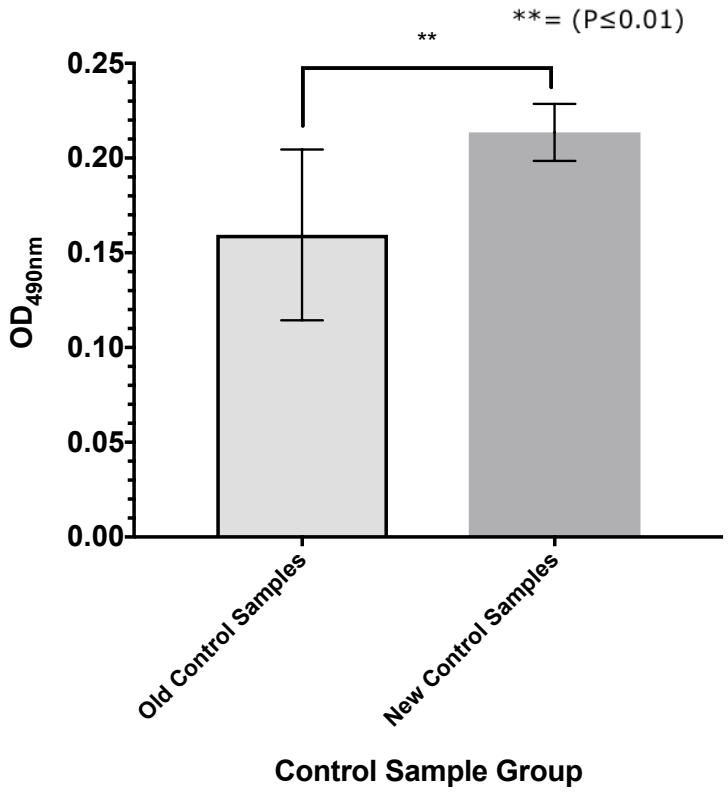

Figure 9-9 - Illustrates optical density measuring mean LDH levels in 20 fresh and 20 previously tested control groups. A statistically significant difference was identified between the two groups at P≤0.01. Results shown are the mean LDH isoenzyme level obtained from one measurement at OD_{490nm} of control sera samples listed in Appendix C.2 and Appendix C.3. Data analysed using the Kolmogorov-Smirnov unpaired statistical test. The error bars represent the standard error of the mean.

9.3.10 Serum LDH Levels with Standardised Controls

The LDH data of fresh control sera (Section 9.3.9) was compared with LDH results from previously tested CIS and MS sera samples (Section 9.3.5). Fresh control sera demonstrated greater LDH activity against CIS and MS sera compared to previously tested controls in Section 9.3.5 (Figure 9-10). Comparable LDH levels were observed between the fresh control sera and CIS sera (Figure 9-10). The difference in sera LDH activity between the control and CIS groups was not statistically significant.

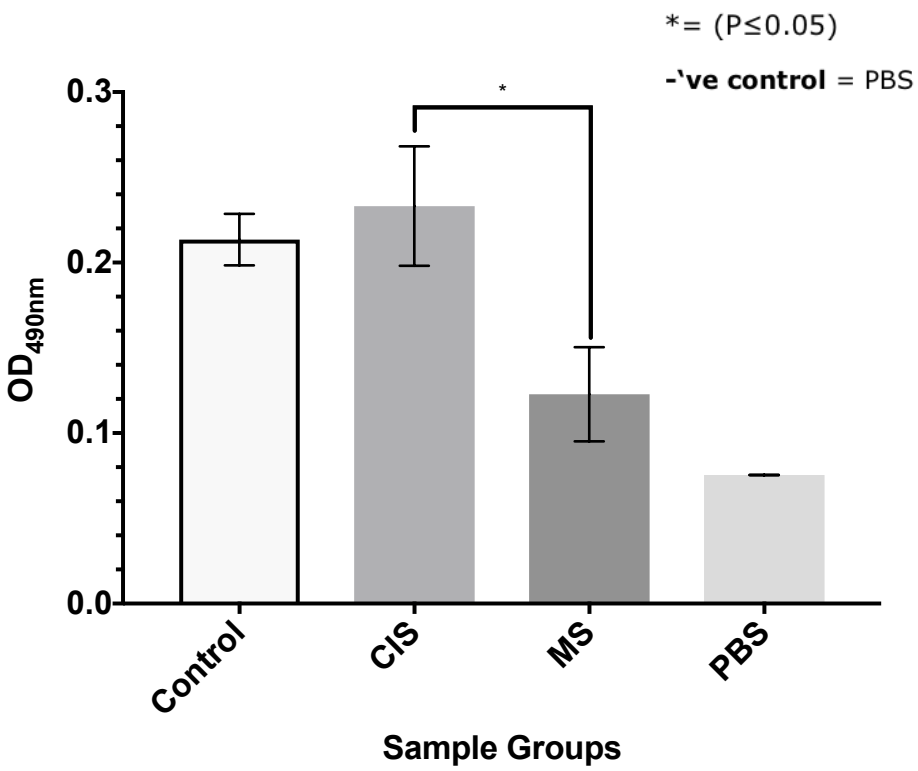

Figure 9-10 - Illustrates optical density measuring mean LDH activity in control, CIS and MS sera groups compared to a PBS negative control. CIS and MS sera groups contain 20 previously tested samples. The control group contains 20 fresh sera samples. A statistically significant difference was identified between the CIS and MS sera at P≤0.05. Results shown are from two measurements recorded at OD_{490nm} of sera samples listed in Appendix C.2 and Appendix C.3. Data analysed using the Kolmogorov-Smirnov unpaired statistical test. The error bars represent the standard error of the mean.

9.3.11 Wild Type ε-toxin CT_{50} Calculation

Using the MTT cytotoxicity assay, the WT ε-toxin CT_{50} dose against CHO-hMAL cells was determined through a two-fold dilution (Figure 9-11). Non-linear regression analysis identified the WT ε-toxin CT_{50} dose at 0.112 µM against CHO-hMAL cells with 95% confidence intervals between 0.077 µM and 0.150 µM.

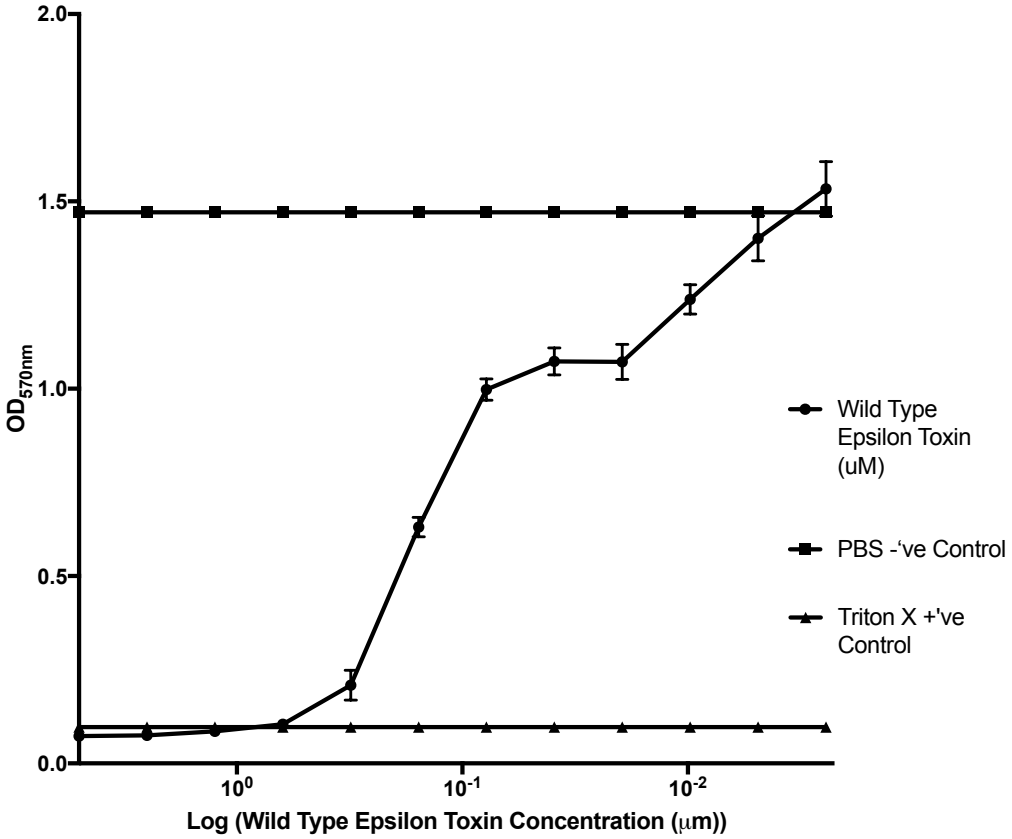

Figure 9-11 - Illustrates optical density measuring formazan production by CHO-hMAL cells. Cells were incubated with a PBS negative control, TritonX positive control or a two-fold dilution of WT ε-toxin at a starting concentration of 5 µM. Results shown are from three replicates measured at OD_{570nm}. The error bars represent the standard error of the mean.

9.3.12 Wild Type ε-toxin Neutralisation Using an Anti-ε PoAb

WT ε-toxin neutralisation was completed with an anti-ε PoAb using MTT cytotoxicity assay. Figure 9-12 illustrates that decreasing the concentration of the anti-ε PoAb corresponds to increased WT ε-toxin ($1xCT_{50}$) cytotoxicity. Evidence of WT ε-toxin neutralisation by the anti-ε PoAb was not observed with cytotoxicity retained at all anti-ε PoAb concentrations used in the assay.

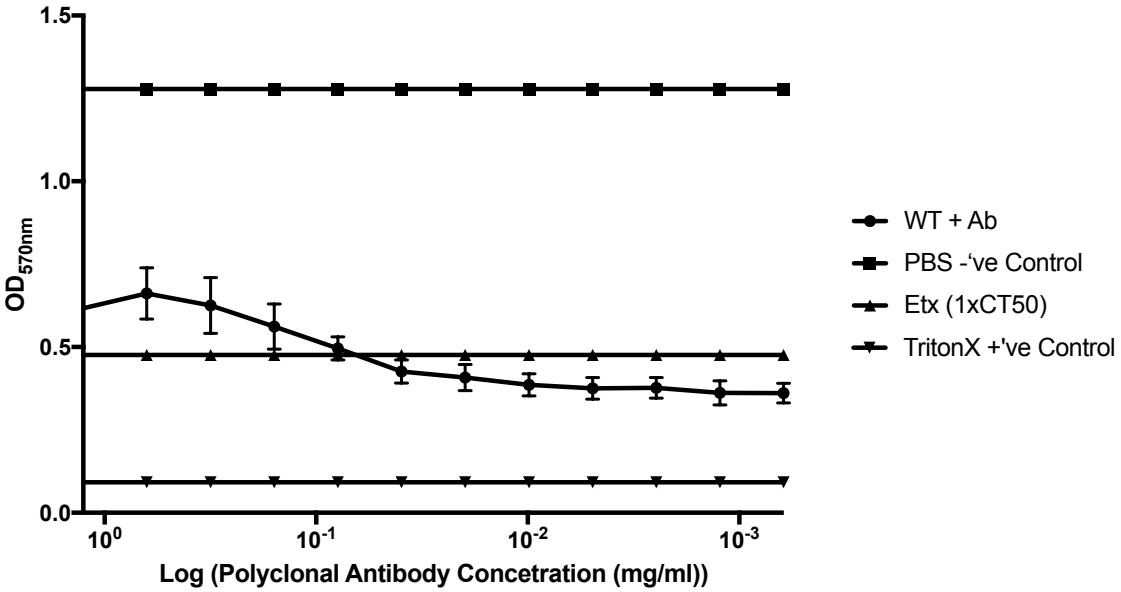

Figure 9-12 - Illustrates optical density measuring mean formazan production by CHO-hMAL cells. Cells were incubated with a PBS negative control, TritonX positive control. WT ε-toxin ($1xCT_{50}$) positive control or WT ε-toxin ($1xCT_{50}$) mixed with anti-ε-PoAb in a two-fold dilution starting at a concentration of 1.26 mg/ml. Results shown are from two replicates measured at OD_{570nm}. The error bars represent the standard error of the mean.

9.4 DISCUSSION

The WT ε-toxin CT_{50} concentration of 0.32 µM obtained in this project was greater than the CT_{50} concentrations of 3.47 nM and 4.00 nM obtained from previous projects (Figure 9-1) [120][85]. The CT_{50} identified in this project illustrates a 92-fold and 8-fold difference compared to the previous CT_{50} results respectively. However, this disparity may be explained by differences in the cell lines and assay methods used between these experiments. WT ε-toxin neutralisation was demonstrated using an anti-ε PoAb up to 0.281 µg/ml and compares closely to a previous experiment where ε-toxin neutralisation was demonstrated up to 0.195 µg/ml in MDCK cells (Figure 9-2) [120]. The results from both of these assays were obtained from two replicates. Consequently, the data presented in Figure 9-1 and Figure 9-2 can only provide the spread of the results without a reliable indication of a statistical mean value. The reliability of the data and conclusions from these assays would therefore be improved with more replicates. Importantly, however, these experiments demonstrated that ε-toxin cytotoxicity and neutralisation could be detected using an LDH based cytotoxicity assay.

WT ε-toxin sera neutralisation results showed that LDH release was greater in the sera groups compared to the ε-toxin positive control (Figure 9-3). These results were unusual since both the sera samples and ε-toxin positive control were incubated with an equivalent $1xCT_{50}$ dose of WT ε-toxin. Therefore it was theoretically impossible for cytotoxicity of the sera/toxin solution to be greater than the $1xCT_{50}$ ε-toxin positive control. Consequently, the neutralisation data strongly suggested that an additional factor was contributing to the cytotoxicity or LDH content in the assay. In order to obtain useable serum neutralisation results, experiments were required to identify the cause of the elevated LDH levels.

Serum samples were first investigated for cytotoxicity against CHO-hMAL cells. Sera cytotoxicity would result in elevated LDH activity that would be detected by the assay. However, no scientific literature had documented the cytotoxicity of human sera to CHO-hMAL cells suggesting that this theory was unlikely to explain the results in Figure 9-3. Serum cytotoxicity results in Figure 9-4

showed consistent OD readings between the sera groups and the PBS negative control. These data suggest that sera from the control, CIS and MS groups were non-toxic to CHO-hMAL cells. As a result, the disproportionate LDH results obtained in Figure 9-3 were highly unlikely to be due to sera cytotoxicity and were probably due to another factor.

Control, CIS and MS sera samples were therefore analysed for levels of the LDH enzyme that could also have contributed to the disproportionate results in Figure 9-3. The presence of LDH in human sera is well documented and was used to investigate a variety of medical conditions [151][152][153][154]. The control, CIS and MS sera all demonstrated elevated LDH results compared to the PBS negative control (Figure 9-5). This suggested that sera LDH activity was responsible for the disproportionate LDH activity observed in Figure 9-3.

Elevated sera LDH activity is normally associated with cellular damage caused by disease and has been previously used by the healthcare industry to investigate illnesses in humans [155][156]. The statistically significant differences identified between the control and CIS sera groups as well as the CIS and MS sera groups suggest that sera LDH levels may be related to differences in tissue damage realised by these conditions (Figure 9-5). Consequently, sera LDH activity could potentially be used as a diagnostic method to distinguish between MS, CIS and healthy patients. The elevated sera LDH activity in CIS sera appears to suggest that there is a possible link between the CIS condition and sera LDH activity. It is possible that the CIS sera LDH levels are related to neurological damage initiated by the CIS condition. However, no previous research has investigated this and therefore it remains unclear if sera LDH levels are indicative of CIS. Conversely, MS patients demonstrated relatively low sera LDH activity suggesting that it is not linked with the condition. However, previous research has reported much greater LDH activity in MS sera compared to the results in this experiment [157].

A possible explanation for this is that the MS sera used in this experiment may have been obtained from patients recovering from CNS damage. This is particularly plausible for patients suffering from remitting relapsing MS, which is characterised by long recovery periods. Patients recovering from tissue damage

could possess reduced sera LDH levels potentially explaining the lower MS sera LDH results observed in Figure 9-5.

However, elevated serum LDH activity can be symptomatic of a wide variety of disorders and therefore cannot be used to identify the cause or origin of LDH within a patient [155]. For example, control sera that was obtained from healthy patients, also showed elevated sera LDH activity potentially symptomatic of tissue damage (Figure 9-5). This emphasises that sera LDH activity can originate from other non-related tissue damage and therefore cannot be linked directly to a particular condition. Further analysis was therefore required to identify the cause of LDH activity within the CIS and MS patients. This was achieved by LDH isoenzyme analysis. The LDH enzyme is composed of four separate peptide chains consisting of H or M sub-units. Varying sub-unit combinations form the five different LDH tetramers, known as isoenzymes (Table 9-7) [158]. These five different LDH isoenzymes demonstrate tissue specificity and can therefore be used clinically to localise the source of LDH release within a patient [155]. To do this, electrophoresis is used to separate the isoenzymes based on their differing electrophoretic mobility's [155]. The proportion of each LDH isoenzyme can then be calculated to estimate the source of the LDH release.

LDH Isoenzyme	Tetramer Subunit Composition	Sera Concentration	Tissue Localisation
LDH-1	H_4	19 -30% [155]	Cardiac muscle, Erthrocytes and kidneys
LDH-2	H_3M_1	32-48% [155]	Cardiac muscle, erythrocytes, kidneys
LDH-3	H_2M_2	12-22% [155]	Lung, Pancreas, Lymphatic Tissue
LDH-4	H_1M_3	5-11% [155]	Placenta, pancreas
LDH-5	M_4	5-13% [155]	Skeletal Muscle and Liver

Table 9-7 - Structural composition, serum concentrations and tissue localisation and of the five LDH isoenzymes in humans.

LDH isoenzyme concentrations in CIS and control sera were largely consistent with reported sera concentrations ranges described in Table 9-7 and the typical LDH ratios identified in human sera (Figure 9-6) [155]. No statistical differences were identified between the control and CIS LDH isoenzyme activity suggesting that it cannot be used to differentiate between control and CIS patients. Arguably, the mean CIS LDH1 activity of 34% was slightly elevated and may be suggestive of tissue damage related to demyelination events characteristic of the condition (Figure 9-6). Previous research investigating sera LDH levels in MS sera suggested that these abnormal LDH concentrations may also be consistent with erythrocyte haemolysis [157][159]. Erythrocytes contain high LDH1 concentrations and are more osmotically fragile during acute stages of disease in MS patients compared to control patients [160][159]. Consequently, these data could suggest that the elevated CIS LDH1 activity in Figure 9-6 is suggestive of erythrocyte haemolysis. However, LDH1 activity is common with many other medical conditions and therefore may be unrelated to CIS. As a result, the data from Figure 9-6 largely suggests that there is no link between

sera LDH activity and the development of CIS.

Furthermore, comparison between the GOSH isoenzyme assay and the LDH cytotoxicity assay revealed a line of best fit between the sera LDH results of both datasets (Figure 9-7). This demonstrated that the LDH cytotoxicity data showed close reproducibility to the GOSH LDH data that was completed independently and indicated that the previous LDH cytotoxicity assay results were reliable.

The high LDH variability between the different sera groups in Figure 9-5 suggested that sera samples within a patient group demonstrated different LDH activities. Since sera samples were obtained from four different hospitals it was proposed that sera LDH variability may be linked to the sera's hospital of origin. The data demonstrated clear differences in sera LDH activity between control and MS sera samples obtained from different hospitals (Figure 9-8). Highly significant differences were identified between control sera obtained from the Exeter RILD, Exeter Medical School and Barts NHS Trust. Similarly MS sera obtained from the Exeter Medical School and Barts NHS Trust was also shown to be very statistically different (Figure 9-8). These data strongly suggest that sera LDH variability observed in Figure 9-5 is related to the hospital of origin, and may be caused by differences in sera handling procedures at these different hospitals.

Scientific literature has documented the susceptibility of the LDH enzyme to inactivation by freeze thaw cycles [161][162]. *Nema* et al. identified that LDH activity decreased sharply following successive freeze thaw cycles with 95% inactivation of LDH observed after five freeze thaw cycles [161]. This research suggests that the sera LDH variability seen in Figure 9-8 could be related to differences in the freeze thaw cycle history of each sera sample. Although undocumented, it is possible that sera samples used in this project were exposed to different numbers of freeze thaw cycles at different hospitals which could explain the variable LDH profiles observed in Figure 9-8. Furthermore, sera samples were exposed to freeze thaw cycles during the course of the project that could also have affected sera LDH activity observed during different

experiments in the project.

The data in Figure 9-8 suggests that sera handling differences between different hospitals contributed to variability in LDH levels between sera samples. This sera LDH variability could potentially invalidate the previously obtained sera LDH and sera neutralisation data (Figure 9-2) and (Figure 9-5). To investigate this further, fresh standardised control sera were obtained from the Exeter RILD and compared to previously tested control, MS and CIS sera from Figure 9-8. The fresh Exeter RILD control sera were subject to identical handling and storage conditions and were therefore unaffected by LDH inactivation by repeated freeze thaw cycles. Figure 9-9 identified that the fresh control sera demonstrated significantly greater LDH activity compared to the previously tested control group and increased LDH activity compared to the previously tested CIS and MS sera groups (Figure 9-10). In both experiments, the fresh control sera demonstrated reduced error bars compared to the other sera groups. This suggested that there was reduced LDH variability between individual samples, possibly due to the more consistent handling conditions. Furthermore, the statistically significant difference between the previously tested control sera and CIS sera in Figure 9-5 was not present using the fresh control sera in Figure 9-10. This suggested that the LDH levels between the CIS and fresh control sera were similar. This therefore negated the previous claim that sera LDH activity could be used to diagnose between control, CIS and MS patients. As a result, the sera LDH data suggested that the fresh standardised sera produced more reliable sera LDH results compared to sera obtained from different hospitals. This indicated that consistent sera handling practices were required in order to mitigate sera LDH variability between sera samples.

Sera LDH variability observed in Figure 9-5 suggested that the LDH based cytotoxicity assay was inappropriate for investigating sera neutralisation of WT ε-toxin. Consequently, an LDH independent MTT assay was employed to investigate sera neutralisation of ε-toxin. Using the MTT assay, WT ε-toxin CT_{50} dose was calculated at 0.112 μM. This demonstrated a 2.8 fold reduction compared to the LDH assay CT_{50} of 0.322 μM, which suggests that the MTT assay is more sensitive to cytotoxicity than the LDH method. The MTT assay CT_{50} concentration also demonstrated a 32 fold and 2.8 fold difference

compared to the CT_{50} concentrations described in other experiments [120][85]. However, differences in cell lines and assay could explain this disparity. WT ε-toxin anti-ε PoAb neutralisation levels remained consistent around the $1xCT_{50}$ positive control for all antibody concentrations used in the MTT assay (Figure 9-12). This suggested that the anti-ε PoAb failed to neutralise WT ε-toxin. These data are in contrast to the previous LDH based WT ε-toxin neutralisation assay where strong neutralisation was demonstrated using the same anti-ε PoAb solution (Figure 9-2). Furthermore, the WT ε-toxin neutralisation analysis in Figure 9-12 was completed using two replicates only. Consequently, the data presented in Figure 9-12 can only provide the spread of the results without a reliable indication of a statistical mean value. Despite the small spread of the results, the reliability of the WT ε-toxin neutralisation analysis shown in Figure 9-12 would be improved with more replicates.

Differences between the Triton X positive control and PBS negative control in Figure 9-12 suggest that the CHO-hMAL cells were sufficiently confluent for the experiment to work. This therefore suggests that cell viability differences were not responsible for the observed neutralisation profile. As a result, there are two variables that may explain the data observed in Figure 9-12:

1) The anti-ε PoAb may have become ineffective for WT ε-toxin neutralisation. However, this is considered unlikely since the antibody was stored undisturbed at -80°C, and therefore its activity should have remained unchanged.

2) The similarity between the WT ε-toxin neutralisation and $1xCT_{50}$ control data in Figure 9-12 suggests that WT ε-toxin could have been overly concentrated for anti-ε PoAb neutralisation. This suggests that there may have been a previous error in calculating WT ε-toxin's CT_{50} concentration in Figure 9-11 or in generating the WT ε-toxin + anti-ε PoAb solution for the MTT neutralisation assay.

Further testing is therefore required to correct the MTT WT ε-toxin neutralisation error. Serum neutralisation of WT ε-toxin can then be investigated using the MTT assay.

Amendments could be made to the sera neutralisation method to produce a more robust analysis. For example, the current neutralisation method assumes that WT ε-toxin neutralisation levels will be representative of the total anti ε-toxin antibodies present in the sera. However, this method does not consider the relative differences in antibody levels between the different sera samples. This means that, irrespective of their antibody content, sera samples with more concentrated antibody levels are more likely to display greater neutralisation than those with less concentrated antibody levels. To correct this, antibody levels should be analysed for each serum sample. Comparing the sera antibody levels with their respective neutralisation results will identify the relative neutralisation profile of each serum sample.

To complete this analysis, purification of the immunoglobulin fraction is required for each serum sample. Centrifugation, dextran substrate treatment and ammonium sulphate precipitation of the sera samples will first be required to remove cell debris, lipoproteins and low molecular weight contaminants from the sera respectively [163]. Following resolubilisation, the antibody levels can then be compared using affinity chromatography. The most suitable analytical method would be to compare serum IgG levels, as this immunoglobulin class represents 70-75% of all antibodies present in human serum. This can be achieved using Protein G or Protein A purification. These techniques bind IgG antibodies based on their high affinity for the protein G and protein A bacterial components from the Group G *Streptococci* and *Staphylococcus aureus,* bacteria respectively [163]. Both methods are highly reliable with purity results commonly exceeding 95% [163]. However, while protein G binds to all human IgG subclasses, protein A is unable to bind IgG_3, and also possesses moderate binding affinity for human IgM [164][165]. This suggests that the protein G affinity chromatography technique would be the most appropriate technique for accurate IgG purification.

Following antibody purification, the purified IgG concentrations can be quantified for all serum samples using the NanoDrop A280 function. IgG levels could also be analysed using the Bradford, Lowry, or BCA techniques and concentrations identified by comparison to a known IgG standard. Alternatively, commercially available indirect human IgG ELISA kits can also be used to

quantify sera IgG [166]. The resulting colour change is proportional to the sample IgG concentration that can be determined by comparison to a known IgG standard. Used in conjugation with previously described purification methods, the high specificity of the ELISA technique would further protect against any sample contaminants following antibody purification. This method would therefore ensure greater accuracy compared to the NanoDrop, BCA, Bradford, and Lowry techniques that measure protein concentrations more indiscriminately. However, the reportedly high purity results of the affinity chromatography methods (>95%) mean that any sample contamination is likely to be very low [163]. As a result, the increased accuracy afforded by the ELISA technique may not be necessary. The indirect human IgG ELISA can also be performed using crude sera samples without any prior purification steps [166]. This technique could therefore help to save time by eliminating the need for the previously mentioned antibody purification steps. Although faster to complete, the ELISA method would be a more expensive technique to perform.

Furthermore, the IgG quantification procedure would require the testing of a large number of sera samples. Consequently, the suitability of each quantification method for mass analysis should also be considered. For example, the NanoDrop IgG quantification method would most likely require the individual testing of each purified sera IgG sample. Whereas the ELISA, Bradford, BCA, and Lowry techniques are compatible, or can be adapted, for use with a 96-well plate. The latter methods may therefore be more applicable for sera IgG quantification due to their increased suitability for mass sample analysis.

Following quantification, sera IgG concentrations can be directly compared to their respective MTT assay neutralisation results. WT ε-toxin neutralisation can then be better analysed between the different sera groups. This will produce a more relevant neutralisation assay that accounts for differences in sera antibody levels.

The sera neutralisation assay results presented in Figure 9-3 demonstrated disproportionate cytotoxicity for the control, CIS and MS sera. Consequently, the results in Project 2 neither support nor reject the hypothesis. Further

investigation in Figure 9-5 suggests that these results were due to sera LDH activity interfering with the assay. Consequently, the data from Figure 9-3 cannot establish if control, MS or CIS patient sera confers cytotoxic protection to CHO-hMAL cells against ε-toxin. Furthermore, the project data cannot validate the presence of anti ε-toxin antibodies in the different sera groups.

Results from Figure 9-8 strongly suggest that serum sample variability is due to differences in sera handling techniques between different hospitals. This suggests that future sera neutralisation analysis should be completed using standardised sera samples. Relative differences between sera antibody levels should also be considered. Sera LDH interference with the LDH cytotoxicity assay also suggests that the alternative MTT assay should be employed for future sera neutralisation experiments. With these improvements, future experiments will yield a superior analysis to support or reject the project hypothesis statement that: “Compared to control sera, MS and CIS patient sera will confer greater cytotoxic protection to CHO-hMAL cells against ε-toxin due to the presence of anti ε-toxin antibodies”.

9.5 FUTURE WORK

9.5.1 GOSH LDH Data

The data in Figure 9-6 revealed increased LDH-1 activity in CIS sera compared to control sera. Previous research has suggested that elevated LDH-1 activity could be indicative of increased erythrocyte haemolysis in MS sera [157]. Erythrocytes are known to contain high LDH-1 concentrations suggesting that erythrocyte haemolysis could also be consistent with the elevated CIS LDH-1 activity observed in Figure 9-6. Consequently, it may be of value to investigate haemolysis and erythrocyte fragility in the CIS samples. MS sera was not investigated in this assay, however, it may be of value to investigate LDH isoenzyme patterns in MS patients and to identify if there are signs of erythrocyte haemolysis.

9.5.2 Standardised Sera Samples

Data in Figure 9-8 suggests that the sera LDH differences are due to sera handling differences between different hospitals. These differences may have also influenced the sera antibody levels between different sera samples that could have affected the neutralisation data in Figure 9-3. Consequently, these data suggest that future sera experiments require fresh standardised sera samples obtained from a single hospital to reduce the risk of sera antibody variability between serum samples.

9.5.3 MTT Neutralisation

The negligible WT ε-toxin neutralisation results in Figure 9-12 suggests there is an issue regarding the efficacy of the anti-ε PoAb or in the WT ε-toxin 1xCT_{50} concentration. Consequently, further testing is required to identify the error responsible for the neutralisation data in Figure 9-12. Once corrected, the project can then advance to the sera neutralisation work using the MTT assay. The sera neutralisation assay could be further improved by investigating differences in IgG levels between the different serum samples. Comparing sera IgG activity with their respective neutralisation results will produce a more robust analysis that accounts for differences in sera antibody levels.

9.5.4 Conclusions

The experiments completed in this project aimed to investigate WT ε-toxin neutralisation using sera obtained from control, CIS and MS patients. However, subsequent work identified that the sera samples contained high levels of the LDH enzyme that distorted neutralisation results obtained using the LDH cytotoxicity assay. Variability in sera LDH activity indicated that sera LDH levels may be useful as a diagnostic biomarker for CIS and MS development. However, later experiments identified that this variability was likely introduced through differences in sera handling techniques performed between different sera banks and hospitals. This variability strongly suggests that sera experiments should be completed using fresh standardised sera samples to ensure greater experimental control. Consequently, future work should concentrate on investigating sera neutralisation of WT ε-toxin using the LDH independent MTT assay. However, experiments investigating sera LDH levels indicate that erythrocyte haemolysis in CIS and MS patients could be of value to investigate further.

10 THESIS CONCLUSION

The research completed as part of this thesis addressed two different topics concerning *C. perfringens* ε-toxin. Project 1 investigated the suitability of several SDM targets for development of a next generation veterinary vaccine against ε-toxin. Using the methods described in this project, SDM was successfully used to introduce several mutations into ε-toxin's BOG binding domain. These mutants were subsequently transformed, expressed, purified and analysed for cytotoxicity against CHO-hMAL cells. Cytotoxicity analysis demonstrated that all seven mutants reduced ε-toxin cytotoxicity towards CHO-hMAL cells, with the V72F, V166F and A168F samples resulting in considerable cytotoxicity reductions. Despite contamination of the V72A, V166A and V166F samples, the results obtained in Project 1 suggest that the BOG binding site is important in mediating ε-toxin's cytotoxicity towards CHO-hMAL cells. This also provides further evidence to suggest that the MAL protein is a receptor, or forms part of a co-receptor complex for ε-toxin binding. Importantly, the results from this project have identified several mutagenesis targets that will advance the development of a next generation veterinary vaccine against ε-toxin. This vaccine will help to provide a more reliable, controlled and safer ε-toxin immunisation platform compared to the current formaldehyde vaccine

Project 2 investigated MS, CIS and control sera for ε-toxin immunogenicity, to identify if sera obtained from MS patients could confer cytotoxic protection to CHO-hMAL cells. Using the methods described in this project, ε-toxin's CT_{50} concentration against CHO-hMAL cells was identified. ε-toxin neutralisation was then successfully demonstrated using a polyclonal antibody. Sera neutralisation analysis of ε-toxin was unsuccessful. Subsequent analysis strongly suggests that this was due to sera LDH activity interfering with the cytotoxicity assay. Results from further investigation indicate that a more effective sera neutralisation analysis could be completed using standardised sera samples and using an LDH independent MTT cytotoxicity assay. Relative differences between sera antibody levels should also be analysed to better compare the neutralisation profile of each sera sample. Consequently, this project was unable to establish if MS sera samples possess different ε-toxin immunoreactivity levels compared to control of CIS sera. Several improvements

have been recommended to provide a more robust analysis that will identify if there is a credible link between ε-toxin and the development of MS in humans.

APPENDIX A SITE DIRECTED MUTAGENESIS DNA SEQUENCES

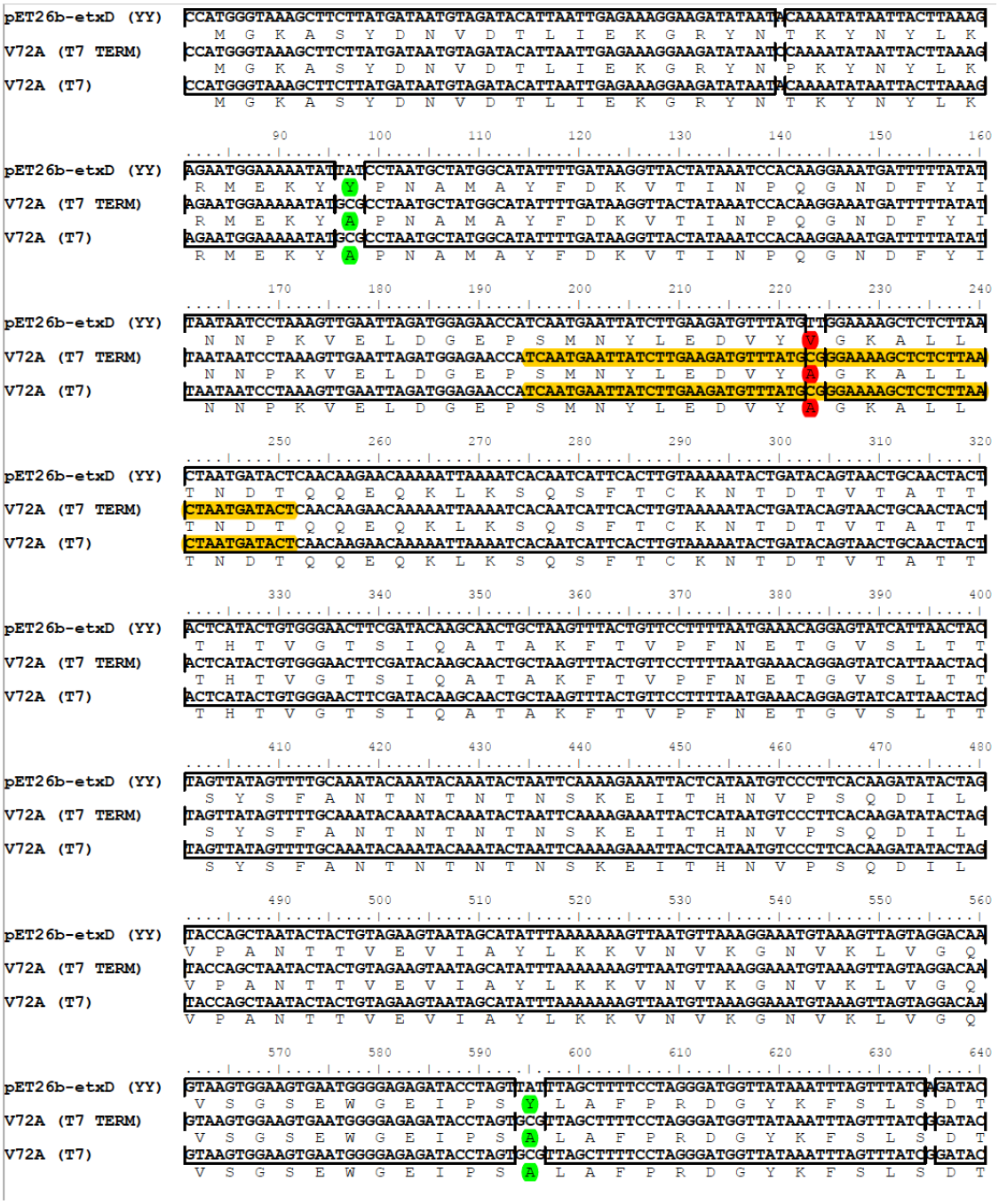

Figure A - 1 - V72A partial DNA sequence following transformation into XL10 Gold E.coli. Sequencing analysis was completed using T7 and T7 term primers. The figure shows the V72A primers heighted in yellow with the V72A amino acid substitution in red. The Y43A and Y209A mutations are highlighted in green

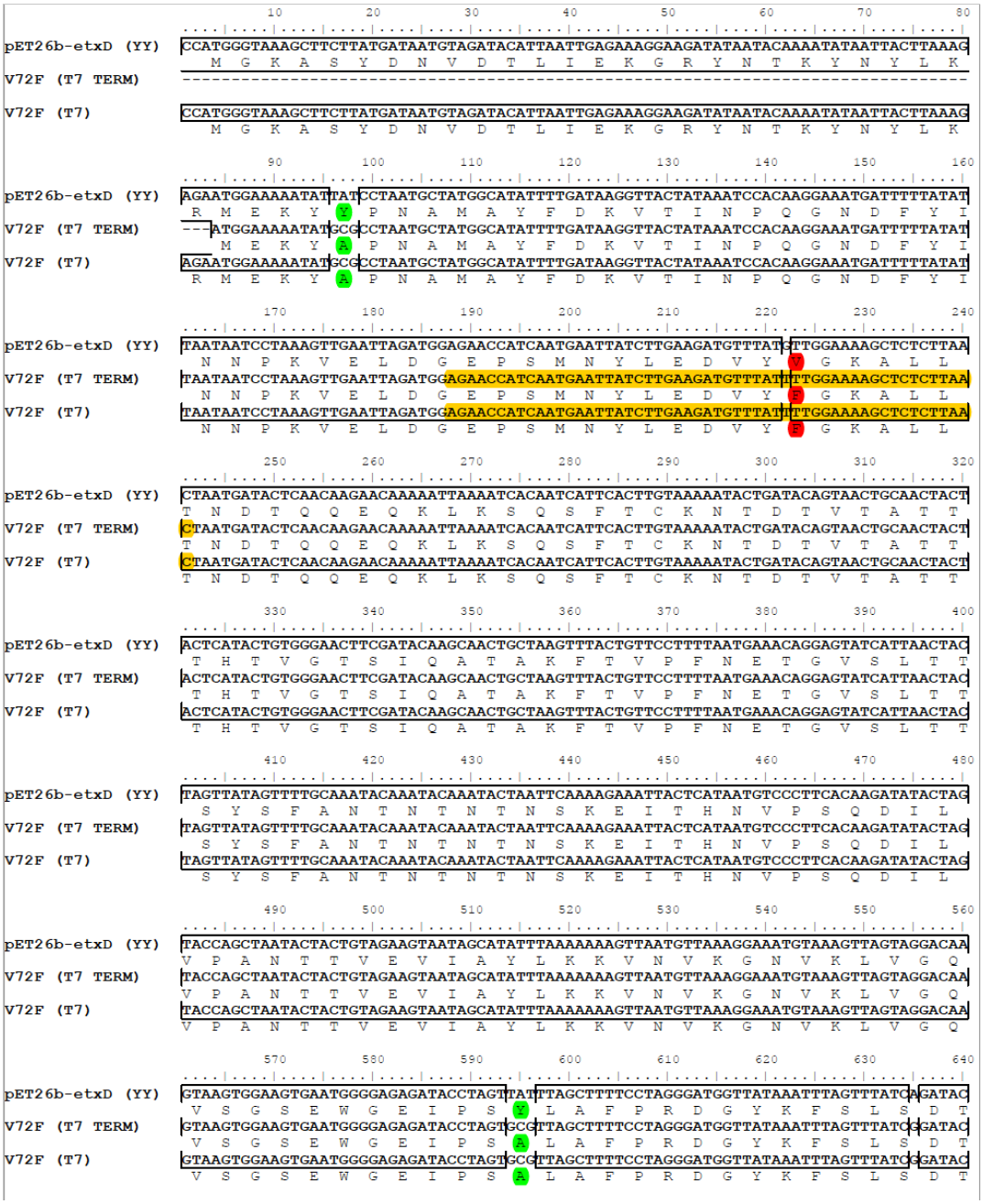

Figure A - 2 - V72F partial DNA sequence following transformation into XL10 Gold E.coli. Sequencing analysis was completed using T7 and T7 term primers. The figure shows the V72F primers heighted in yellow with the V72F amino acid substitution in red. The Y43A and Y209A mutations are highlighted in green

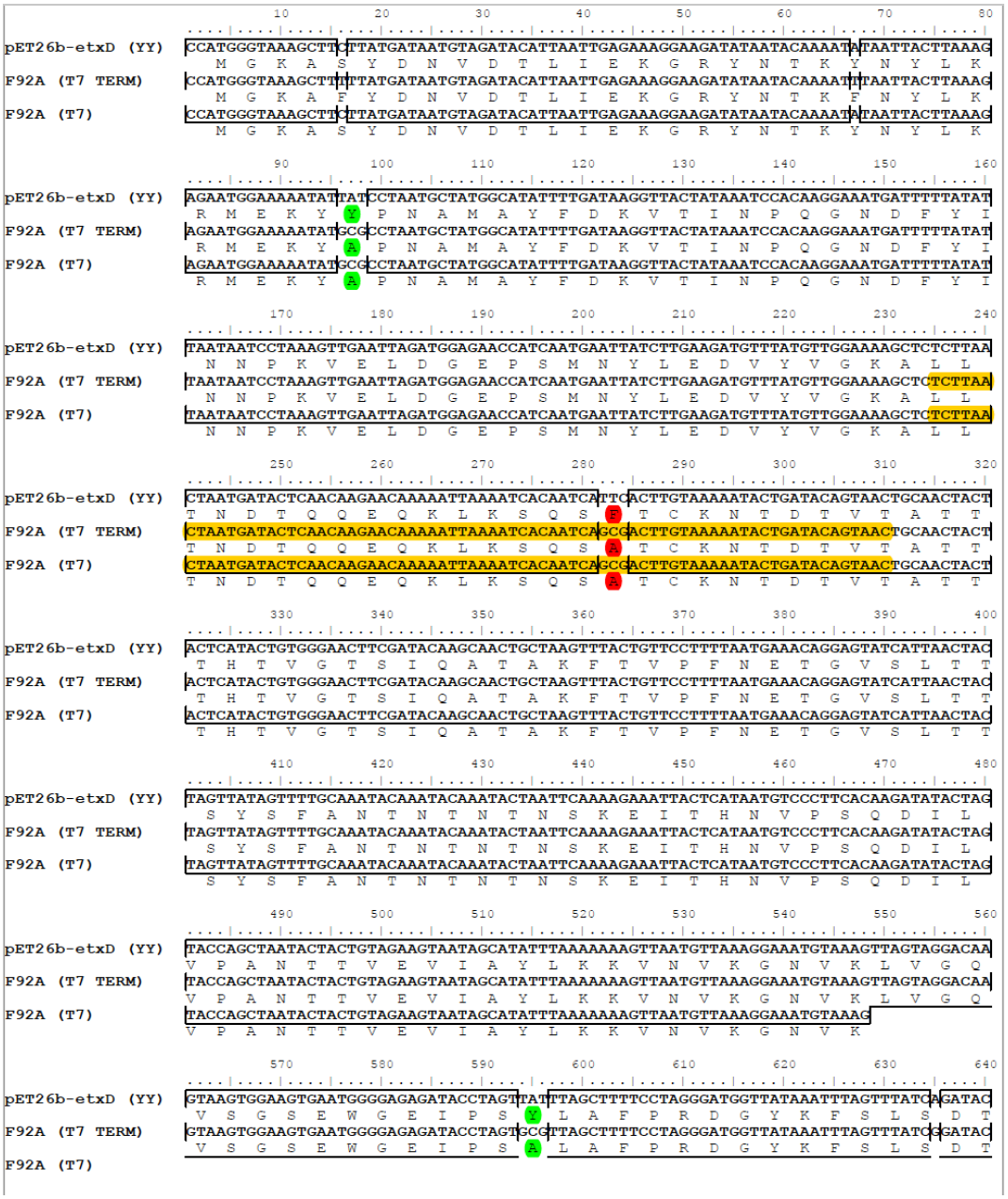

Figure A - 3 - F92A partial DNA sequence following transformation into XL10 Gold E.coli. Sequencing analysis was completed using T7 and T7 term primers. The figure shows the F92A primers heighted in yellow with the F92A amino acid substitution in red. The Y43A and Y209A mutations are highlighted in green.

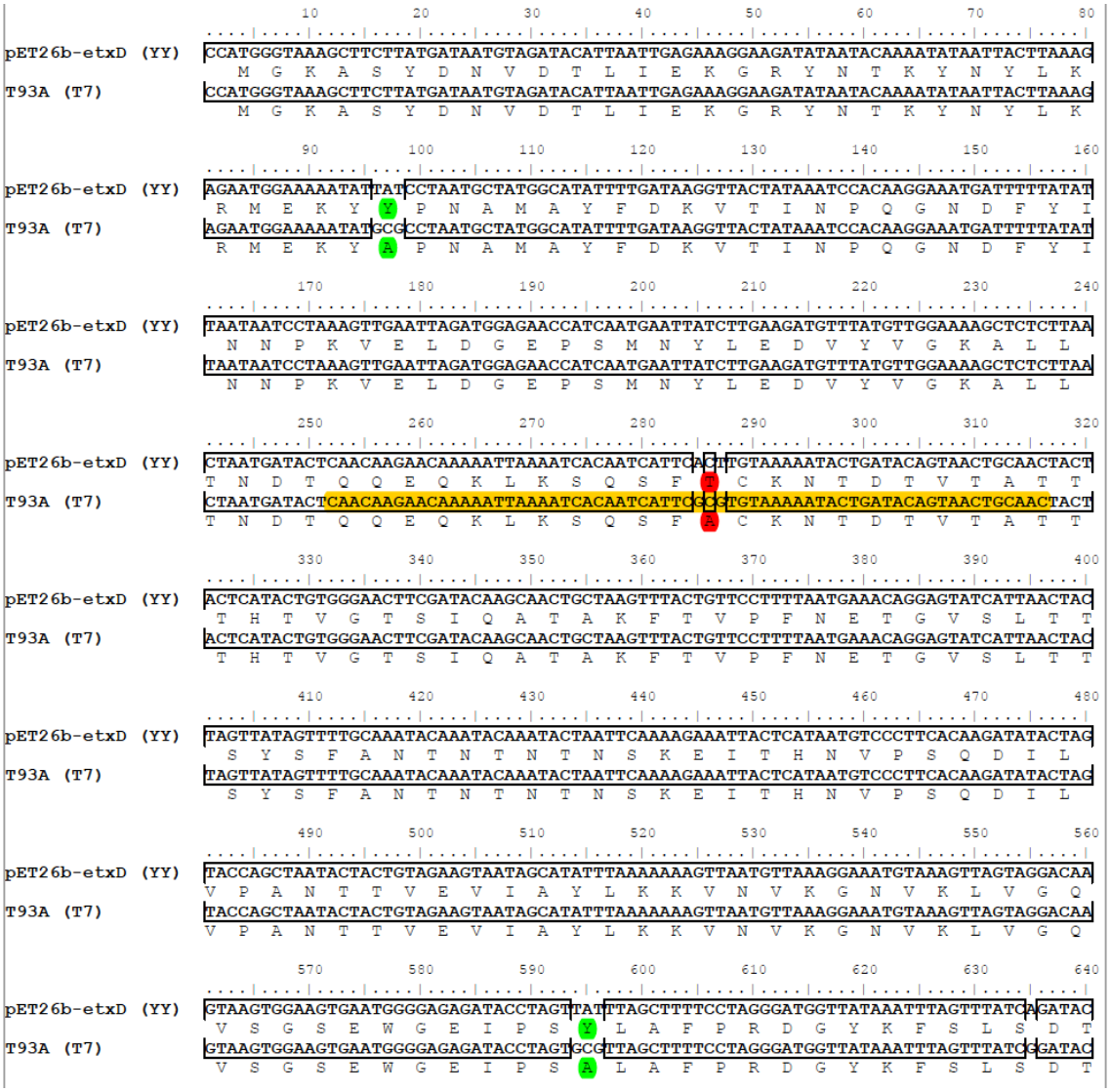

Figure A - 4 - T93A partial DNA sequence following transformation into XL10 Gold E.coli. Sequencing analysis was completed using T7 and T7 term primers. The figure shows the T93A primers heighted in yellow with the T93A amino acid substitution in red. The Y43A and Y209A mutations are highlighted in green.

Figure A - 5 - V166A partial DNA sequence following transformation into XL10 Gold E.coli. Sequencing analysis was completed using T7 and T7 term primers. The figure shows the V166A primers heighted in yellow with the V166A amino acid substitution in red. The Y43A and Y209A mutations are highlighted in green.

Figure A - 6 - V166F partial DNA sequence following transformation into XL10 Gold E.coli. Sequencing analysis was completed using T7 and T7 term primers. The figure shows the V166F primers heighted in yellow with the V166F amino acid substitutions in red. The Y43A and Y209A mutations are highlighted in green.

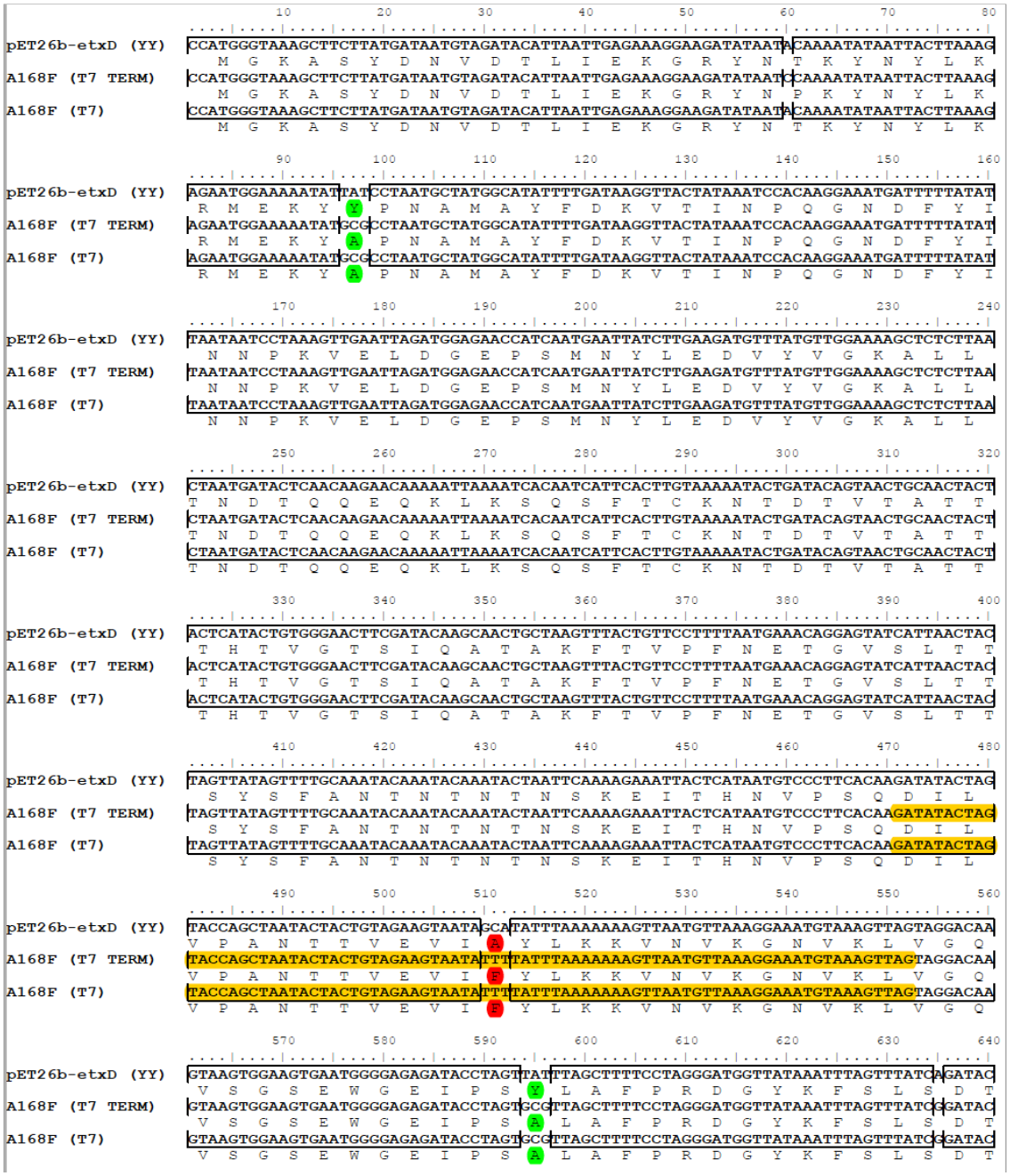

Figure A - 7 - A168F partial DNA sequence following transformation into XL10 Gold E.coli. Sequencing analysis was completed using T7 and T7 term primers. The figure shows the A168F primers heighted in yellow with the A168F amino acid substitutions in red. The Y43A and Y209A mutations are highlighted in green.

APPENDIX B LIST OF MUTAGENESIS OLIGONUCLEOTIDE SEQUENCES

Oligonucleotide	Sequence (5’ to 3’)	Details
V72F_rev	5'GTTAAGAGAGCTTTTC CAAAATAAACATCTTCAA GATAATTCATTGATGGTT CT 3'	SDM reverse primer coding for V72F Amino acid substitution
V72F_fwd	5'AGAACCATCAATGAATT ATCTTGAAGATGTTTATT TTGGAAAAGCTCTCTTAA C 3'	SDM forward primer coding for V72F Amino acid substitution
V72A_rev	5'GAGTATCATTAGTTAAG AGAGCTTTTCCCGCATA AACATCTTCAAGATAATT CATTGA 3'	SDM reverse primer coding for V72A Amino acid substitution
V72A_fwd	5'TCAATGAATTATCTTGA AGATGTTTATGCGGGAA AAGCTCTCTTAACTAATG ATACTC 3'	SDM forward primer coding for V72A Amino acid substitution
F92A_rev	5'GTTACTGTATCAGTATT TTTACAAGTCGCTGATTG TGATTTTAATTTTTGTTCT TGTTGAGTATCATTAGTT AAGA 3'	SDM reverse primer coding for F92A Amino acid substitution

Oligonucleotide	Sequence (5’ to 3’)	Details
F92A_fwd	5'TCTTAACTAATGATACT CAACAAGAACAAAAATTA AAATCACAATCAGCGAC TTGTAAAAATACTGATAC AGTAAC 3'	SDM forward primer coding for F92A Amino acid substitution
T93A_rev	5'GTTGCAGTTACTGTAT CAGTATTTTTACACGCGA ATGATTGTGATTTTAATT TTTGTTCTTGTTG 3'	SDM reverse primer coding for T93A Amino acid substitution
T93A_fwd	5'CAACAAGAACAAAAATT AAAATCACAATCATTCGC GTGTAAAAATACTGATAC AGTAACTGCAAC 3'	SDM forward primer coding for T93A Amino acid substitution
V166F_rev	5'CCTTTAACATTAACTTT TTTTAAATATGCTATAAA TTCTACAGTAGTATTAGC TGGTACTAGTATAT 3'	SDM reverse primer coding for V166F Amino acid substitution
V166F_fwd	5'ATATACTAGTACCAGCT AATACTACTGTAGAATTT ATAGCATATTTAAAAAAA GTTAATGTTAAAGG 3'	SDM forward primer coding for V166F Amino acid substitution
V166A_rev	5'CTTTAACATTAACTTTT TTTAAATATGCTATCGCT TCTACAGTAGTATTAGCT GGTACTAGTAT 3'	SDM reverse primer coding for V166A Amino acid substitution

Oligonucleotide	Sequence (5’ to 3’)	Details
V166A_fwd	5'ATACTAGTACCAGCTA ATACTACTGTAGAAGCG ATAGCATATTTAAAAAAA GTTAATGTTAAAG 3'	SDM forward primer coding for V166A Amino acid substitution
A168F_rev	5'CTAACTTTACATTTCCT TTAACATTAACTTTTTTTA AATAAAATATTACTTCTA CAGTAGTATTAGCTGGT ACTAGTATATC 3'	SDM reverse primer coding for A168F Amino acid substitution
A168F_fwd	5'GATATACTAGTACCAG CTAATACTACTGTAGAAG TAATATTTTATTTAAAAAA AGTTAATGTTAAAGGAAA TGTAAAGTTAG 3'	SDM forward primer coding for A168F Amino acid substitution

Table B - 1 - Illustrates the oligonucleotide primers for used for the site directed mutagenesis of ε-toxin

APPENDIX C LIST OF SERA SAMPLES

C.1 HUMAN SERA SAMPLE INFORMATION (SAMPLE GROUP 1)

Serum ID	Patient Group	Gender	Hospital of Origin	Year of Birth
PEGN 2	MS	F	Exeter Medical School	1958
PEGN 3	MS	F	Exeter Medical School	1972
PEGN 11	Control	F	Exeter Medical School	1961
PEGN 12	Control	F	Exeter Medical School	1970
PEGN 13	Control	F	Exeter Medical School	1963
PEGN 23	MS	F	Exeter Medical School	1967
CIS-301	CIS	F	Charing Cross Hospital	1944
CIS-303	CIS	F	Charing Cross Hospital	1966
CIS-304	CIS	F	Charing Cross Hospital	1965
CIS-305	CIS	M	Charing Cross Hospital	1969
CIS-309	CIS	F	Charing Cross Hospital	1955
CIS-310	CIS	F	Charing Cross Hospital	1972
CIS-311	CIS	F	Charing Cross Hospital	1996
BLT-126	MS	N/A	Barts NHS Trust	N/A
BLT-128	MS	M	Barts NHS Trust	1967
BLT-129	MS	M	Barts NHS Trust	1972
BLT-134	MS	F	Barts NHS Trust	1989
BUH-174	Control	M	Barts NHS Trust	1941
BUH-226	Control	F	Barts NHS Trust	1964
BUG-241	Control	M	Barts NHS Trust	1971

C.2 HUMAN SERA SAMPLE INFORMATION (SAMPLE GROUP 2)

Serum ID	Patient Group	Gender	Hospital of Origin	Year of Birth
A1	Control	N/A	Exeter RILD	N/A
A2	Control	F	Exeter RILD	1963
A3	Control	F	Exeter RILD	1980
A4	Control	F	Exeter RILD	1959
PEGN 11	Control	F	Exeter Medical School	1961
PEGN 12	Control	F	Exeter Medical School	1970
PEGN 13	Control	F	Exeter Medical School	1963
PEGN-14	Control	F	Exeter Medical School	1970
PEGN-15	Control	F	Exeter Medical School	1960
PEGN-16	Control	F	Exeter Medical School	1980
PEGN-17	Control	M	Exeter Medical School	1968
PEGN-18	Control	F	Exeter Medical School	1979
PEGN-19	Control	F	Exeter Medical School	1990
PEGN-20	Control	F	Exeter Medical School	1965
PEGN-22	Control	F	Exeter Medical School	1970
BUH-228	Control	N/A	Barts NHS Trust	N/A
BUH-233	Control	N/A	Barts NHS Trust	N/A
BUH-236	Control	N/A	Barts NHS Trust	N/A
BUH-239	Control	N/A	Barts NHS Trust	N/A
BUH-241	Control	M	Barts NHS Trust	1971
CIS-300	CIS	F	Charing Cross	1973
CIS-301	CIS	F	Charing Cross	1944
CIS-302	CIS	N/A	Charing Cross	N/A
CIS-303	CIS	F	Charing Cross	1966

Serum ID	Patient Group	Gender	Hospital of Origin	Year of Birth
CIS-304	CIS	F	Charing Cross	1965
CIS-305	CIS	M	Charing Cross	1969
CIS-306	CIS	F	Charing Cross	1974
CIS-307	CIS	N/A	Charing Cross	N/A
CIS-308	CIS	N/A	Charing Cross	N/A
CIS-309	CIS	F	Charing Cross	1955
CIS-310	CIS	F	Charing Cross	1972
CIS-311	CIS	F	Charing Cross	1996
CIS-312	CIS	F	Charing Cross	1992
CIS-313	CIS	F	Charing Cross	1987
CIS-314	CIS	N/A	Charing Cross	N/A
CIS-315	CIS	M	Charing Cross	1965
CIS-316	CIS	F	Charing Cross	1978
CIS-317	CIS	F	Charing Cross	1984
CIS-318	CIS	F	Charing Cross	1985
CIS-319	CIS	M	Charing Cross	1988
PEGN-1	MS	N/A	Exeter Medical School	N/A
PEGN-2	MS	F	Exeter Medical School	1958
PEGN-3	MS	F	Exeter Medical School	1972
PEGN-4	MS	N/A	Exeter Medical School	N/A
PEGN-6	MS	N/A	Exeter Medical School	N/A
PEGN-7	MS	N/A	Exeter Medical School	N/A
PEGN-8	MS	N/A	Exeter Medical School	N/A
PEGN-9	MS	N/A	Exeter Medical School	N/A
PEGN-10	MS	N/A	Exeter Medical School	N/A

Serum ID	Patient Group	Gender	Hospital of Origin	Year of Birth
PEGN-21	MS	N/A	Exeter Medical School	N/A
PEGN-23	MS	F	Exeter Medical School	1967
BLT-128	MS	M	Barts NHS trust	1967
BLT-129	MS	M	Barts NHS trust	1972
BLT-130	MS	M	Barts NHS trust	1952
BLT-131	MS	F	Barts NHS trust	1967
BLT-132	MS	N/A	Barts NHS trust	N/A
BLT-133	MS	F	Barts NHS trust	1978
BUH-135	MS	M	Barts NHS trust	1943
BUH-136	MS	F	Barts NHS trust	1944
BUH-137	MS	M	Barts NHS trust	1969

C.3 HUMAN SERA SAMPLE INFORMATION (SAMPLE GROUP 3)

Serum ID	Patient Group	Gender	Hospital of Origin	Year of Birth
A1	Control	N/A	Exeter RILD	N/A
A2	Control	F	Exeter RILD	1963
A3	Control	F	Exeter RILD	1980
A4	Control	F	Exeter RILD	1959
A5	Control	F	Exeter RILD	1959
A6	Control	F	Exeter RILD	1953
A7	Control	M	Exeter RILD	1972
A8	Control	F	Exeter RILD	1974
A9	Control	M	Exeter RILD	1965
A10	Control	F	Exeter RILD	1946
A11	Control	F	Exeter RILD	1956
A12	Control	M	Exeter RILD	1943
B1	Control	N/A	Exeter RILD	N/A
B2	Control	F	Exeter RILD	1952
B3	Control	M	Exeter RILD	1956
B4	Control	N/A	Exeter RILD	N/A
B5	Control	F	Exeter RILD	1965
B6	Control	F	Exeter RILD	1947
B7	Control	F	Exeter RILD	1961
B8	Control	N/A	Exeter RILD	N/A

BIBLIOGRAPHY

1. Hailegebreal G. 2017 A Review on Clostridium Perfringens Food Poisoning. **4**, 104–109.

2. Matches JR, Liston J, Curran D. 1974 Clostridium perfringens in the Environment. *Appl. Microbiol.* **28**, 655–660.

3. Craven SE. 2000 Colonization of the intestinal tract by Clostridium perfringens and fecal shedding in diet-stressed and unstressed broiler chickens. *Poult. Sci.* **79**, 843–9.

4. Paredes-Sabja D, Li J, McClane BA, Sarker MR. In press. Clostridium perfringens Sporulation and Sporulation-Associated Toxin Production. In *The Bacterial Spore: from Molecules to Systems*, pp. 331–347. American Society of Microbiology. (doi:10.1128/microbiolspec.TBS-0022-2015)

5. CDC. 2017 Clostridium perfringens. *FOOD Saf.* See https://www.cdc.gov/foodsafety/diseases/clostridium-perfringens.html (accessed on 11 July 2017).

6. McClane BA, Uzal FA, Fernandez Miyakawa ME, Lyerly D, Wilkins T. 2006 The Enterotoxic Clostridia BT - The Prokaryotes: Volume 4: Bacteria: Firmicutes, Cyanobacteria. In (eds M Dworkin, S Falkow, E Rosenberg, K-H Schleifer, E Stackebrandt), pp. 698–752. New York, NY: Springer US. (doi:10.1007/0-387-30744-3_22)

7. Rood JI, McClane BA, Songer JG, Titball RW. 1997 *The Clostridia: Molecular Biology and Pathogenesis*. Elsevier Science.

8. Freedman JC, Shrestha A, McClane BA. 2016 Clostridium perfringens Enterotoxin: Action, Genetics, and Translational Applications. *Toxins (Basel).* **8**, 73. (doi:10.3390/toxins8030073)

9. Hoffmann S, Batz MB, Morris JG. 2012 Annual cost of illness and quality-adjusted life year losses in the United States due to 14 foodborne pathogens. *J. Food Prot.* **75**, 1292–302. (doi:10.4315/0362-028X.JFP-11-417)

10. Wormser GP, Stratton C. 2008 Manual of Clinical Microbiology, 9th Edition Edited by Patrick R. Murray, Ellen Jo Baron, James H. Jorgensen, Marie Louise Landry, and Michael A. Pfaller Washington, DC: ASM Press, 2007 2488 pp., illustrated. *Clin. Infect. Dis.* **46**, 153–153. (doi:10.1086/524076)

11. Li J, Miyamoto K, Sayeed S, McClane BA. 2010 Organization of the cpe locus in CPE-positive clostridium perfringens type C and D isolates. *PLoS One* **5**, 465–489. (doi:10.1371/journal.pone.0010932)

12. Daube G, Simon P, Limbourg B, Manteca C, Mainil J, Kaeckenbeeck A. 1996 Hybridization of 2,659 Clostridium perfringens isolates with gene probes for seven toxins (alpha, beta, epsilon, iota, theta, mu, and

enterotoxin) and for sialidase. *Am. J. Vet. Res.* **57**, 496–501.

13. Kokai-Kun JF, Songer JG, Czeczulin JR, Chen F, McClane BA. 1994 Comparison of Western immunoblots and gene detection assays for identification of potentially enterotoxigenic isolates of Clostridium perfringens. *J. Clin. Microbiol.* **32**, 2533–2539.

14. Doyle MP, Beuchat LR. 2007 *Food Microbiology: Fundamentals and Frontiers*. ASM Press.

15. Briggs DC, Naylor CE, Smedley JG, Lukoyanova N, Robertson S, Moss DS, McClane BA, Basak AK. 2011 Structure of the food-poisoning Clostridium perfringens enterotoxin reveals similarity to the aerolysin-like pore-forming toxins. *J. Mol. Biol.* **413**, 138–49. (doi:10.1016/j.jmb.2011.07.066)

16. Kitadokoro K *et al.* 2011 Crystal structure of Clostridium perfringens enterotoxin displays features of beta-pore-forming toxins. *J. Biol. Chem.* **286**, 19549–55. (doi:10.1074/jbc.M111.228478)

17. Titball RW. 2005 Gas gangrene: an open and closed case. *Microbiology* **151**, 2821–2828. (doi:10.1099/mic.0.28248-0)

18. Günzel D, Fromm M. 2012 Claudins and other tight junction proteins. *Compr. Physiol.* **2**, 1819–52. (doi:10.1002/cphy.c110045)

19. Saitoh Y, Suzuki H, Tani K, Nishikawa K, Irie K, Ogura Y, Tamura A, Tsukita S, Fujiyoshi Y. 2015 Tight junctions. Structural insight into tight junction disassembly by Clostridium perfringens enterotoxin. *Science* **347**, 775–8. (doi:10.1126/science.1261833)

20. Robertson SL, Smedley JG, Singh U, Chakrabarti G, Van Itallie CM, Anderson JM, McClane BA. 2007 Compositional and stoichiometric analysis of Clostridium perfringens enterotoxin complexes in Caco-2 cells and claudin 4 fibroblast transfectants. *Cell. Microbiol.* **9**, 2734–55. (doi:10.1111/j.1462-5822.2007.00994.x)

21. Chen J, Theoret JR, Shrestha A, Smedley JG, McClane BA. 2012 Cysteine-scanning mutagenesis supports the importance of Clostridium perfringens enterotoxin amino acids 80 to 106 for membrane insertion and pore formation. *Infect. Immun.* **80**, 4078–88. (doi:10.1128/IAI.00069-12)

22. Matsuda M, Sugimoto N. 1979 Calcium-independent and dependent steps in action of Clostridiumperfringens enterotoxin on HeLa and Vero cells. *Biochem. Biophys. Res. Commun.* **91**, 629–636. (doi:http://dx.doi.org/10.1016/0006-291X(79)91568-7)

23. Chakrabarti G, McClane BA. 2005 The importance of calcium influx, calpain and calmodulin for the activation of CaCo-2 cell death pathways by Clostridium perfringens enterotoxin. *Cell. Microbiol.* **7**, 129–46. (doi:10.1111/j.1462-5822.2004.00442.x)

24. Singh U, Van Itallie CM, Mitic LL, Anderson JM, McClane BA. 2000 CaCo-2 cells treated with Clostridium perfringens enterotoxin form multiple large complex species, one of which contains the tight junction protein occludin. *J. Biol. Chem.* **275**, 18407–17. (doi:10.1074/jbc.M001530200)

25. Clooten JK, Kruth SA, Weese JS. In press. Genotypic and phenotypic characterization of Clostridium perfringens and Clostridium difficile in diarrheic and healthy dogs. *J. Vet. Intern. Med.* **17**, 533–540.

26. Grafarholti D. 2007 The prevalence of Clostridium perfringens enterotoxin in dogs with acute diarrhea in southwestern Iceland. , 1–18. See https://www.ddd.dk/sektioner/fagdyrlægeforeninger/hundkatsmaedyr/opgaver/Documents/2007-16 Steinunn Geirsdóttir.pdf (accessed on 17 August 2017).

27. Schlegel BJ, Van Dreumel T, Slavić D, Prescott JF. 2012 Clostridium perfringens type A fatal acute hemorrhagic gastroenteritis in a dog. *Can. Vet. J.* **53**, 555–557.

28. Titball RW. 1993 Bacterial phospholipases C. *Microbiol. Rev.* **57**, 347–366.

29. Takahashi T, Sugahara T, Ohsaka A. 1974 Purification of Clostridium perfringens phospholipase C (α-toxin) by affinity chromatography on agarose-linked egg-yolk lipoprotein. *Biochim. Biophys. Acta - Protein Struct.* **351**, 155–171. (doi:http://dx.doi.org/10.1016/0005-2795(74)90074-9)

30. Cavalcanti MTH, Porto T, Porto ALF, Brandi IV, Lima Filho JL de, Pessoa Junior A. 2004 Large scale purification of Clostridium perfringens toxins: a review. *Rev. Bras. Ciências Farm.* **40**, 151–164. (doi:10.1590/S1516-93322004000200004)

31. Canard B, Cole ST. 1989 Genome organization of the anaerobic pathogen Clostridium perfringens. *Proc. Natl. Acad. Sci. U. S. A.* **86**, 6676–80.

32. Okumura K, Ohtani K, Hayashi H, Shimizu T. 2008 Characterization of Genes Regulated Directly by the VirR/VirS System in Clostridium perfringens. *J. Bacteriol.* **190**, 7719–7727. (doi:10.1128/JB.01573-07)

33. Oda M, Terao Y, Sakurai J, Nagahama M. 2015 Membrane-Binding Mechanism of Clostridium perfringens Alpha-Toxin. *Toxins (Basel).* **7**, 5268–5275. (doi:10.3390/toxins7124880)

34. Naylor CE, Eaton JT, Howells A, Justin N, Moss DS, Titball RW, Basak AK. 1998 Structure of the key toxin in gas gangrene. *Nat. Struct. Biol.* **5**, 738–46. (doi:10.1038/1447)

35. Sakurai J, O M. 2011 Effect of Macrolide Antibiotics on Biological Activities Induced by Clostridium perfringens Alpha-Toxin. In *Gangrene* -

Current Concepts and Management Options, InTech. (doi:10.5772/22404)

36. Titball RW, Leslie DL, Harvey S, Kelly D. 1991 Hemolytic and sphingomyelinase activities of Clostridium perfringens alpha-toxin are dependent on a domain homologous to that of an enzyme from the human arachidonic acid pathway. *Infect. Immun.* **59**, 1872–1874.

37. Titball RW, Rubidge T. 1990 The role of histidine residues in the alpha toxin of Clostridium perfringens. *FEMS Microbiol. Lett.* **68**, 261–266. (doi:10.1111/j.1574-6968.1990.tb13948.x)

38. Guillouard I, Garnier T, Cole ST. 1996 Use of site-directed mutagenesis to probe structure-function relationships of alpha-toxin from Clostridium perfringens. *Infect. Immun.* **64**, 2440–4.

39. Jepson M, Bullifent HL, Crane D, Flores-Diaz M, Alape-Giron A, Jayasekeera P, Lingard B, Moss D, Titball RW. 2001 Tyrosine 331 and phenylalanine 334 in Clostridium perfringens α-toxin are essential for cytotoxic activity. *FEBS Lett.* **495**, 172–177. (doi:http://dx.doi.org/10.1016/S0014-5793(01)02385-7)

40. Alape-Girón A *et al.* 2000 Identification of residues critical for toxicity in Clostridium perfringens phospholipase C, the key toxin in gas gangrene. *Eur. J. Biochem.* **267**, 5191–7.

41. Titball RW, Naylor CE, Basak AK. 1999 The Clostridium perfringens alpha-toxin. *Anaerobe* **5**, 51–64. (doi:10.1006/anae.1999.0191)

42. Bryant AE, Stevens DL. 2010 Clostridial myonecrosis: new insights in pathogenesis and management. *Curr. Infect. Dis. Rep.* **12**, 383–91. (doi:10.1007/s11908-010-0127-y)

43. Bryant AE, Chen RY, Nagata Y, Wang Y, Lee CH, Finegold S, Guth PH, Stevens DL. 2000 Clostridial gas gangrene. II. Phospholipase C-induced activation of platelet gpIIbIIIa mediates vascular occlusion and myonecrosis in Clostridium perfringens gas gangrene. *J. Infect. Dis.* **182**, 808–15. (doi:10.1086/315757)

44. Bryant AE, Stevens DL. 1996 Phospholipase C and perfringolysin O from Clostridium perfringens upregulate endothelial cell-leukocyte adherence molecule 1 and intercellular leukocyte adherence molecule 1 expression and induce interleukin-8 synthesis in cultured human umbilical vein en. *Infect. Immun.* **64**, 358–62.

45. Stevens DL, Bryant AE. 2002 The role of clostridial toxins in the pathogenesis of gas gangrene. *Clin. Infect. Dis.* **35**, 93–100. (doi:10.1086/341928)

46. Bryant AE, Chen RY, Nagata Y, Wang Y, Lee CH, Finegold S, Guth PH, Stevens DL. 2000 Clostridial gas gangrene. I. Cellular and molecular mechanisms of microvascular dysfunction induced by exotoxins of

Clostridium perfringens. *J. Infect. Dis.* **182**, 799–807. (doi:10.1086/315756)

47. Peek SF, Semrad SD. 2010 Clostridial myonecrosis in horses. *Equine Vet. Educ.* **14**, 163–168. (doi:10.1111/j.2042-3292.2002.tb00162.x)

48. Goossens E, Valgaeren BR, Pardon B, Haesebrouck F, Ducatelle R, Deprez PR, Van Immerseel F. 2017 Rethinking the role of alpha toxin in Clostridium perfringens-associated enteric diseases: a review on bovine necro-haemorrhagic enteritis. *Vet. Res.* **48**, 1–17. (doi:10.1186/s13567-017-0413-x)

49. Gurjar A, Li J, McClane BA. 2010 Characterization of Toxin Plasmids in Clostridium perfringens Type C Isolates . *Infect. Immun.* **78**, 4860–4869. (doi:10.1128/IAI.00715-10)

50. Nagahama M, Ochi S, Oda M, Miyamoto K, Takehara M, Kobayashi K. 2015 Recent Insights into Clostridium perfringens Beta-Toxin. *Toxins (Basel).* **7**, 396–406. (doi:10.3390/toxins7020396)

51. Theoret JR, Uzal FA, McClane BA. 2015 Identification and Characterization of Clostridium perfringens Beta Toxin Variants with Differing Trypsin Sensitivity and In Vitro Cytotoxicity Activity. *Infect. Immun.* **83**, 1477–1486. (doi:10.1128/IAI.02864-14)

52. Sakurai J, Nagahama M. 2006 CLOSTRIDIUM PERFRINGENS BETA-TOXIN: CHARACTERIZATION AND ACTION. *Toxin Rev.* **25**, 89–108. (doi:10.1080/15569540500320979)

53. Ferreira M, Moreira G, Cunha C, Mendonça M, Salvarani F, Moreira Â, Conceição F. 2016 Recombinant Alpha, Beta, and Epsilon Toxins of Clostridium perfringens: Production Strategies and Applications as Veterinary Vaccines. *Toxins (Basel).* **8**, 340. (doi:10.3390/toxins8110340)

54. Songer JG. 1996 Clostridial enteric diseases of domestic animals. *Clin. Microbiol. Rev.* **9**, 216–34.

55. Hagan WA, Bruner DW, Timoney JF. 1988 *Hagan and Bruner's Microbiology and Infectious Diseases of Domestic Animals: With Reference to Etiology, Epizootiology, Pathogenesis, Immunity, Diagnosis, and Antimicrobial Susceptibility*. Comstock Pub. Associates.

56. Lawrence G, Walker PD. 1976 PATHOGENESIS OF ENTERITIS NECROTICANS IN PAPUA NEW GUINEA. *Lancet* **307**, 125–126. (doi:10.1016/S0140-6736(76)93160-3)

57. Ma M, Li J, McClane BA. 2012 Genotypic and Phenotypic Characterization of Clostridium perfringens Isolates from Darmbrand Cases in Post-World War II Germany. *Infect. Immun.* **80**, 4354–4363. (doi:10.1128/IAI.00818-12)

58. Gurtner C, Popescu F, Wyder M, Sutter E, Zeeh F, Frey J, von Schubert C, Posthaus H. 2010 Rapid Cytopathic Effects of Clostridium perfringens

Beta-Toxin on Porcine Endothelial Cells. *Infect. Immun.* **78**, 2966–2973. (doi:10.1128/IAI.01284-09)

59. Popescu F, Wyder M, Gurtner C, Frey J, Cooke RA, Greenhill AR, Posthaus H. 2011 Susceptibility of primary human endothelial cells to C. perfringens beta-toxin suggesting similar pathogenesis in human and porcine necrotizing enteritis. *Vet. Microbiol.* **153**, 173–7. (doi:10.1016/j.vetmic.2011.02.017)

60. Nagahama M, Hayashi S, Morimitsu S, Sakurai J. 2003 Biological Activities and Pore Formation of Clostridium perfringens Beta Toxin in HL 60 Cells. *J. Biol. Chem.* **278**, 36934–36941. (doi:10.1074/jbc.M306562200)

61. Autheman D, Wyder M, Popoff M, D'Herde K, Christen S, Posthaus H. 2013 Clostridium perfringens Beta-Toxin Induces Necrostatin-Inhibitable, Calpain-Dependent Necrosis in Primary Porcine Endothelial Cells. *PLoS One* **8**, e64644. (doi:10.1371/journal.pone.0064644)

62. Sakurai J, Nagahama M, Oda M, Tsuge H, Kobayashi K. 2009 Clostridium perfringens Iota-Toxin: Structure and Function. *Toxins (Basel).* **1**, 208–228. (doi:10.3390/toxins1020208)

63. Uzal FA, Vidal JE, McClane BA, Gurjar AA. 2010 Clostridium Perfringens Toxins Involved in Mammalian Veterinary Diseases. *open toxinology J.* **2**, 24–42.

64. STILES BG, HALE ML, MARVAUD JC, POPOFF MR. 2002 Clostridium perfringens iota toxin: characterization of the cell-associated iota b complex. *Biochem. J.* **367**, 801–808. (doi:10.1042/bj20020566)

65. Gibert M, Petit L, Raffestin S, Okabe A, Popoff MR. 2000 Clostridium perfringens Iota-Toxin Requires Activation of Both Binding and Enzymatic Components for Cytopathic Activity. *Infect. Immun.* **68**, 3848–3853. (doi:10.1128/IAI.68.7.3848-3853.2000)

66. Richard JF, Mainguy G, Gibert M, Marvaud JC, Stiles BG, Popoff MR. 2002 Transcytosis of iota-toxin across polarized CaCo-2 cells. *Mol. Microbiol.* **43**, 907–17.

67. Schering B, Bärmann M, Chhatwal GS, Geipel U, Aktories K. 1988 ADP-ribosylation of skeletal muscle and non-muscle actin by Clostridium perfringens iota toxin. *Eur. J. Biochem.* **171**, 225–9.

68. Tsuge H, Nagahama M, Oda M, Iwamoto S, Utsunomiya H, Marquez VE, Katunuma N, Nishizawa M, Sakurai J. 2008 Structural basis of actin recognition and arginine ADP-ribosylation by Clostridium perfringens iota-toxin. *Proc. Natl. Acad. Sci. U. S. A.* **105**, 7399–404. (doi:10.1073/pnas.0801215105)

69. Aktories K, Wegner A. 1992 Mechanisms of the cytopathic action of actin-ADP-ribosylating toxins. *Mol. Microbiol.* **6**, 2905–8. (doi:10.1111/j.1365-

2958.1992.tb01749)

70. Hunter SE, Clarke IN, Kelly DC, Titball RW. 1992 Cloning and nucleotide sequencing of the Clostridium perfringens epsilon-toxin gene and its expression in Escherichia coli. *Infect. Immun.* **60**, 102–10.

71. Popoff MR. 2011 Epsilon toxin: a fascinating pore-forming toxin. *FEBS J.* **278**, 4602–15. (doi:10.1111/j.1742-4658.2011.08145.x)

72. Gill DM. 1982 Bacterial toxins: a table of lethal amounts. *Microbiol. Rev.* **46**, 86–94.

73. Stiles B, Barth G, Barth H, Popoff M. 2013 Clostridium perfringens Epsilon Toxin: A Malevolent Molecule for Animals and Man? *Toxins (Basel).* **5**, 2138–2160. (doi:10.3390/toxins5112138)

74. Uzal FA, Kelly WR. 1997 Effects of the intravenous administration of Clostridium perfringens type D epsilon toxin on young goats and lambs. *J. Comp. Pathol.* **116**, 63–71. (doi:10.1053/jcpa.2001.0514)

75. Rumah KR, Linden J, Fischetti VA, Vartanian T. 2013 Isolation of Clostridium perfringens Type B in an Individual at First Clinical Presentation of Multiple Sclerosis Provides Clues for Environmental Triggers of the Disease. *PLoS One* **8**, e76359. (doi:10.1371/journal.pone.0076359)

76. Hughes ML, Poon R, Adams V, Sayeed S, Saputo J, Uzal FA, McClane BA, Rood JI. 2007 Epsilon-Toxin Plasmids of Clostridium perfringens Type D Are Conjugative. *J. Bacteriol.* **189**, 7531–7538. (doi:10.1128/JB.00767-07)

77. Sayeed S, Li J, McClane BA. 2007 Virulence Plasmid Diversity in Clostridium perfringens Type D Isolates. *Infect. Immun.* **75**, 2391–2398. (doi:10.1128/IAI.02014-06)

78. Sayeed S, Li J, McClane BA. 2010 Characterization of Virulence Plasmid Diversity among Clostridium perfringens Type B Isolates. *Infect. Immun.* **78**, 495–504. (doi:10.1128/IAI.00838-09)

79. Bokori-Brown M, Savva CG, Fernandes da Costa SP, Naylor CE, Basak AK, Titball RW. 2011 Molecular basis of toxicity of Clostridium perfringens epsilon toxin. *FEBS J.* **278**, 4589–4601. (doi:10.1111/j.1742-4658.2011.08140.x)

80. Harvard HL, Hunter SEC, Titball RW. 1992 Comparison of the nucleotide sequence and development of a PCR test for the epsilon toxin gene of Clostridium perfringens type B and type D. *FEMS Microbiol. Lett.* **97**, 77–81. (doi:10.1111/j.1574-6968.1992.tb05443.x)

81. Alves GG, Machado de Ávila RA, Chávez-Olórtegui CD, Lobato FCF. 2014 Clostridium perfringens epsilon toxin: The third most potent bacterial toxin known. *Anaerobe* **30**, 102–107.

(doi:10.1016/j.anaerobe.2014.08.016)

82. Manni MM, Sot J, Goñi FM. 2015 Interaction of Clostridium perfringens epsilon-toxin with biological and model membranes: A putative protein receptor in cells. *Biochim. Biophys. Acta - Biomembr.* **1848**, 797–804. (doi:https://doi.org/10.1016/j.bbamem.2014.11.028)

83. Bullen JJ. 1952 Enterotoxæmia of sheep:Clostridium welchii type D in the alimentary tract of normal animals. *J. Pathol. Bacteriol.* **64**, 201–206. (doi:10.1002/path.1700640120)

84. Uzal FA, Songer JG. 2008 Diagnosis of Clostridium perfringens intestinal infections in sheep and goats. *J. Vet. Diagn. Invest.* **20**, 253–65. (doi:10.1177/104063870802000301)

85. Rumah KR *et al.* 2015 The Myelin and Lymphocyte Protein MAL Is Required for Binding and Activity of Clostridium perfringens ε-Toxin. *PLOS Pathog.* **11**, e1004896. (doi:10.1371/journal.ppat.1004896)

86. Oliveira DM, Pimentel LA, Pessoa AF, Dantas AFM, Uzal F, Riet-Correa F. 2010 Focal symmetrical encephalomalacia in a goat. *J. Vet. Diagn. Invest.* **22**, 793–6. (doi:10.1177/104063871002200527)

87. Tamai E, Ishida T, Miyata S, Matsushita O, Suda H, Kobayashi S, Sonobe H, Okabe A. 2003 Accumulation of Clostridium perfringens Epsilon-Toxin in the Mouse Kidney and Its Possible Biological Significance. *Infect. Immun.* **71**, 5371–5375. (doi:10.1128/IAI.71.9.5371-5375.2003)

88. Linden JR, Ma Y, Zhao B, Harris JM, Rumah KR, Schaeren-Wiemers N, Vartanian T. 2015 Clostridium perfringens Epsilon Toxin Causes Selective Death of Mature Oligodendrocytes and Central Nervous System Demyelination. *MBio* **6**, 2513–14. (doi:10.1128/mBio.02513-14)

89. Lonchamp E *et al.* 2010 Clostridium perfringens epsilon toxin targets granule cells in the mouse cerebellum and stimulates glutamate release. *PLoS One* **5**, 1–15. (doi:10.1371/journal.pone.0013046)

90. Dorca-Arévalo J, Soler-Jover A, Gibert M, Popoff MR, Martín-Satué M, Blasi J. 2008 Binding of epsilon-toxin from Clostridium perfringens in the nervous system. *Vet. Microbiol.* **131**, 14–25. (doi:10.1016/j.vetmic.2008.02.015)

91. Wioland L *et al.* 2015 Epsilon toxin from C lostridium perfringens acts on oligodendrocytes without forming pores, and causes demyelination. *Cell. Microbiol.* **17**, 369–388. (doi:10.1111/cmi.12373)

92. Miyamoto O. 2000 Clostridium perfringens epsilon toxin causes excessive release of glutamate in the mouse hippocampus. *FEMS Microbiol. Lett.* **189**, 109–113. (doi:10.1016/S0378-1097(00)00262-7)

93. Finnie JW. 2004 Neurological disorders produced by Clostridium perfringens type D epsilon toxin. *Anaerobe* **10**, 145–150.

(doi:10.1016/j.anaerobe.2003.08.003)

94. de la Rosa C, Hogue DE, Thonney ML. 1997 Vaccination schedules to raise antibody concentrations against epsilon-toxin of Clostridium perfringens in ewes and their triplet lambs. *J. Anim. Sci.* **75**, 2328–34.

95. Titball RW. 2009 Clostridium perfringens vaccines. *Vaccine* **27 Suppl 4**, D44-7. (doi:10.1016/j.vaccine.2009.07.047)

96. WHO. 2016 WHO Vaccine Safety Basics. Module 2 - Types of Vaccine and Adverse Reaction. See http://vaccine-safety-training.org/summary-module2.html (accessed on 20 June 2017).

97. Walker PD. 1992 Bacterial vaccines: old and new, veterinary and medical. *Vaccine* **10**, 977–90.

98. Stokka GL, Edwards AJ, Spire MF, Brandt RT, Smith JE. 1994 Inflammatory response to clostridial vaccines in feedlot cattle. *J. Am. Vet. Med. Assoc.* **204**, 415–9.

99. Lobato FCFF, Lima CGRDRD, Assis RA, Pires PS, Silva ROSS, Salvarani FM, Carmo AO, Contigli C, Kalapothakis E. 2010 Potency against enterotoxemia of a recombinant Clostridium perfringens type D epsilon toxoid in ruminants. *Vaccine* **28**, 6125–7. (doi:10.1016/j.vaccine.2010.07.046)

100. Pelish TM, McClain MS. 2009 Dominant-negative inhibitors of the Clostridium perfringens epsilon-toxin. *J. Biol. Chem.* **284**, 29446–53. (doi:10.1074/jbc.M109.021782)

101. Worthington RW, Mülders MS. 1977 Physical changes in the epsilon prototoxin molecule of Clostridium perfringens during enzymatic activation. *Infect. Immun.* **18**, 549–51.

102. Miyata S, Matsushita O, Minami J, Katayama S, Shimamoto S, Okabe A. 2001 Cleavage of a C-terminal Peptide Is Essential for Heptamerization of Clostridium perfringens ε-Toxin in the Synaptosomal Membrane. *J. Biol. Chem.* **276**, 13778–13783. (doi:10.1074/jbc.M011527200)

103. Harkness JM, Li J, McClane BA. 2012 Identification of a lambda toxin-negative Clostridium perfringens strain that processes and activates epsilon prototoxin intracellularly. *Anaerobe* **18**, 546–52. (doi:10.1016/j.anaerobe.2012.09.001)

104. Goldstein J, Morris WE, Loidl CF, Tironi-Farinati C, Tironi-Farinatti C, McClane BA, Uzal FA, Fernandez Miyakawa ME. 2009 Clostridium perfringens epsilon toxin increases the small intestinal permeability in mice and rats. *PLoS One* **4**, e7065. (doi:10.1371/journal.pone.0007065)

105. Li J, Sayeed S, Robertson S, Chen J, McClane BA. 2011 Sialidases affect the host cell adherence and epsilon toxin-induced cytotoxicity of Clostridium perfringens type D strain CN3718. *PLoS Pathog.* **7**,

e1002429. (doi:10.1371/journal.ppat.1002429)

106. Adamson RH, Ly JC, Fernandez-Miyakawa M, Ochi S, Sakurai J, Uzal F, Curry FE. 2005 Clostridium perfringens epsilon-toxin increases permeability of single perfused microvessels of rat mesentery. *Infect. Immun.* **73**, 4879–87. (doi:10.1128/IAI.73.8.4879-4887.2005)

107. Buxton D. 1978 Further studies on the mode of action of Clostridium welchii type-D epsilon toxin. *J. Med. Microbiol.* **11**, 293–8. (doi:10.1099/00222615-11-3-293)

108. Soler-Jover A, Blasi J, Gómez de Aranda I, Navarro P, Gibert M, Popoff MR, Martín-Satué M. 2004 Effect of epsilon toxin-GFP on MDCK cells and renal tubules in vivo. *J. Histochem. Cytochem.* **52**, 931–42. (doi:10.1369/jhc.4A6254.2004)

109. Shortt SJ, Titball RW, Lindsay CD. 2000 An assessment of the in vitro toxicology of Clostridium perfringens type D epsilon-toxin in human and animal cells. *Hum. Exp. Toxicol.* **19**, 108–16. (doi:10.1191/096032700678815710)

110. Uzal FA, Rolfe BE, Smith NJ, Thomas AC, Kelly WR. 1999 Resistance of ovine, caprine and bovine endothelial cells to Clostridium perfringens type D epsilon toxin in vitro. *Vet. Res. Commun.* **23**, 275–84. (doi:10.1023/A:1006362819202)

111. Türkcan S, Masson J-B, Casanova D, Mialon G, Gacoin T, Boilot J-P, Popoff MR, Alexandrou A. 2012 Observing the confinement potential of bacterial pore-forming toxin receptors inside rafts with nonblinking Eu(3+)-doped oxide nanoparticles. *Biophys. J.* **102**, 2299–308. (doi:10.1016/j.bpj.2012.03.072)

112. Petit L, Gibert M, Gillet D, Laurent-Winter C, Boquet P, Popoff MR. 1997 Clostridium perfringens epsilon-toxin acts on MDCK cells by forming a large membrane complex. *J. Bacteriol.* **179**, 6480–7.

113. Chassin C *et al.* 2007 Pore-forming epsilon toxin causes membrane permeabilization and rapid ATP depletion-mediated cell death in renal collecting duct cells. *Am. J. Physiol. Renal Physiol.* **293**, F927-37. (doi:10.1152/ajprenal.00199.2007)

114. Miyata S, Minami J, Tamai E, Matsushita O, Shimamoto S, Okabe A. 2002 Clostridium perfringens epsilon-toxin forms a heptameric pore within the detergent-insoluble microdomains of Madin-Darby canine kidney cells and rat synaptosomes. *J. Biol. Chem.* **277**, 39463–8. (doi:10.1074/jbc.M206731200)

115. Knapp O, Maier E, Benz R, Geny B, Popoff MR. 2009 Identification of the channel-forming domain of Clostridium perfringens Epsilon-toxin (ETX). *Biochim. Biophys. Acta* **1788**, 2584–93. (doi:10.1016/j.bbamem.2009.09.020)

116. Gil C, Dorca-Arévalo J, Blasi J. 2015 Clostridium Perfringens Epsilon Toxin Binds to Membrane Lipids and Its Cytotoxic Action Depends on Sulfatide. *PLoS One* **10**, e0140321. (doi:10.1371/journal.pone.0140321)

117. Fennessey CM, Sheng J, Rubin DH, McClain MS. 2012 Oligomerization of Clostridium perfringens epsilon toxin is dependent upon caveolins 1 and 2. *PLoS One* **7**, e46866. (doi:10.1371/journal.pone.0046866)

118. Payne DW, Williamson ED, Havard H, Modi N, Brown J. 1994 Evaluation of a new cytotoxicity assay for Clostridium perfringens type D epsilon toxin. *FEMS Microbiol. Lett.* **116**, 161–167. (doi:10.1111/j.1574-6968.1994.tb06695.x)

119. Ivie SE, Fennessey CM, Sheng J, Rubin DH, McClain MS. 2011 Gene-Trap Mutagenesis Identifies Mammalian Genes Contributing to Intoxication by Clostridium perfringens ε-Toxin. *PLoS One* **6**, e17787. (doi:10.1371/journal.pone.0017787)

120. Bokori-Brown M *et al.* 2014 Clostridium perfringens epsilon toxin mutant Y30A-Y196A as a recombinant vaccine candidate against enterotoxemia. *Vaccine* **32**, 2682–2687. (doi:10.1016/j.vaccine.2014.03.079)

121. Bokori-Brown M, Kokkinidou MC, Savva CG, Fernandes da Costa S, Naylor CE, Cole AR, Moss DS, Basak AK, Titball RW. 2013 Clostridium perfringens epsilon toxin H149A mutant as a platform for receptor binding studies. *Protein Sci.* **22**, 650–9. (doi:10.1002/pro.2250)

122. Schaeren-Wiemers N, Bonnet A, Erb M, Erne B, Bartsch U, Kern F, Mantei N, Sherman D, Suter U. 2004 The raft-associated protein MAL is required for maintenance of proper axon--glia interactions in the central nervous system. *J. Cell Biol.* **166**, 731–42. (doi:10.1083/jcb.200406092)

123. Antón O, Batista A, Millán J, Andrés-Delgado L, Puertollano R, Correas I, Alonso MA. 2008 An essential role for the MAL protein in targeting Lck to the plasma membrane of human T lymphocytes. *J. Exp. Med.* **205**, 3201–13. (doi:10.1084/jem.20080552)

124. Antón OM, Andrés-Delgado L, Reglero-Real N, Batista A, Alonso MA. 2011 MAL protein controls protein sorting at the supramolecular activation cluster of human T lymphocytes. *J. Immunol.* **186**, 6345–56. (doi:10.4049/jimmunol.1003771)

125. Alonso MA, Weissman SM. 1987 cDNA cloning and sequence of MAL, a hydrophobic protein associated with human T-cell differentiation. *Proc. Natl. Acad. Sci. U. S. A.* **84**, 1997–2001.

126. Ramnarayanan SP, Cheng CA, Bastaki M, Tuma PL. 2007 Exogenous MAL reroutes selected hepatic apical proteins into the direct pathway in WIF-B cells. *Mol. Biol. Cell* **18**, 2707–15. (doi:10.1091/mbc.E07-02-0096)

127. Morinaga G, Nakamura T, Yoshizawa J, Nishida S. 1965 Isolation of Clostridium perfringens Type D from a Case of Gas Gangrene. *J.*

Bacteriol. **90**, 826.

128. Miller C *et al.* 2004 Fulminant and fatal gas gangrene of the stomach in a healthy live liver donor. *Liver Transpl.* **10**, 1315–9. (doi:10.1002/lt.20227)

129. Greenfield RA, Brown BR, Hutchins JB, Iandolo JJ, Jackson R, Slater LN, Bronze MS. 2002 Microbiological, biological, and chemical weapons of warfare and terrorism. *Am. J. Med. Sci.* **323**, 326–40.

130. Anderson PD. 2012 Bioterrorism: toxins as weapons. *J. Pharm. Pract.* **25**, 121–9. (doi:10.1177/0897190012442351)

131. Markowitz CE. 2013 Multiple sclerosis update. *Am. J. Manag. Care* **19**, s294-300.

132. Murrell TG, O'Donoghue PJ, Ellis T. 1986 A review of the sheep-multiple sclerosis connection. *Med. Hypotheses* **19**, 27–39.

133. Chandran D, Naidu SS, Sugumar P, Rani GS, Vijayan SP, Mathur D, Garg LC, Srinivasan VA. 2010 Development of a Recombinant Epsilon Toxoid Vaccine against Enterotoxemia and Its Use as a Combination Vaccine with Live Attenuated Sheep Pox Virus against Enterotoxemia and Sheep Pox. *Clin. Vaccine Immunol.* **17**, 1013–1016. (doi:10.1128/CVI.00013-10)

134. Agilent Technologies. 2015 QuikChange Lightning Site-Directed Mutagenesis Kit - Instruction Manual. , 4–15. See http://www.agilent.com/cs/library/usermanuals/public/210518.pdf (accessed on 16 November 2016).

135. Thermo Scientific. 2014 Thermo Scientific - GeneJET Plasmid Miniprep Kit. , 4–5. See http://www.thermoscientificbio.com/uploadedFiles/Resources/k0502-product-information.pdf (accessed on 16 February 2015).

136. Eurofins Genomics. In press. Sample Submission Guide - Value Read Tube. , 1. See http://www.eurofinsgenomics.eu/media/892645/samplesubmissionguide_valuereadtube.pdf (accessed on 22 February 2015).

137. Hall TA. 1999 BioEdit: a user-friendly biological sequence alignment editor and analysis program for Windows 95/98/NT. *Nucleic Acids Symp. Ser.* **41**, 95–98.

138. Novagen. 2016 Rosetta^{TM}(DE3) Competent Cells - Novagen. *N/A*. See http://www.merckmillipore.com/GB/en/product/Rosetta%25E2%2584%25A2%2528DE3%2529-Competent-Cells---Novagen,EMD_BIO-70954?ReferrerURL=https%253A%252F%252Fwww.google.co.uk%252F&bd=1#overview (accessed on 16 November 2016).

139. Studier FW. 2005 Protein production by auto-induction in high-density shaking cultures. *Protein Expr. Purif.* **41**, 207–234.

(doi:10.1016/j.pep.2005.01.016)

140. GE Healthcare. 2006 His Gravitrap. *GE Healthc.* , 1–2. See https://www.gelifesciences.com/gehcls_images/GELS/Related Content/Files/1314750913712/litdoc11003690_20161014103044.pdf (accessed on 16 November 2016).

141. GE Healthcare. 2007 PD-10 Desalting Columns. *GE Healthc.* , 1–8. See https://www.gelifesciences.com/gehcls_images/GELS/Related Content/Files/1478781880316/litdoc52130800_20161110134421.pdf (accessed on 16 November 2016).

142. Olson BJSC, Markwell J. 2007 Assays for Determination of Protein Concentration. In *Current Protocols in Protein Science*, p. 3.4.1-3.4.29. Hoboken, NJ, USA: John Wiley & Sons, Inc. (doi:10.1002/0471140864.ps0304s48)

143. Johnson M. 2012 Protein Quantitation. *Mater. Methods* **2**. (doi:10.13070/mm.en.2.115)

144. Cunningham BC, Wells JA. 1989 High-resolution epitope mapping of hGH-receptor interactions by alanine-scanning mutagenesis. *Science* **244**, 1081–5.

145. Kyte J, Doolittle RF. 1982 A simple method for displaying the hydropathic character of a protein. *J. Mol. Biol.* **157**, 105–132. (doi:http://dx.doi.org/10.1016/0022-2836(82)90515-0)

146. ProImmune. 2013 Amino Acid Properties. See http://www.thinkpeptides.com/aminoacidproperties.html (accessed on 6 June 2017).

147. Unversity of California. 2017 An introduction to circular dichroism spectroscopy. See https://www.chem.uci.edu/~dmitryf/manuals/Fundamentals/CD spectroscopy.pdf (accessed on 7 June 2017).

148. Clore GM, Gronenborn AM. 1998 NMR structure determination of proteins and protein complexes larger than 20 kDa. *Curr. Opin. Chem. Biol.* **2**, 564–70.

149. Smyth MS, Martin JHJ. 2000 x Ray crystallography. *Mol. Pathol.* **53**, 8–14.

150. University of Semmelweis. 2014 The Isoenzyme Profile of Lactate Dehydrogenase. , 1–4. See http://semmelweis.hu/biokemia/files/2014/01/EN_lab_LDH_or_BAK-KOK_20150130.pdf (accessed on 13 January 2017).

151. Menon MP, Anderson G, Nambiar GK. 1983 Determination of human serum lactate dehydrogenase isoenzymes by anion exchange chromatography. *Anal. Chem.* **55**, 1385–1390.

(doi:10.1021/ac00259a044)

152. Rothwell DJ, Jendrzejczak B, Becker M, Doumas BT. 1976 Lactate dehydrogenase activities in serum and plasma. *Clin. Chem.* **22**, 1024–1026.

153. Vesell ES, Bearn AG. 1961 Isozymes of Lactic Dehydrogenase in Human Tissues. *J. Clin. Invest.* **40**, 586–591. (doi:10.1172/JCI104287)

154. Schneider RJ, Seibert K, Passe S, Little C, Gee T, Lee BJ, Mik? V, Young CW. 1980 Prognostic significance of serum lactate dehydrogenase in malignant lymphoma. *Cancer* **46**, 139–143. (doi:10.1002/1097-0142(19800701)46:1<139::AID-CNCR2820460122>3.0.CO;2-8)

155. Drent M, Cobben NAM, Henderson RF, Wouters EFM, van Dieijen-Visser M. 1996 Usefulness of lactate dehydrogenase and its isoenzymes as indicators of lung damage or inflammation. *Eur. Respir. J.* **9**, 1736–1742. (doi:10.1183/09031936.96.09081736)

156. Huijgen HJ, Sanders GT, Koster RW, Vreeken J, Bossuyt PM. 1997 The clinical value of lactate dehydrogenase in serum: a quantitative review. *Eur. J. Clin. Chem. Clin. Biochem.* **35**, 569–579.

157. Lewin A, Hamilton S, Witkover A, Langford P, Nicholas R, Chataway J, Bangham CRM. 2016 Free serum haemoglobin is associated with brain atrophy in secondary progressive multiple sclerosis. *Wellcome Open Res.* **1**, 1–23. (doi:10.12688/wellcomeopenres.9967.1)

158. Valvona CJ, Fillmore HL, Nunn PB, Pilkington GJ. 2016 The Regulation and Function of Lactate Dehydrogenase A: Therapeutic Potential in Brain Tumor. *Brain Pathol.* **26**, 3–17. (doi:10.1111/bpa.12299)

159. Schauf CL, Frischer H, Davis FA. 1980 Mechanical fragility of erythrocytes in multiple sclerosis. *Neurology* **30**, 323–323. (doi:10.1212/WNL.30.3.323)

160. Caspary EA, Sewell F, Field EJ. 1967 Red blood cell fragility in multiple sclerosis. *Br. Med. J.* **2**, 610–611.

161. Nema S, Avis KE. In press. Freeze-thaw studies of a model protein, lactate dehydrogenase, in the presence of cryoprotectants. *J. Parenter. Sci. Technol.* **47**, 76–83.

162. Lugovoi VI, Volovel'skaia EL, Grek AM. In press. [Effect of freezing-thawing on the activity of lactate dehydrogenase isoenzymes]. *Ukr. biokhimicheskii zhurnal* **54**, 274–9.

163. GE Lifesciences. 2015 Antibody Purification Handbook. **1**, 1–171. See https://www.google.co.uk/url?sa=t&rct=j&q=&esrc=s&source=web&cd=1&ved=0ahUKEwjI78OAvunZAhVMBsAKHTP3CUoQFgg4MAA&url=http%3A%2F%2Fproteins.gelifesciences.com%2F~%2Fmedia%2Fprotein-purification-ib%2Fdocuments%2Fhandbooks%2Fantibody_purification_handbook.pdf

%3Fla%3Den&usg=AOvVaw1uIQbN11tRNNaK8pMIHjPh (accessed on 21 February 2018).

164. LOGHEM E, FRANGIONE B, RECHT B, FRANKLIN EC. 1982 Staphylococcal Protein A and Human IgG Subclasses and Allotypes. *Scand. J. Immunol.* **15**, 275–278. (doi:10.1111/j.1365-3083.1982.tb00649.x)

165. Grov A. 1975 HUMAN IgM INTERACTING WITH STAPHYLOCOCCAL PROTEIN A. *Acta Pathol. Microbiol. Scand. Sect. C Immunol.* **83C**, 173–176. (doi:10.1111/j.1699-0463.1975.tb01622.x)

166. ThermoFisher Scientific. 2017 IgG (Total) Human ELISA Kit. *Invitrogen*. , 1–20. See https://www.thermofisher.com/order/catalog/product/BMS2091 (accessed on 13 March 2018).